Csaba Fábri

Quantum chemical computation and characterization of rotational-vibrational states of semirigid and flexible polyatomic molecules

Supervisor

Prof. Dr. Attila G. Császár

Laboratory of Molecular Structure and Dynamics, Institute of Chemistry

Eötvös Loránd University

Chemistry Doctoral School

Head of the Doctoral School: Prof. Dr. György Inzelt

Theoretical and Physical Chemistry, Materials Science Research Doctoral Programme

Head of the Doctoral Programme: Prof. Dr. Péter Surján

Eötvös Loránd University

Budapest, 2012

Acknowledgements

First of all, I would like to thank my supervisor, Professor Attila G. Császár, for his help and support.

I thank Dr. Edit Mátyus, Tamás Szidarovszky, Dr. Tibor Furtenbacher, Dr. Gábor Czakó, István Szabó and János Sarka for their help and for the valuable scientific discussions we had during the past three years.

Collaboration with Drs. Wesley D. Allen, Sergei Yurchenko, László Nemes, Tucker Carrington, Georg Mellau, as well as Ms. Tímea Mihály and Mr. Béla Mihály is gratefully acknowledged.

The European Union and the European Social Fund have provided financial support to this research under Grant No. TÁMOP-4.2.1/B-09/1/KMR-2010-0003. The work described was also supported by the Hungarian Scientific Research Fund (OTKA, Grant Nos. K72885 and NK83583).

I thank Ms. Margit Katalin Kapocsi, my high school chemistry teacher, for turning my attention to chemistry.

Finally, I am grateful to my family and friends for their support and encouragement during my doctoral work.

Contents

1 Introduction **9**

2 Variational rotational-vibrational computations for N-atomic molecules **12**

2.1 DEWE 12

2.1.1 The Eckart–Watson (EW) Hamiltonian for semirigid molecules . . . 12

2.1.2 Summary of the vibration-only algorithm 15

2.1.3 Solution of the rotational-vibrational problem 18

2.2 GENIUSH 22

2.2.1 Formulation of the classical Hamiltonian in generalized internal coordinates 22

2.2.2 Formulation of the quantum mechanical Hamiltonian in generalized coordinates 25

2.2.3 Reduced-dimensional computational models 26

2.2.4 Brief summary of the vibration-only algorithm 26

2.2.5 Solution of the rotational-vibrational problem 27

2.3 Symmetry-adapted Lanczos method (SAL) 31

2.3.1 Iterative Lanczos eigensolver 31

2.3.2 Theory of the SAL method 32

2.3.3 Considerations for the C_{2v}(M) molecular symmetry group within DEWE 33

2.4 Eckart embedding 36

2.4.1 Summary of the Eckart conditions and Eckart related applications . 36

2.4.2 Theory of maintaining the rotational Eckart condition 37

2.5 Labelling of rovibrational states 40

2.5.1 Normal mode decomposition (NMD) 40

2.5.2 Rigid rotor decomposition (RRD) 40

2.6 The vibrational subspace (VS) method 44

2.6.1 General description 44

2.6.2 DEWE-VS matrix elements 46

2.6.3 GENIUSH-VS matrix elements 47

2.6.4 Symmetry considerations 48

3 Results and discussion **50**
3.1 Rovibrational states of NH_3 computed by GENIUSH 50
3.1.1 Computational details 51
3.1.2 Full-dimensional results 53
3.1.3 Convergence of the rovibrational levels 55
3.1.4 Reduced-dimensional results 59
3.2 Rovibrational results for the C_2H_2O computed by DEWE 60
3.2.1 Model of the PES 62
3.2.2 Rovibrational energy levels and wave functions 63
3.2.3 MARVEL analysis 64
3.2.4 Vibrational band origins 65
3.2.5 Rovibrational energy levels 75
3.2.6 MARVEL energy levels 81
3.2.7 New assignments 83
3.3 GENIUSH-VS computations for $H_2{}^{16}O$ 84

4 Future plans **89**
4.1 Clustering of the highly-excited rovibrational states of CH_4 89
4.2 Eckart embedding for the NH_3 molecule 93

5 Summary **94**

A Appendix **96**
A.1 Angular momentum algebra 96
A.2 Elements of the **g** matrix 98
A.3 Derivation of Eq. (143) 99

1 Introduction

The Born–Oppenheimer (BO) approximation [1, 2], being central to the definition of many concepts of chemistry, separates adiabatically the motion of electrons and nuclei and thus defines two important fields for computational quantum chemistry: electronic structure theory and nuclear motion theory. This thesis is dedicated to the field of nuclear motion theory and introduces methods for the effective variational solution of the time-independent nuclear-motion Schrödinger equation.

Similarly to the field of electronic structure theory, the nuclear Hamiltonian is the sum of the nuclear kinetic and potential energy operators. The potential energy operator, also known as the potential energy surface (PES), contrary to electronic structure computations, is never known in an exact and analytical form. The value of the PES at distinct nuclear geometries can be obtained by the tools of electronic structure theory.

Also in contrast to electronic structure computations, the nuclear kinetic energy operator is not expressed in terms of Cartesian coordinates. Instead of the Cartesian formulation it is common to utilize more specific coordinates which allow the introduction of different types of motions, namely translations, rotations and vibrations. The three translational degrees of freedom are described by three center-of-mass coordinates [3], while the three rotational degrees of freedom are usually characterized by the widely employed Euler angles [3]. For the vibrational motions there are many possible coordinate sets and the actual choice of the vibrational coordinates often depends on the semirigid or flexible nature and on the bonding arrangement of the molecule under examination.

There are three main categories of the nuclear kinetic energy operators. The first one is the so-called tailor-made nuclear kinetic energy operator [4, 5, 6]. These operators have been successfully applied, also in our group [7, 8, 9, 10], to molecules containing 3, 4, and even 5 atoms [11, 12, 13, 14, 15, 16, 17]. An important drawback of the tailor-made Hamiltonians is their specificity: separate programs need to be developed for molecules with different atom count and bonding arrangement. Within the second category this problem is circumvented by employing the exact and general N-atomic Eckart–Watson [18, 19] nuclear kinetic energy operator expressed in rectilinear internal coordinates. Several programs were implemented either in our laboratory, where it is called DEWE [20, 21, 22], or by other research groups [23, 24, 25, 26, 27, 28, 29, 30, 31]. Though these programs do apply to N-atomic molecules, it is important to note that they are limited to semirigid molecules exhibiting a well-defined single minimum on their PES. The third and most general approach

allows nuclear motion computations employing arbitrarily chosen internal coordinates and body-fixed frame embeddings for N-atomic molecules. Besides the GENIUSH program [32, 33] developed in our group, notable examples of this black-box-like approach can be found in Refs. [34, 35, 36, 37, 38, 39, 40].

During my doctoral research I extended the original vibrational-only DEWE and GENIUSH programs, developed principally by Dr. Edit Mátyus, with the capability of variational computation of rotational-vibrational energy levels and wave functions, as described in Sections 2.1 and 2.2, respectively. Section 2.3 summarizes the symmetry-adapted Lanczos method (SAL) allowing the assignment of molecular symmetry (MS) group symmetry labels to the computed rovibrational energy levels and wave functions. After a general introduction to SAL I give the details of my SAL implementation [22] within DEWE. Section 2.4 introduces how the rotational Eckart condition [41], leading to an optimal separation of vibrations and rotations, can be maintained for the case of general N-atomic rovibrational Hamiltonians expressed in arbitrary curvilinear internal coordinates. The practical implementation of the Eckart frame within GENIUSH is also described. Section 2.5 is dedicated to the labelling of the computed rovibrational energy levels and wave functions with zeroth-order harmonic oscillator and rigid rotor quantum numbers by the normal mode decomposition (NMD) and rigid rotor decomposition (RRD) procedures [42], helping the interpretation of the computed rovibrational states. Section 2.6 gives an insight into the vibrational subspace (VS) method [22] allowing the computation of rovibrational states for high values of the J rotational quantum number. Labelling of the computed rovibrational states with symmetry labels, and zeroth-order harmonic oscillator and rigid rotor quantum numbers within the framework of VS is also discussed.

My application-oriented results are summarized in Section 3. Section 3.1 focuses on the rovibrational results for the four-atomic NH_3 obtained by GENIUSH. Special emphasis is put on the comparison of the full-dimensional and different reduced-dimensional rovibrational models. In Section 3.2 the rovibrational spectroscopy of the five-atomic C_2H_2O (ketene) molecule is examined. Variational computations (employing the DEWE, VS, NMD, RRD and SAL methods) and the Measured Active Rotational-Vibrational Energy Levels (MARVEL) [43] procedure were applied to propose new assignments in the experimental spectrum of C_2H_2O. In Section 3.3 labels of the MARVEL energy levels of $H_2{}^{16}O$ up to $J = 25$ are validated. The validation process has employed the VS procedure implemented within GENIUSH.

Finally, in Section 4 I introduce my future plans concerning the CH_4 and NH_3 molecules. In case of CH_4, rovibrational clustering of the energy levels corresponding to high J values is examined. For NH_3, rovibrational computations employing the Eckart frame have been executed and the results with different choices of the Eckart reference structure are analysed briefly.

2 Variational rotational-vibrational computations for N-atomic molecules

2.1 DEWE

This section is dedicated to the DEWE (Discrete variable representation of the Eckart–Watson Hamiltonian with a numerically Exact inclusion of arbitrary potential energy surfaces) program developed by our research group. DEWE employs the universal and exact Eckart–Watson (EW) Hamiltonian [18, 19] and the iterative Lanczos [44] eigensolver for obtaining the eigenvalues and eigenvectors of the Hamiltonian matrix. Though DEWE can be applied for N-atomic systems, it is limited to the case of semirigid molecules with a single well-defined minimum structure. My contribution to DEWE was to add the capability of computing rotational-vibrational energy levels and wave functions to the original vibrational-only code [20, 21]. After introducing the EW Hamiltonian and summarizing the vibrational-only implementation I give a detailed description on the variational solution of the rotational-vibrational problem [22] within the framework of DEWE.

2.1.1 The Eckart–Watson (EW) Hamiltonian for semirigid molecules

The formalism given in this section is restricted to molecules having nonlinear reference configurations. Details concerning the special case of molecules with linear reference structure are discussed in the literature [19].

Let us denote the position vectors of the nuclei of an N-atomic nonlinear molecule by $\mathbf{x}_i$ $(i = 1, \cdots, N)$, expressed in the laboratory-fixed frame. In practice, it is preferable to work with the body-fixed nuclear position vectors $\mathbf{z}_i$, defined as

$$\mathbf{z}_i = \mathbf{C}^{\mathrm{T}}(\mathbf{x}_i - \mathbf{X}). \tag{1}$$

In Eq. (1) $\mathbf{X}$ refers to the nuclear center of mass and $\mathbf{C}$ stands for the orthogonal direction cosine matrix [3], which gives the orientation of the body-fixed frame with respect to the laboratory-fixed one. It is important to note that only $3N-6$ coordinates are independent out of the $3N$ body-fixed Cartesian coordinates.

The translational motion of the molecule can be separated by employing the

$$\sum_{i=1}^{N} m_i \mathbf{z}_i = \mathbf{0} \tag{2}$$

translational Eckart condition [41], where m_i is the mass of the ith nucleus. The $\boldsymbol{\rho}_i$ displacement vectors are defined as

$$\boldsymbol{\rho}_i = \mathbf{z}_i - \mathbf{c}_i, \tag{3}$$

where the $\mathbf{c}_i$ $(i = 1, \cdots, N)$ vectors belong to the reference structure of the molecule. In most of the applications the reference structure corresponds to a minimum of the potential energy surface (PES). In terms of the $\mathbf{c}_i$ and $\boldsymbol{\rho}_i$ vectors the rotational Eckart condition [41] reads as

$$\sum_{i=1}^{N} m_i \mathbf{c}_i \times \boldsymbol{\rho}_i = \mathbf{0}, \tag{4}$$

defining the coordinate axes of the body-fixed frame.

Out of the many coordinate systems developed to describe the vibrational motion of the nuclei, the present formalism employs the

$$Q_k = \sum_{i=1}^{N} \sum_{\alpha} b_{\alpha ik} \rho_{\alpha i} = \sum_{i=1}^{N} \mathbf{b}_{ik}^{\mathrm{T}} \boldsymbol{\rho}_i,$$

$$Q_k \in (-\infty, +\infty), \quad k = 1, 2, \ldots, 3N-6, \quad \alpha = x, y, z \tag{5}$$

rectilinear vibrational coordinates constructed as the linear combinations of the $\boldsymbol{\rho}_i$ displacement vectors. In Eq. (5) $\mathbf{b} \in \Re^{3N \times (3N-6)}$ is a constant matrix whose elements were chosen as

$$\mathbf{b}_{ik} = \sqrt{m_i}\, \mathbf{l}_{ik} \tag{6}$$

by Watson [18]. The rows and columns of the $\mathbf{l}$ matrix satisfy the

$$\sum_{i=1}^{N} \mathbf{l}_{ik}^{\mathrm{T}} \mathbf{l}_{il} = \delta_{kl} \quad \text{and} \quad \sum_{k=1}^{N} \mathbf{l}_{ik}^{\mathrm{T}} \mathbf{l}_{jk} = \delta_{ij} \tag{7}$$

orthogonality relations. In view of Eq. (6), the Q_k rectilinear vibrational coordinates are

given by

$$Q_k = \sum_{i=1}^{N} \sqrt{m_i}\, \mathbf{l}_{ik}^{\mathrm{T}} \boldsymbol{\rho}_i, \quad k = 1, 2, \ldots, 3N-6 \tag{8}$$

with regard to the elements of the $\mathbf{l}$ matrix.

If Eq. (8) is inverted, the $\boldsymbol{\rho}_i$ displacement vectors can be expressed in terms of the Q_k vibrational coordinates:

$$\boldsymbol{\rho}_i = \frac{1}{\sqrt{m_i}} \sum_{k=1}^{3N-6} \mathbf{l}_{ik} Q_k, \quad i = 1, \ldots, N. \tag{9}$$

In practical applications of DEWE, the reference configurations are usually chosen to be an equilibrium (minimum) structure of the PES and the Q_k rectilinear vibrational coordinates defined in Eq. (8) are chosen to be the $3N-6$ normal coordinates of the molecule under examination.

The exact rotational-vibrational kinetic energy operator for an N-atomic nonlinear molecule employing the Eckart embedding and rectilinear vibrational coordinates of Eq. (8) was simplified by Watson in 1968 [18] and has the form

$$\hat{H} = \frac{1}{2} \sum_{k=1}^{3N-6} \hat{P}_k^2 + \frac{1}{2} \sum_{\alpha,\beta} (\hat{J}_\alpha - \hat{\pi}_\alpha) \mu_{\alpha\beta} (\hat{J}_\beta - \hat{\pi}_\beta) - \frac{\hbar^2}{8} \sum_{\alpha} \mu_{\alpha\alpha} + \hat{V}, \tag{10}$$

where α,$\beta = x, y, z$. In Eq. (10), $\hat{P}_k = -i\hbar \frac{\partial}{\partial Q_k}$, the $\hat{J}_x$, $\hat{J}_y$, and $\hat{J}_z$ operators correspond to the body-fixed components of the total angular momentum, and $\hat{V}$ is the potential energy surface determining the motion of the nuclei. Definitions of the $\hat{\pi}_\alpha$ vibrational angular momentum and $\mu_{\alpha\beta}$ generalized inverse inertia tensor operators are given by the

$$\hat{\pi}_\alpha = \sum_{k,l=1}^{3N-6} \zeta_{kl}^{\alpha} Q_k \hat{P}_l, \tag{11}$$

$$\mu_{\alpha\beta} = \left(\mathbf{I}'^{-1}\right)_{\alpha\beta}, \tag{12}$$

$$I'_{\alpha\beta} = I_{\alpha\beta} - \sum_{k,l,m=1}^{3N-6} \zeta_{km}^{\alpha} \zeta_{lm}^{\beta} Q_k Q_l, \tag{13}$$

and

$$\zeta_{kl}^{\alpha} = \sum_{\beta\gamma} \epsilon_{\alpha\beta\gamma} \sum_{i=1}^{N} l_{\beta ik} l_{\gamma il} \tag{14}$$

relations. In the previous expressions $\epsilon_{\alpha\beta\gamma}$ stands for the Levi-Cività symbol and $\mathbf{I}$ refers to the inertia tensor.

The $\boldsymbol{\mu}$ matrix can be decomposed as

$$\mu_{\alpha\beta} = \sum_{\gamma\delta} (\mathbf{I}''^{-1})_{\alpha\gamma} I^0_{\gamma\delta} (\mathbf{I}''^{-1})_{\delta\beta}, \tag{15}$$

where

$$I''_{\alpha\beta} = I^0_{\alpha\beta} + \frac{1}{2} \sum_{k=1}^{3N-6} a_k^{\alpha\beta} Q_k, \tag{16}$$

and

$$a_k^{\alpha\beta} = 2 \sum_{\gamma\delta\nu} \epsilon_{\alpha\gamma\nu} \epsilon_{\beta\delta\nu} \sum_{k=1}^{N} \sqrt{m_i} c_{\gamma i} l_{\delta ik}, \tag{17}$$

with $\mathbf{I}^0$ being the inertia tensor corresponding to the reference structure. In order to compute matrix elements corresponding to the Eckart–Watson Hamiltonian the integral volume element is needed, which has the simple form

$$\mathrm{d}V = \sin\theta \mathrm{d}\phi \mathrm{d}\theta \mathrm{d}\chi \mathrm{d}Q_1 \cdots \mathrm{d}Q_{3N-6}, \tag{18}$$

where ϕ, θ, and χ denote the well-known Euler angles [3].

2.1.2 Summary of the vibration-only algorithm

The description of the vibrational DEWE algorithm given in this section follows closely the work of Mátyus and coworkers [20, 21]. For the $J = 0$ value of the J rotational quantum number, the Eckart–Watson Hamiltonian takes the form

$$\hat{H}^{\mathrm{v}} = \frac{1}{2} \sum_{k=1}^{3N-6} \hat{P}_k^2 + \frac{1}{2} \sum_{\alpha,\beta} \hat{\pi}_\alpha \mu_{\alpha\beta} \hat{\pi}_\beta - \frac{\hbar^2}{8} \sum_{\alpha} \mu_{\alpha\alpha} + \hat{V}. \tag{19}$$

The $\hat{H}^{\mathrm{v}}$ pure vibrational operator can be regarded as an effective nuclear-motion Hamiltonian yielding the $J = 0$ energy levels and wave functions of the molecule under examination.

In order to apply the linear variational method to the eigenproblem of $\hat{H}^{\mathrm{v}}$ a suitable

basis has to be found. As molecular vibrations are examined, a plausible choice is the set of one-dimensional harmonic oscillator eigenfunctions [45],

$$f_{i_k}(Q_k) = H_{i_k-1}(\gamma_k^{\frac{1}{4}} Q_k) e^{-\frac{\gamma_k^{\frac{1}{2}} Q_k^2}{2}}. \tag{20}$$

In Eq. (20) Q_k is the kth rectilinear vibrational coordinate, γ_k is the quadratic force constant corresponding to Q_k and the $H_{i_k-1}(\gamma_k^{\frac{1}{4}} Q_k)$s denote the well-known normalized Hermite polynomials. As a first attempt, one can define the $3N-6$-dimensional vibrational basis as the direct product of the $f_{i_k}(Q_k)$ one-dimensional functions,

$$\{\prod_{k=1}^{3N-6} f_{i_k}(Q_k)\}_{i_1=1,i_2=1,\cdots,i_{3N-6}=1}^{n_1,n_2,\ldots,n_{3N-6}}. \tag{21}$$

As a result, $3N-6$-dimensional integrals arise during the evaluation of the potential energy matrix elements which can highly increase the computational cost. Our strategy to circumvent this problem employs the discrete variable representation (DVR) [14, 46, 47, 48, 49, 50], which greatly reduces the numerical work needed for the evaluation of the potential energy matrix elements. The DVR technique has proven to be a powerful tool for solving problems in the fields of computational molecular spectroscopy and molecular dynamics since its introduction in these fields in 1965 [46].

The Hermite-DVR [51] applied by DEWE necessitates the matrix representation of the Q_k coordinate operators for $k = 1, \ldots, 3N-6$. These matrix elements are defined by the

$$\langle f_{i_k}(Q_k)|Q_k|f_{j_k}(Q_k)\rangle = \int_{-\infty}^{+\infty} H_{i_k-1}(\gamma_k^{\frac{1}{4}} Q_k) Q_k H_{j_k-1}(\gamma_k^{\frac{1}{4}} Q_k) e^{-\gamma_k^{\frac{1}{2}} Q_k^2} dQ_k \tag{22}$$

integrals, where the matrix representation of Q_k is of dimension n_k. The only nonzero values of Eq. (22) are given by

$$\langle f_{i_k}(Q_k)|Q_k|f_{j_k}(Q_k)\rangle = \sqrt{\frac{i_k}{2\gamma_k}}, \quad \text{if } j_k = i_k + 1, \tag{23}$$

and

$$\langle f_{i_k}(Q_k)|Q_k|f_{j_k}(Q_k)\rangle = \sqrt{\frac{i_k - 1}{2\gamma_k}}, \quad \text{if } j_k = i_k - 1. \tag{24}$$

The q_{k,i_k} quadrature points for the Q_k coordinate correspond to the eigenvalues of $\mathbf{Q}_k$, while the DVR basis can be built according to the expression

$$F_{i_k}(Q_k) = \sum_{j_k=1}^{n_k} (\mathbf{T}_k)_{i_k,j_k} f_{j_k}(Q_k), \tag{25}$$

where the columns of $\mathbf{T}_k$ contain the eigenvectors of $\mathbf{Q}_k$. These one-dimensional DVR basis functions are combined into the direct product basis according to the equation

$$\{\prod_{k=1}^{3N-6} F_{i_k}(Q_k)\}_{i_1=1,i_2=1,\cdots,i_{3N-6}=1}^{n_1,n_2,\ldots,n_{3N-6}}. \tag{26}$$

The $\mathbf{Q}_k$ matrices become diagonal as a result of applying the DVR basis. Moreover, the matrix representation of an arbitrary $\hat{A}$ operator depending only on the vibrational coordinates can be approximated by a diagonal matrix and the diagonal elements equal to the values of $\hat{A}$ at the DVR grid points. This statement applies to the $\hat{V}$ potential energy surface whose matrix elements are simply

$$\langle F_i|\hat{V}(\mathbf{Q})|F_j\rangle = V(q_{1,i_1}, q_{2,i_2}, \ldots, q_{3N-6,n_{3N-6}})\delta_{i_1,j_1}\delta_{i_2,j_2}\cdots\delta_{i_{3N-6},j_{3N-6}}, \tag{27}$$

where $F_i = F_{i_1}(Q_1)F_{i_2}(Q_2)\cdots F_{i_{3N-6}}(Q_{3N-6})$, and the i and j direct product indices can be uniquely expressed in terms of the $i_1, i_2, \ldots, i_{3N-6}$ and $j_1, j_2, \ldots, j_{3N-6}$ indices:

$$i = n_2 \ldots n_{3N-6}(i_1 - 1) + n_3 \ldots n_{3N-6}(i_2 - 1) + \cdots + n_{3N-6}(i_{3N-7} - 1) + i_{3N-6}, \tag{28}$$

and

$$j = n_2 \ldots n_{3N-6}(j_1 - 1) + n_3 \ldots n_{3N-6}(j_2 - 1) + \cdots + n_{3N-6}(j_{3N-7} - 1) + j_{3N-6}.$$

Matrix elements of the $\mu_{\alpha\beta}$ operators take the form

$$\langle F_i|\mu_{\alpha\beta}(\mathbf{Q})|F_j\rangle = \mu_{\alpha\beta}(q_{1,i_1}, q_{2,i_2}, \ldots, q_{3N-6,i_{3N-6}})\delta_{i_1,j_1}\delta_{i_2,j_2}\cdots\delta_{i_{3N-6},j_{3N-6}}, \tag{29}$$

where $\mu_{\alpha\beta}(q_{1,i_1}, q_{2,i_2}, \ldots, q_{3N-6,i_{3N-6}})$ is evaluated according to Eq. (15). Once the matrix elements corresponding to the $\mu_{\alpha\beta}$ operators are known it is easy to set up the matrix representation of $-\frac{\hbar^2}{8}\sum_\alpha \mu_{\alpha\alpha}$, the so-called extrapotential term of the EW Hamiltonian.

DVR matrix elements of the $\frac{\partial}{\partial Q_k}$ and $\frac{\partial^2}{\partial Q_k^2}$ differential operators needed for the $\frac{1}{2}\sum_{k=1}^{3N-6}\hat{P}_k^2$ and $\frac{1}{2}\sum_{\alpha,\beta}\hat{\pi}_\alpha\mu_{\alpha\beta}\hat{\pi}_\beta$ terms can be given by simple analytic expressions [51].

The last step in solving the vibrational problem is the construction of the matrix representation of the

$$\frac{1}{2}\sum_{\alpha,\beta}\hat{\pi}_\alpha\mu_{\alpha\beta}\hat{\pi}_\beta$$

Coriolis coupling operator. To move forward, two resolution of identities are to be inserted amongst $\hat{\pi}_\alpha$ and $\mu_{\alpha\beta}$, and $\mu_{\alpha\beta}$ and $\hat{\pi}_\beta$. This step results in the matrix element expression

$$\langle F_i|\frac{1}{2}\sum_{\alpha,\beta}\hat{\pi}_\alpha\mu_{\alpha\beta}\hat{\pi}_\beta|F_j\rangle = \frac{1}{2}\sum_{\alpha,\beta}\sum_{k=1}^{n}(\boldsymbol{\pi}_\alpha)_{ik}(\boldsymbol{\mu}_{\alpha\beta})_{kk}(\boldsymbol{\pi}_\beta)_{kj}, \tag{30}$$

where $n = n_1 n_2 \cdots n_{3N-6}$ is the size of the direct-product basis.

2.1.3 Solution of the rotational-vibrational problem

In order to derive formulae suitable for practical implementations, it is advantageous to rewrite the Eckart–Watson Hamiltonian defined by Eq. (10) as

$$\hat{H} = \hat{T}^{\mathrm{v}} + \hat{T}^{\mathrm{r}} + \hat{T}^{\mathrm{rv}} + \hat{V}, \tag{31}$$

where

$$\hat{T}^{\mathrm{v}} = \frac{1}{2}\sum_{k=1}^{3N-6}\hat{P}_k^2 + \frac{1}{2}\sum_{\alpha,\beta}\hat{\pi}_\alpha\mu_{\alpha\beta}\hat{\pi}_\beta - \frac{\hbar^2}{8}\sum_{\alpha}\mu_{\alpha\alpha}, \tag{32}$$

$$\hat{T}^{\mathrm{r}} = \frac{1}{2}\sum_{\alpha,\beta}\mu_{\alpha\beta}\hat{J}_\alpha\hat{J}_\beta = \frac{1}{2}\sum_{\alpha}\mu_{\alpha\alpha}\hat{J}_\alpha^2 + \frac{1}{2}\sum_{\alpha}\sum_{\beta>\alpha}\mu_{\alpha\beta}[\hat{J}_\alpha,\hat{J}_\beta]_+, \tag{33}$$

where

$$[\hat{J}_\alpha,\hat{J}_\beta]_+ = \hat{J}_\alpha\hat{J}_\beta + \hat{J}_\beta\hat{J}_\alpha,$$

and

$$\hat{T}^{\mathrm{rv}} = -\frac{1}{2}\sum_{\alpha,\beta}\mu_{\alpha\beta}\hat{\pi}_\beta\hat{J}_\alpha - \frac{1}{2}\sum_{\alpha,\beta}\mu_{\alpha\beta}\hat{\pi}_\alpha\hat{J}_\beta = -\sum_{\alpha,\beta}\mu_{\alpha\beta}\hat{\pi}_\beta\hat{J}_\alpha, \tag{34}$$

where the $\mu_{\alpha\beta} = \mu_{\beta\alpha}$ relation is utilized. In the previous equations the $\hat{T}^{\mathrm{v}}$, $\hat{T}^{\mathrm{r}}$, and $\hat{T}^{\mathrm{rv}}$ operators denote the vibrational, rotational, and rotational-vibrational coupling parts of the kinetic energy operator, respectively.

In order to set up the matrix representation of the rovibrational Hamiltonian of Eq. (31) a suitable rotational basis has to be chosen. The simplest choice is the orthonormal set of the $|JKM\rangle$ eigenfunctions of the symmetric-top rigid rotor [52], where $K = -J, \ldots, J$ is the body-fixed and $M = -J, \ldots, J$ is the space-fixed projection quantum number. Properties of the $|JKM\rangle$ functions and elements of the angular momentum algebra are briefly summarized in Appendix A.1. The nonzero matrix elements of the $\hat{J}_\alpha$ operators can be given by the following simple analytic formulae [52]:

$$\begin{aligned}
\langle JKM|\hat{J}_x|J(K\pm 1)M\rangle &= \frac{1}{2}\sqrt{J(J+1)-K(K\pm 1)} \\
\langle JKM|\hat{J}_y|J(K\pm 1)M\rangle &= \mp\frac{i}{2}\sqrt{J(J+1)-K(K\pm 1)} \\
\langle JKM|\hat{J}_z|JKM\rangle &= K,
\end{aligned} \tag{35}$$

where i is the imaginary unit.

Matrix elements of the $\hat{J}_\alpha^2$ and $[\hat{J}_\alpha, \hat{J}_\beta]_+$ operators present in Eqs. (33) and (34) can be constructed by simple matrix multiplication, by inserting the resolution of identity between $\hat{J}_\alpha$ and $\hat{J}_\beta$, thus,

$$\langle JKM|\hat{J}_\alpha\hat{J}_\beta|JK'M\rangle = \sum_{J'}\sum_{K''=-J'}^{J'}\langle JKM|\hat{J}_\alpha|J'K''M\rangle\langle J'K''M|\hat{J}_\beta|JK'M\rangle =$$

$$= \sum_{K''=-J}^{J}\langle JKM|\hat{J}_\alpha|JK''M\rangle\langle JK''M|\hat{J}_\beta|JK'M\rangle. \tag{36}$$

It is important to emphasize that Eq. (36) does not utilize any approximations, as

$$\langle JKM|\hat{J}_\alpha|J'K''M\rangle = \delta_{JJ'}\langle JKM|\hat{J}_\alpha|JK''M\rangle. \tag{37}$$

To facilitate symmetry considerations (see Sections 2.3 and 2.6.4) and to avoid complex rovibrational matrix elements present in Eq. (35), it is worth combining the simple $|JKM\rangle$ functions into the so-called Wang functions [52],

1. $\frac{1}{\sqrt{2}}\left(|JKM\rangle + |J-KM\rangle\right)$, where K is even

2. $\frac{1}{\sqrt{2}}\left(|JKM\rangle - |J-KM\rangle\right)$, where K is odd (38)

3. $\frac{i}{\sqrt{2}}\left(|JKM\rangle - |J-KM\rangle\right)$, where K is even

4. $\frac{i}{\sqrt{2}}\left(|JKM\rangle + |J-KM\rangle\right)$, where K is odd.

The four sets resulting from the use of the Wang functions correspond to the four irreducible representations of the D_2 rotational group.

One can construct a rovibrational basis of dimension $n(2J+1)$ as a direct product of the $2J+1$ Wang functions for a given J and the n vibrational basis functions defined in Eq. (26). Thus, the rovibrational Hamiltonian can be represented by the

$$\mathbf{H} = \mathbf{T}^{\mathrm{v}} + \mathbf{T}^{\mathrm{r}} + \mathbf{T}^{\mathrm{rv}} + \mathbf{V} \tag{39}$$

rovibrational Hamiltonian matrix of dimension $n(2J+1)$, where

$$\mathbf{T}^{\mathrm{v}} = \mathbf{E}_{2J+1} \otimes \left(\frac{1}{2} \sum_{k=1}^{3N-6} \mathbf{P}_k^2 + \frac{1}{2} \sum_{\alpha,\beta} \boldsymbol{\pi}_\alpha \boldsymbol{\mu}_{\alpha\beta} \boldsymbol{\pi}_\beta - \frac{\hbar^2}{8} \sum_\alpha \boldsymbol{\mu}_{\alpha\alpha} \right),$$

$$\mathbf{T}^{\mathrm{r}} = \frac{1}{2} \sum_\alpha \mathbf{J}_\alpha^2 \otimes \boldsymbol{\mu}_{\alpha\alpha} + \frac{1}{2} \sum_\alpha \sum_{\beta>\alpha} [\mathbf{J}_\alpha, \mathbf{J}_\beta]_+ \otimes \boldsymbol{\mu}_{\alpha\beta}, \tag{40}$$

and

$$\mathbf{T}^{\mathrm{rv}} = -\sum_{\alpha,\beta} \mathbf{J}_\alpha \otimes \left(\boldsymbol{\mu}_{\alpha\beta} \boldsymbol{\pi}_\beta \right).$$

In Eq. (40) $\mathbf{E}_{2J+1}$ refers to the $2J+1$-dimensional identity matrix and $\otimes$ denotes the direct product operation. Matrix elements of the potential energy $\hat{V}$ can be computed by the equation

$$(\mathbf{V})_{n\cdot(K+J)+i,n\cdot(K'+J)+j} = V(q_{1,i_1}, q_{2,i_2}, \ldots, q_{3N-6,i_{3N-6}}) \delta_{i_1,j_1} \delta_{i_2,j_2} \cdots \delta_{i_{3N-6},j_{3N-6}} \delta_{K,K'}, \tag{41}$$

where q_{k,n_k}s are grid points of the kth vibrational degree of freedom and n is the size of the vibrational basis.

According to the definitions of the $\hat{\pi}_\alpha$ vibrational angular momentum operators and vibrational basis functions, elements of the $\boldsymbol{\pi}_\alpha$ matrices are purely imaginary. In order to eliminate complex arithmetics, it is favorable to construct real Hamiltonian matrix elements

by employing imaginary $\mathbf{J}_\alpha$ matrices. Thus, all the $\mathbf{J}_\alpha^2$, $[\mathbf{J}_\alpha, \mathbf{J}_\beta]_+$, and $\mathbf{J}_\alpha \otimes \left(\boldsymbol{\mu}_{\alpha\beta}\boldsymbol{\pi}_\beta\right)$ matrices become real. The fact, that matrices of the $\hat{J}_\alpha$ operators expressed in the Wang basis have imaginary matrix elements, can be simply proven.

2.2 GENIUSH

In this section the theory of the GENIUSH (General rovibrational code with Numerical, Internal coordinate, User-Specified Hamiltonians) approach [32, 33] is described. The GENIUSH approach successfully circumvents the main drawbacks of DEWE and thus can be applied to N-atomic molecules exhibiting multiple accessible PES minima and large amplitude motions. The main idea behind GENIUSH is the numerical representation of the rovibrational kinetic energy operator which allows us to employ arbitrary sets of internal coordinates and body-fixed frame embeddings during the rovibrational computations. Another important characteristics of GENIUSH is the possibility to introduce reduced-dimensional vibrational models in a straightforward manner. My task was to formulate and add the rotational functionality to the original vibrational-only GENIUSH code. Before the detailed description of the variational solution of the rovibrational problem is given, formulation of the general N-atomic rovibrational Hamiltonian and the vibrational-only implementation are discussed.

2.2.1 Formulation of the classical Hamiltonian in generalized internal coordinates

The nonrelativistic Lagrangian of an isolated N-particle system with masses m_i, $i = 1, ..., N$, can be written as

$$L = \frac{1}{2} \sum_{k=1}^{D+6} \sum_{l=1}^{D+6} g_{kl} \dot{q}_k \dot{q}_l - V, \tag{42}$$

where $D < 3N - 6$ for reduced-dimensional models ($D = 3N - 6$ for the full problem), V is the potential energy depending on the generalized coordinates q_k, and

$$g_{kl} = \sum_{i=1}^{N} m_i \frac{\partial \mathbf{X}_i^{\mathrm{T}}}{\partial q_k} \frac{\partial \mathbf{X}_i}{\partial q_l} = \sum_{i=1}^{N} m_i \mathbf{t}_{ik}^{\mathrm{T}} \mathbf{t}_{il}, \quad k, l = 1, \ldots, D + 6. \tag{43}$$

In Eq. (43), $\mathbf{X}_i$ is the position vector of the ith atom in the *space-fixed* reference frame (X, Y, Z), and $\mathbf{t}_{ik}$ is the $\mathbf{t}$ vector [53] of the q_k generalized coordinate on the ith atom. After introducing the $p_k = \frac{\partial L}{\partial \dot{q}_k}$ $(k = 1, \ldots, D + 6)$ generalized momenta conjugate to q_k,

the classical Hamiltonian takes the following simple form:

$$H^{\text{full}} = \frac{1}{2} \sum_{k=1}^{D+6} \sum_{l=1}^{D+6} G_{kl} p_k p_l + V, \tag{44}$$

where

$$G_{kl} = \left(\mathbf{g}^{-1}\right)_{kl}, \tag{45}$$

if $\mathbf{g} \in \mathbb{R}^{(D+6)\times(D+6)}$ is not singular.

To construct the $\mathbf{g}$ and $\mathbf{G}$ matrices, let us describe the configuration of the system by the $q_k = q_k$ active ($k = 1, \ldots, D$) and constrained ($k = D+1, \ldots, 3N-6$) internal coordinates, the three rotational $q_{D+1} = \alpha_1$, $q_{D+2} = \alpha_2$, $q_{D+3} = \alpha_3$, and the three center-of-mass ($q_{D+4} = X_1$, $q_{D+5} = X_2$, $q_{D+6} = X_3$) coordinates. Then,

$$\mathbf{X}_i = \mathbf{X} + \mathbf{C}\mathbf{x}_i, \quad i = 1, \ldots, N, \tag{46}$$

where $\mathbf{C}$ is an orthogonal rotation matrix depending on the three rotational coordinates, and the $\mathbf{x}_i$ *body-fixed* position vectors in the body-fixed frame (x, y, z) are functions of the q_k internal coordinates. Derivation of the g_{kl} matrix elements is equivalent, see Eq. (43), to giving the $\mathbf{t}_{ik}$ vectors in terms of the generalized coordinates.

The *translational* $\mathbf{t}_{i,k+D+3}$ ($k = 1, 2, 3$) vectors are simply

$$t^a_{i,k+D+3} = \frac{\partial X_{ia}}{\partial X_k} = \delta_{ak}, \quad a = 1, 2, 3, \tag{47}$$

where a refers to the three components of the vector $\mathbf{t}$.

By making use of Eq. (43), the translational $\mathbf{g}$ matrix elements can be expressed as

$$g_{k+D+3,l+D+3} = M \cdot \delta_{kl}, \quad k, l = 1, 2, 3, \tag{48}$$

where M is the total mass of the system; thus, these are constants.

For isolated systems, the *rotational-translational* and the *vibrational-translational* coupling matrix elements of $\mathbf{g}$ are all equal to zero. Therefore, the motion of the center of mass can be separated exactly from the rest of the coordinates. This allows the introduction of the

$$H = T + V = \frac{1}{2} \sum_{k=1}^{D+3} \sum_{l=1}^{D+3} G_{kl} p_k p_l + V \tag{49}$$

rovibrational Hamiltonian.

The *rotational* $\mathbf{t}_{i,k+D}$ $(k = 1, 2, 3)$ vectors take the form

$$t^a_{i,k+D} = \frac{\partial X_{ia}}{\partial \alpha_k} = \sum_{b=1}^{3} \frac{\partial C_{ab}}{\partial \alpha_k} x_{ib}. \tag{50}$$

Thus, the rotational $\mathbf{g}$ matrix elements are equal to

$$g_{k+D,l+D} = \sum_{i=1}^{N} m_i (\mathbf{e}_k \times \mathbf{x}_i)^{\mathrm{T}} (\mathbf{e}_l \times \mathbf{x}_i), \tag{51}$$

where the direction of the unit vector $\mathbf{e}_k$ coincides with the axis of rotation assigned to the α_k rotational coordinate [see Appendix A.2 for the derivation of Eq. (51)].

The *vibrational* $\mathbf{t}_{ik}$ $(k = 1, \ldots, D)$ vectors are

$$t^a_{ik} = \frac{\partial X_{ia}}{\partial q_k} = \sum_{b=1}^{3} C_{ab} \frac{\partial x_{ib}}{\partial q_k}. \tag{52}$$

Thus, the corresponding vibrational $\mathbf{g}$ matrix elements are given as

$$g_{kl} = \sum_{i=1}^{N} m_i \frac{\partial \mathbf{x}_i^{\mathrm{T}}}{\partial q_k} \frac{\partial \mathbf{x}_i}{\partial q_l}, \tag{53}$$

where $k, l = 1, \ldots, D$ [see Appendix A.2 for the derivation of Eq. (53)]. To determine g_{kl}, choice of the embedding of the molecule-fixed frame has to be established, which gives the dependence of the $\mathbf{x}_i$ body-fixed nuclear position vectors on the q_k internal coordinates.

According to previous expressions, the $\mathbf{g}$ matrix elements of the *rotational-vibrational coupling* block have the form

$$g_{k,l+D} = \sum_{i=1}^{N} m_i \frac{\partial \mathbf{x}_i^{\mathrm{T}}}{\partial q_k} (\mathbf{e}_l \times \mathbf{x}_i), \tag{54}$$

where $k = 1, \ldots, D$, $l = 1, 2, 3$, and $\mathbf{g}$ is a symmetric matrix [see Appendix A.2 for the derivation of Eq. (54)].

The elements of $\mathbf{G}$ can be expressed in two different ways: (a) by inversion of $\mathbf{g}$; and (b) by introduction of the so-called $\mathbf{s}_{ki}$ vectors [40, 53, 54], $\mathbf{s}_{ki} = \frac{\partial q_k}{\partial \mathbf{X}_i}, k = 1, \ldots, D + 6$ and $i = 1, \ldots, N$. In the present implementation of GENIUSH only the first approach is

utilized to construct $\mathbf{G}$.

2.2.2 Formulation of the quantum mechanical Hamiltonian in generalized coordinates

In this subsection the rovibrational quantum Hamiltonian $\hat{H}$ is introduced in analogy with the rovibrational classical Hamiltonian H. Within the Born–Oppenheimer approximation, the potential energy acting on the nuclei, $\hat{V}$, can be obtained by electronic structure computations. Thus, we will focus on constructing the $\hat{T}$ rovibrational kinetic energy operator in terms of the q_k $(k = 1, \ldots, D)$ vibrational and the α_k $(k = 1, 2, 3)$ rotational coordinates. According to differential geometry [55, 56, 57], $\hat{T}$ becomes

$$\hat{T} = \frac{1}{2} \sum_{k=1}^{D+3} \sum_{l=1}^{D+3} \tilde{g}^{-1/4} \hat{p}_k^{\dagger} G_{kl} \tilde{g}^{1/2} \hat{p}_l \tilde{g}^{-1/4}, \tag{55}$$

where $\tilde{g} = \det(\mathbf{g})$, $\mathbf{g}$ is either the full or the rotational-vibrational $\mathbf{g}$ matrix, $\hat{p}_k$ are the quasi-momenta [35], and the volume element contains no extra factors.

In units of $\hbar$, for the vibrational coordinates $\hat{p}_k = -i\frac{\partial}{\partial q_k}, \quad k = 1, \ldots, D$, while for the rotational coordinates $\hat{p}_{k+D} = -i\frac{\partial}{\partial \alpha_k}, \quad k = 1, 2, 3$. Next, let us utilize that infinitesimal rotations are generated [52] by the projection of the total angular momentum $\hat{\mathbf{J}}$ onto the rotational axis:

$$\mathbf{n}\hat{\mathbf{J}} = -i\frac{\partial}{\partial \phi}, \tag{56}$$

where $\mathbf{n}$ has unit length, its direction gives the rotational axis, and ϕ is an angle associated with the rotation.

According to Eq. (56), it is straightforward to identify the rotational $\hat{p}_{k+D}$ quasi-momenta as the components of the total angular momentum in the body-fixed frame. After specifying three unique rotational axes, three successive rotations can be performed in order to define the transformation between the space-fixed and body-fixed frames. As the α_k rotational coordinate describes a rotation around the kth of these three rotational axes, it is obvious that

$$\hat{p}_{k+D} = -i\frac{\partial}{\partial \alpha_k} = \hat{J}_k, \tag{57}$$

where $\hat{J}_k$ is the component of the total angular momentum vector along the kth rotational axis. The three rotational axes have been chosen to coincide with the three axes of the body-

fixed frame. Therefore, the $\hat{J}_k$ operators correspond to the angular momentum components expressed in the body-fixed frame, and the α_k rotational angles define three successive rotations around the three orthogonal axes of the body-fixed system. This work employs these infinitesimal rotational coordinates [58, 59] instead of the widely used Eulerian angles. This choice has two significant advantages: (a) one can directly insert the body-fixed components of the total angular momentum into the rovibrational Hamiltonian by utilizing Eq. (57), which greatly reduces the effort to construct $\hat{T}$; and (b) the rotational and rotational-vibrational blocks of $\mathbf{g}$ (and thus of $\mathbf{G}$) can be computed trivially, as according to Eqs. (51) and (54) one needs to evaluate the $\mathbf{e}_k \times \mathbf{x}_i$ cross products of the unit vectors pointing along the body-fixed axes and the body-fixed atomic position vectors, which clearly requires the choice of the embedding.

2.2.3 Reduced-dimensional computational models

If larger molecules are examined it is often a good approximation to introduce reduced dimensional models by constraining the motion along certain internal coordinates. Two possible choices of defining reduced-dimensional models [60] are (a) deleting rows and columns of the $\mathbf{g}$ matrix, (b) deleting rows and columns of the $\mathbf{G}$ matrix. The first case, when the ith row and ith column of $\mathbf{g}$ is deleted, corresponds to the $\dot{q}_i = 0$ constraint, while the second one, when the ith row and ith column of $\mathbf{G}$ is omitted, gives rise to the $p_i = 0$ relation. If orthogonal coordinates are applied, the two approaches lead to the same effective Hamiltonian. However, in general the two different strategies provide different reduced models and numerical results, see Ref. [32] for numerical examples. Reduced-dimensional results given in this thesis have been computed by using the first approach as its physical meaning seems to be clearer than that of the second one.

2.2.4 Brief summary of the vibration-only algorithm

If the vibration-only problem is solved, one can introduce the effective vibrational Hamiltonian as

$$\hat{H}^{\mathrm{v}} = \hat{T}^{\mathrm{v}} + \hat{V} = \frac{1}{2} \sum_{k=1}^{D} \sum_{l=1}^{D} \tilde{g}^{-1/4} \hat{p}_k^{\dagger} G_{kl} \tilde{g}^{1/2} \hat{p}_l \tilde{g}^{-1/4} + \hat{V} \tag{58}$$

for the D active vibrational degrees of freedom. The matrix representation of $\hat{H}^{\mathrm{v}}$, similarly to that of the EW Hamiltonian, is set up in the basis of D-dimensional DVR vibrational

basis functions:

$$\mathbf{H}^{\mathrm{v}} = \mathbf{T}^{\mathrm{v}} + \mathbf{V} = \frac{1}{2}\sum_{k=1}^{D}\sum_{l=1}^{D}\tilde{\mathbf{g}}^{-1/4}\mathbf{p}_k^{\dagger}\mathbf{G}_{kl}\tilde{\mathbf{g}}^{1/2}\mathbf{p}_l\tilde{\mathbf{g}}^{-1/4} + \mathbf{V}, \tag{59}$$

where five resolution of identities have been inserted amongst the operators present in $\hat{T}^{\mathrm{v}}$. It is important to note the two possible forms of $\hat{H}^{\mathrm{v}}$ outlined in Ref. [32]. As the rearranged vibrational Hamiltonian is numerically less stable than the so-called Podolsky form of $\hat{H}^{\mathrm{v}}$ given in Eqs. (58) and (59), the use of the Podolsky form is preferable over the rearranged form.

In the current implementation of GENIUSH, DVRs based on Hermite [51], Legendre [51], Laguerre [51], and sinc [61] functions are available. Besides the primitive DVR functions it is also possible to employ potential optimized (PO) DVR [49] functions. The basic idea behind PO-DVR is the optimization of the DVR grid points and basis functions by solving the eigenproblem of suitable one-dimensional model Hamiltonians. The main virtue of PO-DVR is its compactness as it is possible to maintain the same computational accuracy with less PO DVR functions than primitive DVR ones.

As a result of applying DVR vibrational basis functions, matrix representation of the coordinate-dependent operators $\tilde{g}^{-1/4}$, G_{kl}, $\tilde{g}^{1/2}$, and $\hat{V}$ are diagonal and the diagonal matrix elements are equal to the values of these operators at the DVR grid points (see Section 2.1.2 for further details). As a direct consequence, the $\mathbf{t}$-vectors (see Eq. (43) for their definition) needed for the construction of $\tilde{g}^{-1/4}$, G_{kl}, and $\tilde{g}^{1/2}$ are to be evaluated only at the grid points, which can be done either numerically or analytically for arbitrary internal coordinates and embeddings. This is the fact which makes the numerical representation of the kinetic energy operator possible; thus, no analytical kinetic energy operators are needed within the GENIUSH algorithm. Matrix elements of the vibrational $\hat{p}_k$ operators are proportional to matrix elements of the $\frac{\partial}{\partial q_k}$ differential operators and can be constructed according to the considerations of Ref. [32].

2.2.5 Solution of the rotational-vibrational problem

In order to compute rovibrational states variationally the matrix representation of the $\hat{H}$ rovibrational Hamiltonian is needed. It is advantageous to split $\hat{T}$ into three terms:

$$\hat{H} = \hat{T} + \hat{V} = \hat{T}^{\mathrm{v}} + \hat{T}^{\mathrm{r}} + \hat{T}^{\mathrm{rv}} + \hat{V}, \tag{60}$$

where

$$\hat{T}^{\mathrm{v}} = \frac{1}{2}\sum_{k=1}^{D}\sum_{l=1}^{D}\tilde{g}^{-1/4}\hat{p}_k^{\dagger}G_{kl}\tilde{g}^{1/2}\hat{p}_l\tilde{g}^{-1/4}, \tag{61}$$

$$\hat{T}^{\mathrm{r}} = \frac{1}{2}\sum_{k=1}^{3}G_{k+D,k+D}\,\hat{J}_k^2 + \frac{1}{2}\sum_{k=1}^{3}\sum_{l>k}^{3}G_{k+D,l+D}\,[\hat{J}_k,\hat{J}_l]_+, \tag{62}$$

and

$$\hat{T}^{\mathrm{rv}} = \frac{1}{2}\sum_{l=1}^{3}\sum_{k=1}^{D}\left(\tilde{g}^{-1/4}\hat{p}_k^{\dagger}G_{k,l+D}\,\tilde{g}^{1/4} + \tilde{g}^{1/4}G_{k,l+D}\,\hat{p}_k\tilde{g}^{-1/4}\right)\hat{J}_l, \tag{63}$$

where $\hat{T}^{\mathrm{v}}$ is the vibrational and $\hat{T}^{\mathrm{r}}$ is the rotational kinetic energy operator and $\hat{T}^{\mathrm{rv}}$ describes the coupling between vibrations and rotations. In Eq. (62), $\hat{J}_k$ is the kth body-fixed component of $\hat{\mathbf{J}}$ and $[\hat{J}_k,\hat{J}_l]_+$ refers to the anticommutator of the operators $\hat{J}_k$ and $\hat{J}_l$.

As the $\hat{J}_k$ angular momentum components correspond to the body-fixed frame, they satisfy the anomalous commutation relations [52]

$$[\hat{J}_k,\hat{J}_l] = -i\sum_m \epsilon_{klm}\hat{J}_m, \tag{64}$$

where $k,l,m = x,y,z$. For a given rotational angular momentum quantum number J (the molecular system is isolated and no external fields are present), the set of $2J+1$ orthonormal $|JKM\rangle$ symmetric rigid rotor eigenfunctions serves as a suitable basis to set up the matrix representation of $\hat{H}$. According to Eqs. (62) and (63), the matrix representation of $\hat{J}_k$, $\hat{J}_k^2$ and $[\hat{J}_k,\hat{J}_l]_+$ is required to solve the rovibrational problem. The complete set of nonzero $\hat{J}_k$ matrix elements is given [52] by

$$\begin{aligned}
\langle JKM|\hat{J}_x|J(K\pm 1)M\rangle &= \frac{1}{2}\sqrt{J(J+1)-K(K\pm 1)}\\
\langle JKM|\hat{J}_y|J(K\pm 1)M\rangle &= \mp\frac{i}{2}\sqrt{J(J+1)-K(K\pm 1)}\\
\langle JKM|\hat{J}_z|JKM\rangle &= K,
\end{aligned} \tag{65}$$

where $K=-J,\ldots,J$ corresponds to the body-fixed z, while $M=-J,\ldots,J$ to the space-fixed Z components of the angular momentum. Matrix representations of the $\hat{J}_k^2$ and $[\hat{J}_k,\hat{J}_l]_+$ operators can be constructed by simple matrix multiplication, by inserting the

resolution of identity between $\hat{J}_k$ and $\hat{J}_l$, and thus

$$\langle JKM|\hat{J}_k\hat{J}_l|JK'M\rangle = \sum_{K''=-J}^{J} \langle JKM|\hat{J}_k|JK''M\rangle\langle JK''M|\hat{J}_l|JK'M\rangle. \tag{66}$$

It is important to emphasize that Eq. (66) does not utilize any approximations as it has been shown in Eqs. (36) and (37).

As a next step, a more sophisticated rotational basis of $2J+1$ orthonormal Wang functions [52] is introduced by the following combinations,

$$\begin{aligned}
&\frac{1}{\sqrt{2}}\left(|JKM\rangle + |J-KM\rangle\right), \text{ where } K \text{ is even} \\
&\frac{1}{\sqrt{2}}\left(|JKM\rangle - |J-KM\rangle\right), \text{ where } K \text{ is odd} \\
&\frac{i}{\sqrt{2}}\left(|JKM\rangle - |J-KM\rangle\right), \text{ where } K \text{ is even} \\
&\frac{i}{\sqrt{2}}\left(|JKM\rangle + |J-KM\rangle\right), \text{ where } K \text{ is odd.}
\end{aligned} \tag{67}$$

This basis has two advantages over the simple $|JKM\rangle$ functions: (a) after some trivial algebra and a careful choice of the vibrational basis it becomes transparent that the matrix representation of $\hat{H}$, $\mathbf{H}$, lacks complex matrix elements; and (b) as shown in the previous four equations, one can separate the Wang functions into four (only three for $J=1$) sets according to the irreducible representations of the D_2 rotational group, which helps exploiting molecular symmetry during the rovibrational computations.

Construction of $\mathbf{H}$ requires the introduction of a rovibrational basis, chosen here as a direct product of the set of vibrational basis functions and the $2J+1$ Wang functions (details concerning the vibrational basis and the necessary matrix elements can be found in Ref. [32]). Using Eqs. (60), (61), (62), and (63), $\mathbf{H}$ takes the form

$$\mathbf{H} = \mathbf{T} + \mathbf{V} = \mathbf{T}^{\mathrm{v}} + \mathbf{T}^{\mathrm{r}} + \mathbf{T}^{\mathrm{rv}} + \mathbf{V}, \tag{68}$$

where

$$\mathbf{T}^{\mathrm{v}} = \frac{1}{2}\mathbf{E}_{2J+1} \otimes \sum_{k=1}^{D}\sum_{l=1}^{D} \tilde{\mathbf{g}}^{-1/4}\mathbf{p}_k^{\dagger}\mathbf{G}_{kl}\tilde{\mathbf{g}}^{1/2}\mathbf{p}_l\tilde{\mathbf{g}}^{-1/4} \tag{69}$$

$$\mathbf{T}^{\mathrm{r}} = \frac{1}{2}\sum_{k=1}^{3} \mathbf{J}_k^2 \otimes \mathbf{G}_{k+D,k+D} + \frac{1}{2}\sum_{k=1}^{3}\sum_{l>k}^{3} [\mathbf{J}_k, \mathbf{J}_l]_+ \otimes \mathbf{G}_{k+D,l+D} \tag{70}$$

and

$$\mathbf{T}^{\mathrm{rv}} = \frac{1}{2}\sum_{l=1}^{3} \mathbf{J}_l \otimes \sum_{k=1}^{D} \left(\tilde{\mathbf{g}}^{-1/4} \mathbf{p}_k^{\dagger} \mathbf{G}_{k,l+D}\, \tilde{\mathbf{g}}^{1/4} + \tilde{\mathbf{g}}^{1/4} \mathbf{G}_{k,l+D}\, \mathbf{p}_k \tilde{\mathbf{g}}^{-1/4} \right), \tag{71}$$

$\mathbf{E}_{2J+1}$ is the identity matrix of dimension $2J+1$, and $\otimes$ refers to the direct product operation.

2.3 Symmetry-adapted Lanczos method (SAL)

This section addresses the problem of assigning symmetry labels to computed rovibrational energy levels and wave functions. As DEWE and GENIUSH employs the iterative Lanczos eigensolver, it seemed to be a good choice to adopt the symmetry-adapted Lanczos method (SAL). During the SAL process Lanczos vectors are projected onto the different irreducible representations of the molecular symmetry (MS) group. This procedure results in rovibrational states belonging to the ith irreducible representation of the MS group if the Lanczos vectors are projected onto the ith irreducible representation.

After a brief review of the Lanczos algorithm and the general theory of the SAL method I describe my own SAL implementation which currently works for the DEWE code employing normal coordinates and Hermite-DVR vibrational basis functions. Though the current implementation applies to Abelian MS groups having ± 1 characters (for the $D_{2\mathrm{h}}(\mathrm{M})$ MS group and its subgroups), the last section only covers the special case of the $C_{2\mathrm{v}}(\mathrm{M})$ group.

2.3.1 Iterative Lanczos eigensolver

As the dimension of the rovibrational Hamiltonian equals $n(2J+1)$, where n is the number of vibrational basis functions, and n grows rapidly with the number of vibrational degrees of freedom, it is not feasible to employ explicit eigensolvers [62] for computing the eigenvalues and eigenvectors of the rovibrational Hamiltonian. The original DEWE and GENIUSH codes employ the iterative Lanczos method [44, 63] to solve the eigenproblem of the Hamiltonian, which needs the evaluation of matrix-vector products. As the rovibrational Hamiltonian has a very special and sparse structure, an effective matrix-vector product algorithm has been implemented, which does not need the Hamiltonian, of rapidly growing dimension, to be stored explicitly.

The shift-fold procedure of the family of polynomial spectral transformation techniques [64, 65] was employed during the Lanczos iterations to obtain the lowest eigenstates corresponding to the chosen Hamiltonian. Semi-orthogonality of the Lanczos vectors was maintained by using the periodic reorthogonalization algorithm [66], whereby every second Lanczos vector is reorthogonalized against all the previous ones. The more sophisticated partial reorthogonalization technique [67, 68] resulted in a similar frequency of reorthogonalization steps as the periodic reorthogonalization, and thus the simpler periodic version was employed [21]. The thick-restart Lanczos method [68, 69] was used to compact the ever-growing Krylov subspace periodically.

2.3.2 Theory of the SAL method

A possible way of exploiting molecular symmetry during variational rovibrational computations is to adopt the symmetry-adapted Lanczos (SAL) technique [70, 71, 72]. Within this procedure the Lanczos vectors are projected onto the required irreducible representation of the molecular symmetry (MS) group [73]. These projections, carried out during the course of the Lanczos iterations regularly, assure that the Lanczos algorithm will result in energy levels and wave functions of the given irreducible representation. This scheme does not decrease the size of the Hamiltonian matrix to be treated. Nevertheless, a considerable advantage of SAL is that the eigenvalues to be determined become considerably sparser resulting in a much improved convergence of the Lanczos procedure. Furthermore, symmetry labels are distributed automatically to the computed rovibrational energy levels and wave functions. The SAL method can be understood as follows.

Each $\hat{A}$ element of the MS group can be constructed as the product of a $\hat{B}$ point-group (PG) and a $\hat{C}$ rotational-group (RG) symmetry element [73]:

$$\hat{A} = \hat{B}\hat{C}. \tag{72}$$

These relations are explored when the projector [74] onto the ith irreducible representation is constructed by considering

$$\hat{P}_i = \frac{1}{h} \sum_{\hat{A} \in G} \chi_i(\hat{A}) \hat{A}, \tag{73}$$

where G is the molecular symmetry group, h is the order of G, and $\chi_i(\hat{A})$ is the character of the MS group element $\hat{A}$ associated with the ith irreducible representation. The effect of $\hat{P}_i$ on the original Lanczos vector $\mathbf{x}$ is

$$\mathbf{x}_i = \mathbf{P}_i \mathbf{x}, \tag{74}$$

where $\mathbf{x}_i$ is the projected Lanczos vector, and $\mathbf{P}_i$ is the matrix representation of the $\hat{P}_i$ projector in the rovibrational basis. Elements of the $\mathbf{P}_i$ matrix can be expressed as

$$(\mathbf{P}_i)_{ab,cd} = \langle F_a R_b | \hat{P}_i | F_c R_d \rangle = \frac{1}{h} \sum_{\hat{A} \in G} \chi_i(\hat{A}) \langle F_a R_b | \hat{A} | F_c R_d \rangle \tag{75}$$

with

$$\langle F_a R_b|\hat{A}|F_c R_d\rangle = \langle F_a|\hat{B}|F_c\rangle\langle R_b|\hat{C}|R_d\rangle \tag{76}$$

in the direct product basis of the F_a vibrational and R_b rotational basis functions. Eq. (76) utilizes the fact that $\hat{B}$ and $\hat{C}$ act only on the vibrational and rotational coordinates, respectively.

According to Eq. (76) the matrix representation of the $\hat{A} = \hat{B}\hat{C}$ molecular symmetry group element is given by the direct product of the matrix representations of $\hat{C}$ and $\hat{B}$. Once the matrix representations of the MS group symmetry elements are available, one can construct the matrix of the $\hat{P}_i$ projectors by taking appropriate linear combinations of the matrix representations of the $\hat{A}$ operators, see Eq. (75).

2.3.3 Considerations for the C_{2v}(M) molecular symmetry group within DEWE

The implementation of the SAL method for Abelian groups having $+1$ and -1 characters is summarized below for the special case of the C_{2v}(M) MS group. The point group and the rotational group needed by the considerations of the present section are C_{2v} and D_2, respectively. Table I gives the character tables of the isomorphic C_{2v}(M), C_{2v}, and D_2 groups.

If the C_{2v} equilibrium structure of the molecule examined is placed into the yz plane and z coincides with the C_2 axis, the following equations relate the C_{2v}(M) symmetry elements to the C_{2v} point-group and D_2 rotation-group elements:

$$\begin{aligned} E(M) &= E(P)E(R) \\ (12) &= C_2(z)R_z \\ E^* &= \sigma_v(yz)R_x \\ (12)^* &= \sigma_v(xz)R_y. \end{aligned} \tag{77}$$

In Eq. (77) the following notations are applied: E = identity, (12) = permutation of the two identical nuclei, E^* = inversion of the nuclear coordinates, $(12)^* = (12)E^*$, $C_2(z)$ = two-fold rotation about the z axis, R_α = two-fold rotation around the α coordinate axis with $\alpha = x, y, z$.

As the current implementation applies only to Abelian groups, having characters $+1$

Table I. Character tables of the isomorphic groups $C_{2v}(M)$ (molecular symmetry group), C_{2v} (point group), and D_2 (rotational group).

$C_{2v}(M)$ / C_{2v} / D_2	$E(M)$ / $E(P)$ / $E(R)$	(12) / $C_2(z)$ / R_z	E^* / $\sigma_v(yz)$ / R_x	$(12)^*$ / $\sigma_v(xz)$ / R_y
A_1 / A_1 / A	1	1	1	1
A_2 / A_2 / B_z	1	1	-1	-1
B_1 / B_1 / B_y	1	-1	-1	1
B_2 / B_2 / B_x	1	-1	1	-1

and -1, the effect of a $\hat{B}$ point-group symmetry element on the Q_i normal coordinate is

$$\hat{B}Q_i = \chi_j(\hat{B})Q_i = \pm Q_i, \tag{78}$$

where Q_i forms the basis of the jth irreducible representation and the $\chi_j(\hat{B})$ character refers to the jth irreducible representation. According to Eq. (78), one can deduce the effect of $\hat{B}$ on the $f_n(Q_i)$ one-dimensional Hermite-DVR vibrational basis functions as

$$\hat{B}f_n(Q_i) = f_n(\hat{B}^{-1}Q_i) = f_n(Q_i), \text{ if } \hat{B}Q_i = Q_i, \text{ or} \tag{79}$$

$$\hat{B}f_n(Q_i) = f_n(\hat{B}^{-1}Q_i) = f_n(-Q_i) = f_{-n}(Q_i), \text{ if } \hat{B}Q_i = -Q_i,$$

where the $f_n(Q_i)$ one-dimensional functions were given the $n = -p, \ldots, -1, 1, \ldots, p$ or $n = -p, \ldots, 0, \ldots, p$ indices for $2p$ even and $2p+1$ odd numbers of basis functions, respectively; thus, the $f_n(Q_i)$ basis functions are enumerated according to the ascending order of the Hermite-DVR grid points. Eq. (79) holds due to the fact that the set of Hermite-DVR grid points is symmetric with respect to the origin and the q_i grid points are transformed to their mirror image q_{-i} by $\hat{B}$ if $\hat{B}Q_i = -Q_i$. In light of these equations the following relations hold:

$$\langle f_m(Q_i)|\hat{B}f_n(Q_i)\rangle = \langle f_m(Q_i)|f_n(Q_i)\rangle = \delta_{mn}, \text{ if } \hat{B}Q_i = Q_i, \text{ or} \tag{80}$$

$$\langle f_m(Q_i)|\hat{B}f_n(Q_i)\rangle = \langle f_m(Q_i)|f_{-n}(Q_i)\rangle = \delta_{m,-n}, \text{ if } \hat{B}Q_i = -Q_i.$$

According to Eq. (80), the matrix representation of $\hat{B}$ in the basis of Hermite-DVR functions is either an identity or an anti-diagonal matrix. Since the vibrational basis is constructed as the direct product of one-dimensional Hermite-DVR functions, the matrix representation of $\hat{B}$ is the direct product of the related matrices. This operation results in the

matrix representation of $\hat{B}$, which is a permutation matrix, and has the dimension of the direct-product vibrational basis.

For the construction of the matrix representation of a $\hat{C}$ rotational-group (D_2) symmetry element it is important to know the symmetry properties of the Wang functions defined by Eq. (67). The Wang functions are basis functions of the irreducible representations of the Abelian D_2 rotational group [73]. Thus, the matrix representation of $\hat{C}$ is diagonal and has $+1$ or -1 in its main diagonal:

$$\langle W_m(\Omega)|\hat{C}W_n(\Omega)\rangle = \chi_n(\hat{C})\delta_{mn}, \tag{81}$$

where $W_n(\Omega)$ refers to the $2J+1$ Wang functions for a given J, Ω stands for the three rotational coordinates, and $\chi_n(\hat{C})$ is the character of $\hat{C}$ in the irreducible representation spanned by $W_n(\Omega)$.

It is important to note that the method described in this section generally applies to Abelian groups having ± 1 characters ($D_{2\mathrm{h}}$(M) MS group and its subgroups). For MS groups with ± 1 characters other than $C_{2\mathrm{v}}$(M) the relations of Eq. (77) have to be derived. As the $\hat{P}_i$ projectors are represented by permutation matrices, an effective matrix-vector multiplication subroutine can be developed for evaluating the necessary $\mathbf{x}_i = \mathbf{P}_i\mathbf{x}$ products without having to construct and store the $\mathbf{P}_i$ matrix explicitly.

2.4 Eckart embedding

In this section the theory of maintaing the rotational Eckart condition in a variational rovibrational computation is discussed. As the DEWE code employs the Eckart–Watson Hamiltonian, the rotational Eckart condition holds automatically in this case. However, when GENIUSH is used, an additional procedure is needed to compute rovibrational energy levels and wave functions with Eckart-embedded kinetic energy operators. After a brief summary of the theory of the rotational Eckart condition, I describe my implementation of the Eckart embedding within the GENIUSH algorithm.

2.4.1 Summary of the Eckart conditions and Eckart related applications

Choosing the frame which minimizes the coupling between the vibrations and rotations of polyatomic molecules is an important topic in nuclear motion theory. It was Eckart [41] who first formulated correctly the equations leading to an optimal separation of the two motions (yielding zero coupling at a reference structure).

The translational Eckart condition (see also Eq. (2)) is

$$\sum_{k=1}^{N} m_k \mathbf{r}_k = \mathbf{0}, \tag{82}$$

where m_k and $\mathbf{r}_k$ stand for the masses and position vectors of the N nuclei under examination, and it is trivial to satisfy it for arbitrary values of N. However, the rotational Eckart condition (see also Eq. (4)),

$$\sum_{k=1}^{N} m_k (\mathbf{r}_k \times \mathbf{a}_k) = \mathbf{0}, \tag{83}$$

where $\mathbf{a}_k$ gives the position of the kth particle in the reference configuration chosen, results in a set of more complex equations. Fulfillment of the rotational Eckart condition, Eq. (83), can be interpreted as finding a $\mathbf{T}$ pseudorotation matrix which transforms the $\mathbf{r}_k$ initial coordinates into the $\mathbf{r}'_k = \mathbf{T}\mathbf{r}_k$ coordinates corresponding to the Eckart frame.

How to construct such a transformation was proposed by Eckart in his groundbreaking paper from 1935 [41]. Later, Pickett and Strauss [75] derived a procedure for finding the $\mathbf{T}$ transformation matrix. An important shortcoming of the methods proposed is the need for computing the inverse of an intermediate matrix which can be singular for some initial geometries. A new method, free of previous limitations, has recently been published by

Dymarsky and Kudin [76].

As the Eckart frame minimizes the rotational-vibrational coupling, several authors attempted to derive Eckart-embedded Hamiltonians for use in computational molecular spectroscopy. For rectilinear vibrational coordinates (including normal coordinates), the form of the operator is well established [18, 19], and the Eckart–Watson operator has been successfully applied for N-atomic molecules. However, this operator is only suitable for semirigid molecules. For curvilinear internal coordinates, analytic Eckart formulae and Eckart-embedded kinetic energy operators have been derived for triatomic [77, 78, 79, 80] as well as more general planar molecules [81]. These Hamiltonians are well suited to treat molecules exhibiting arbitrary motions. Nevertheless, drawbacks of Eckart-embedded Hamiltonians expressed in internal coordinates are as follows: (a) the resulting expressions are rather complex, which makes their implementation less desirable, and (b) analytical Eckart expressions are derived only for special cases.

Thus, it is left as a challenge to construct a general Eckart-embedded kinetic energy operator (KEO) expressed in arbitrary curvilinear coordinates. One way forward is to construct the KEO numerically, for which the GENIUSH algorithm [32, 33] provides the starting point. As in GENIUSH the kinetic energy operator is constructed numerically and represented on a DVR grid, it is sufficient to transform the nuclear geometries corresponding to each different grid point into the Eckart frame.

This new approach exhibits the following significant advantages: (a) it applies to arbitrary internal coordinates and molecular compositions, and (b) no complicated analytical derivations are required.

2.4.2 Theory of maintaining the rotational Eckart condition

The initial step in the method derived by Dymarsky and Kudin [76] is the definition of a matrix $\mathbf{A}$,

$$A_{ij} = \sum_{k=1}^{N} m_k (\mathbf{r}_k)_i (\mathbf{a}_k)_j, \qquad i,j = 1,2,3 \tag{84}$$

computed with the $\mathbf{r}_k$ initial and $\mathbf{a}_k$ reference position vectors, where i and j denote Cartesian indices. If a $\mathbf{T}$ pseudorotation matrix ($\mathbf{T}^{\mathrm{T}} = \mathbf{T}^{-1}$) acts on the initial coordinates $\mathbf{r}_k$ and transforms them into the $\mathbf{r}'_k = \mathbf{T}\mathbf{r}_k$ Eckart coordinates, we can compute the elements

of the symmetric $\mathbf{S}$ matrix,

$$S_{ij} = \sum_{k=1}^{N} m_k (\mathbf{r}'_k)_i (\mathbf{a}_k)_j = (\mathbf{TA})_{ij}. \tag{85}$$

The symmetric nature of $\mathbf{S}$ is assured by the rotational Eckart condition, Eq. (83).

The next step is the introduction of the $\mathbf{A}_1 = \mathbf{A}^{\mathrm{T}}\mathbf{A}$ and $\mathbf{A}_2 = \mathbf{A}\mathbf{A}^{\mathrm{T}}$ symmetric matrices, and the solution of the

$$\mathbf{A}_1 \mathbf{u}_i = \lambda_i \mathbf{u}_i, \tag{86}$$

$$\mathbf{A}_2 \mathbf{v}_i = \lambda_i \mathbf{v}_i$$

eigenproblems for $i = 1, 2, 3$. One can easily prove that the eigenvalue sets of $\mathbf{A}_1$ and $\mathbf{A}_2$ coincide. After considering the

$$\mathbf{S}^2 = \mathbf{S}^{\mathrm{T}}\mathbf{S} = \mathbf{A}^{\mathrm{T}}\mathbf{T}^{\mathrm{T}}\mathbf{TA} = \mathbf{A}_1 \tag{87}$$

and

$$\mathbf{S}^2 = \mathbf{S}\mathbf{S}^{\mathrm{T}} = \mathbf{TA}\mathbf{A}^{\mathrm{T}}\mathbf{T}^{\mathrm{T}} = \mathbf{T}\mathbf{A}_2\mathbf{T}^{\mathrm{T}} \tag{88}$$

relations, we get

$$\mathbf{A}_1\mathbf{T} = \mathbf{T}\mathbf{A}_2, \tag{89}$$

so the $\mathbf{T}$ transformation matrix can be constructed according to the

$$\mathbf{T} = \sum_{i=1}^{3} \mathbf{u}_i \circ \mathbf{v}_i \tag{90}$$

formula, where $\mathbf{u}_i$ and $\mathbf{v}_i$ share the same λ_i eigenvalues for $i = 1, 2, 3$. There are eight possible $\mathbf{T}$ transformations differing in the relative signs of the $\mathbf{u}_i$ and $\mathbf{v}_i$ eigenvectors. Dymarsky and Kudin [76] suggested the use of the

$$\mathbf{u}_i \cdot \mathbf{v}_i \geq 0, \tag{91}$$

with $i = 1, 2, 3$, and

$$\mathbf{u}_3 = \mathbf{u}_1 \times \mathbf{u}_2 \tag{92}$$

$$\mathbf{v}_3 = \mathbf{v}_1 \times \mathbf{v}_2$$

conditions to find the $\mathbf{T}$ transformation matrix which is closest to the identity matrix and represents a pure rotation (det$\mathbf{T} = 1$).

The kinetic energy operator expressed in internal coordinates needs the

$$g_{ij} = \sum_{k=1}^{N} m_k \frac{\partial \mathbf{r}_k}{\partial q_i} \frac{\partial \mathbf{r}_k}{\partial q_j} \tag{93}$$

matrix elements of the well-known $\mathbf{g}$ matrix [54] expressed in terms of the $3N-3$ q_i generalized ($3N-6$ vibrational and 3 rotational) coordinates. Within the framework of GENIUSH, the $\mathbf{g}$ matrix is evaluated by the numerical computation of the so-called $\mathbf{t}$-vectors, $\frac{\partial \mathbf{r}_k}{\partial q_i}$, by the method of finite differences. This needs the generation of the $\mathbf{r}_k$ body-fixed Cartesian coordinates for a given set of the q_i generalized coordinates which is done by the following algorithm: (a) Cartesian coordinate computation with respect to an arbitrary inital embedding, and (b) rotation of the initial Cartesian coordinates into the Eckart frame by the previously described method and maintaining the criteria given by Eqs. (91) and (92).

2.5 Labelling of rovibrational states

Labelling the computed rovibrational energy levels and wave functions with zeroth-order harmonic oscillator and rigid rotor quantum numbers is of great importance as these labels are widely used in the field of experimental spectroscopy. This task can be solved by the normal mode decomposition (NMD) and rigid-rotor decomposition (RRD) procedures [42]. After the concise summary of the NMD procedure I discuss the implementation of the RRD algorithm I used extensively for the interpretation of computed rovibrational states.

2.5.1 Normal mode decomposition (NMD)

The NMD algorithm [42] was developed to facilitate the assignment of zeroth-order harmonic oscillator (HO) quantum numbers to computed variational (ro)vibrational eigenstates. In the case of the NMD, overlaps between the Φ_j variational vibrational and the Φ_i^{HO} harmonic oscillator basis functions are computed. An NMD coefficient is defined as

$$c_{ji} = |\langle \Phi_i^{\mathrm{HO}} | \Phi_j \rangle|^2. \tag{94}$$

Labelling of the Φ_j variational vibrational wave functions with approximate HO quantum numbers can be accomplished by finding the dominant NMD coefficient given by Eq. (94). After finding the dominant c_{ji} contribution (if possible) in Φ_j it is straightforward to assign Φ_j with the HO labels of Φ_i^{HO} .

2.5.2 Rigid rotor decomposition (RRD)

The RRD algorithm [42] was developed to assign zeroth-order rigid rotor (RR) quantum numbers to computed variational rovibrational eigenstates.

Let us consider the n_Jth rovibrational wave function $\Psi_{n_J}^J(\mathbf{Q}, \phi, \theta, \chi)$ (for a given value of the J rotational quantum number) expressed in terms of the $\mathbf{Q}$ vibrational and (ϕ, θ, χ) rotational coordinates as a linear combination of rotational-vibrational basis functions:

$$\Psi_{n_J}^J(\mathbf{Q}, \phi, \theta, \chi) = \sum_{i=1}^{n} \sum_{k=1}^{2J+1} c_{n_J,ik}^J F_i(\mathbf{Q}) R_k^J(\phi, \theta, \chi), \tag{95}$$

where

$$F_i(\mathbf{Q}) = \prod_{k=1}^{3N-6} f_{i_k}(Q_k), \quad i_k = 1, 2 \ldots, n_k, \tag{96}$$

and n_k stands for the number of vibrational basis functions on the kth vibrational coordinate, $n = n_1 n_2 \cdot \ldots \cdot n_{3N-6}$ is the total size of the vibrational basis, and $R_k^J(\phi, \theta, \chi)$ stands for the Wang-transformed symmetric top basis functions defined by Eq. (38). In the present subsection orthonormal vibrational basis functions and real linear combination coefficients are assumed.

For the eigenstates of the field-free rovibrational Hamiltonian the J rotational quantum number is exact and serves as one of the input parameters of the rovibrational computations, while the widely used K_a and K_c labels are approximate and correspond to $|K|$ for the prolate and oblate symmetric-top limits of the rigid rotor [52], respectively. In the present subsection a two-step algorithm based on overlap integrals is proposed to match the computed rovibrational states with pure vibrational states and then generate the K_a and K_c labels.

By rearranging Eq. (95), one obtains

$$\Psi_{n_J}^J(\mathbf{Q}, \phi, \theta, \chi) = \sum_{k=1}^{2J+1} R_k^J(\phi, \theta, \chi) \left(\sum_{i=1}^{n} c_{n_J,ik}^J F_i(\mathbf{Q}) \right) = \sum_{k=1}^{2J+1} R_k^J(\phi, \theta, \chi) \psi_{n_J k}^J(\mathbf{Q}). \quad (97)$$

From now on, $\psi_{n_J k}^J(\mathbf{Q})$ will be referred to as the kth vibrational part of $\Psi_{n_J}^J(\mathbf{Q}, \phi, \theta, \chi)$. Because the eigenfunctions of the rotational-vibrational Hamiltonian are orthonormal, the overlap of a vibration-only wave function,

$$\Phi_m(\mathbf{Q}) = \sum_{j=1}^{n} C_{m,j} F_j(\mathbf{Q}), \quad (98)$$

and a rovibrational wave function, $\Psi_{n_J}^J(\mathbf{Q}, \phi, \theta, \chi)$ $(J > 0)$, is always zero, and thus not useful for making assignments. A way to circumvent this problem is to introduce the overlap of the kth vibrational part of $\Psi_{n_J}^J(\mathbf{Q}, \phi, \theta, \chi)$ and the vibration-only $\Phi_m(\mathbf{Q})$ as

$$\mathcal{S}_{n_J k,m}^J = \langle \psi_{n_J k}^J(\mathbf{Q}) | \Phi_m(\mathbf{Q}) \rangle_\mathbf{Q} = \sum_{i=1}^{n} \sum_{j=1}^{n} c_{n_J,ik}^J C_{m,j} \langle F_i(\mathbf{Q}) | F_j(\mathbf{Q}) \rangle_\mathbf{Q} = \sum_{i=1}^{n} c_{n_J,ik}^J C_{m,i} \ , \quad (99)$$

where the integration is carried out over the $3N-6$ vibrational coordinates. $\mathcal{S}_{n_J k,m}^J$ provides a measure of the similarity of $\psi_{n_J k}^J(\mathbf{Q})$ and $\Phi_m(\mathbf{Q})$: the larger the magnitude of $\mathcal{S}_{n_J k,m}^J$ the more similar the vibrational parts of the two functions are. The next step is to sum the

absolute squares of the $\mathcal{S}^J_{n_Jk,m}$ quantities with respect to k:

$$P^J_{n_J,m} = \sum_{k=1}^{2J+1} \left|\mathcal{S}^J_{n_Jk,m}\right|^2 = \sum_{k=1}^{2J+1} \left| \sum_{i=1}^{n} c^J_{n_J,ik} C_{m,i} \right|^2 . \tag{100}$$

After converging M $J = 0$ and N_J $J \neq 0$ eigenstates by variational procedures, $N_J M$ square-overlap sums are computed over all of the $J = 0$ and $J \neq 0$ pairs. The quantities $P^J_{n_J,m}$ ($n_J = 1, 2, \ldots, N_J$ and $m = 1, 2, \ldots, M$) can be regarded as elements of a rectangular matrix with N_J rows and M columns. For a given J, those $2J + 1$ $\Psi^J_{n_J}(\mathbf{Q}, \phi, \theta, \chi)$ rovibrational states belong to a selected $\Phi_m(\mathbf{Q})$ pure vibrational state which give the $2J+1$ largest $P^J_{n_J,m}$ values. This means of identification is valuable because the rovibrational levels belonging to a given vibrational state appear neither consecutively nor in a predictable manner in the overall eigenspectrum.

It is important to emphasize the pronounced dependence of the quantities $P^J_{n_J,m}$ on the embedding of the body-fixed frame, as exhibited in the previous equations. The Eckart frame [41] is expected to be a trenchant choice for the overlap calculations due to a minimalized rovibrational coupling. Of course, this rotational labelling scheme can be generally applied to variational rovibrational approaches employing arbitrary internal coordinates and embeddings.

After assigning $2J + 1$ rovibrational levels to a pure vibrational state, the next step is to generate the K_a and K_c or $\tau = K_\mathrm{a} - K_\mathrm{c}$ labels. Such assignments could be naively based on the canonical energy stacking of asymmetric-top $J_{K_\mathrm{a}K_\mathrm{c}}$ states, derived from the symmetric-top limits, the symmetry labels of the states, and the noncrossing rule [52]. A rigorous approach is to set up what we call rigid-rotor decomposition (RRD) tables. The two approaches do not necessarily give the same labels. In order to compute the RRD coefficients it is necessary to evaluate the overlap integral

$$S^J_{n_J,m,m_J} = \langle \Psi^J_{n_J}(\mathbf{Q}, \phi, \theta, \chi) | \Phi_m(\mathbf{Q}) \varphi^J_{m_J}(\phi, \theta, \chi) \rangle_{\mathbf{Q},\phi,\theta,\chi} =$$

$$= \sum_{i=1}^{n} \sum_{k=1}^{2J+1} c^J_{n_J,ik} \sum_{j=1}^{n} \sum_{l=1}^{2J+1} C_{m,j} \cdot d^J_{m_J,l} \cdot \langle F_i(\mathbf{Q}) | F_j(\mathbf{Q}) \rangle_{\mathbf{Q}} \cdot \langle R^J_k(\phi, \theta, \chi) | R^J_l(\phi, \theta, \chi) \rangle_{\phi,\theta,\chi} = \tag{101}$$

$$= \sum_{i=1}^{n} \sum_{k=1}^{2J+1} c^J_{n_J,ik} \cdot C_{m,i} \cdot d^J_{m_J,k}$$

between the n_Jth rovibrational state and the product of the mth vibrational state and m_Jth rigid-rotor eigenfunction. The rigid-rotor component of the product is given by a linear combination of the Wang functions $R_k^J(\phi,\theta,\chi)$ with expansion coefficients $d_{m_J,k}^J$:

$$\varphi_{m_J}^J(\phi,\theta,\chi) = \sum_{k=1}^{2J+1} d_{m_J,k}^J R_k^J(\phi,\theta,\chi), \tag{102}$$

where the $d_{m_J,k}^J$ coefficients are the components of the eigenvectors of the rigid-rotor Hamiltonian matrix. Note that the notation employed does not restrict the summation by symmetry; thus, certain blocks of the $d_{m_J,k}^J$ coefficients will necessarily be zero. Recognizing that these coefficients are elements of a unitary matrix, the quantities in Eqs. (100) and (101) are connected by the condition

$$P_{n_J,m}^J = \sum_{m_J=1}^{2J+1} |S_{n_J,m,m_J}^J|^2. \tag{103}$$

Because the $\Phi_m(\mathbf{Q})\varphi_{m_J}^J(\phi,\theta,\chi)$ functions form an orthonormal basis of dimension $n(2J+1)$, it is also obvious that

$$\sum_{m=1}^{n} P_{n_J,m}^J = 1. \tag{104}$$

In light of these relationships, we define the RRD coefficients as the absolute square of the overlaps, $|S_{n_J,m,m_J}^J|^2$, and arrange them in a rectangular table whose rows are the exact states under consideration, $\Psi_{n_J}^J(\mathbf{Q},\phi,\theta,\chi)$, and whose columns are the above-defined "basis" states, $\Phi_m(\mathbf{Q})\varphi_{m_J}^J(\phi,\theta,\chi)$. During the labelling process of the $\Psi_{n_J}^J(\mathbf{Q},\phi,\theta,\chi)$ functions the "basis" state giving the largest RRD coefficient is selected first. Thereafter, $\Psi_{n_J}^J(\mathbf{Q},\phi,\theta,\chi)$ is assigned with the zeroth-order quantum numbers of the dominant "basis" state.

2.6 The vibrational subspace (VS) method

In this section an efficient algorithm for the computation of highly-excited rovibrational states is introduced. After describing the general theory of the VS procedure I discuss my practical VS implementations within the DEWE and GENIUSH programs. Toward the end of the theoretical section relations between the VS and RRD algorithms and generation of symmetry labels are described.

2.6.1 General description

Determination of the large number of rovibrational energy levels and wave functions associated with large J values is computationally extremely demanding when traditional procedures, described in Sec. 2.1, are used. Here a technique employing a vibrational subspace (VS) is presented which can be used for the determination of a large number of rovibrational states and is almost cost free.

The rotational-vibrational Hamiltonian can be partitioned as

$$\hat{H} = \hat{T}^{\mathrm{v}} + \hat{T}^{\mathrm{r}} + \hat{T}^{\mathrm{rv}} + \hat{V} = \hat{H}^{\mathrm{v}} + \hat{T}^{\mathrm{r}} + \hat{T}^{\mathrm{rv}}, \tag{105}$$

where $\hat{T}^{\mathrm{v}}$, $\hat{T}^{\mathrm{r}}$ and $\hat{T}^{\mathrm{rv}}$ denote the vibrational, rotational and rotational-vibrational coupling terms of the kinetic energy operator, respectively, and

$$\hat{H}^{\mathrm{v}} = \hat{T}^{\mathrm{v}} + \hat{V} \tag{106}$$

is the vibration-only Hamiltonian. It is important to note that Eqs. (105) and (106) hold generally irrespective of the applied vibrational coordinates and embeddings and the form of the Hamiltonian. After solving the

$$\hat{H}^{\mathrm{v}}\Phi_i = E_i\Phi_i \tag{107}$$

vibrational Schrödinger equation and obtaining the Φ_i vibrational wave functions and the corresponding E_i vibrational energy levels, a subset of the Φ_i functions can be employed as a compact vibrational basis for the rotational-vibrational computations. In order to construct a new and compact rovibrational basis, consider the direct product of the Φ_i

vibrational states and some R_k rotational basis functions for a given J:

$$\{\Phi_i R_k\}, \text{ where } i = 1, \ldots, n \text{ and } k = 1, \ldots, 2J+1, \tag{108}$$

in which the Ψ_α rovibrational wave functions are expanded as

$$\Psi_\alpha = \sum_{i=1}^{n} \sum_{k=1}^{2J+1} c_{ik}^{\alpha} \Phi_i R_k. \tag{109}$$

The matrix representation of $\hat{H}^{\mathrm{v}}$ is diagonal,

$$\langle \Phi_i R_j | \hat{H}^{\mathrm{v}} | \Phi_k R_l \rangle = E_i \delta_{ik} \delta_{jl}. \tag{110}$$

While the latter equation holds irrespective of the actual form of the Hamiltonian applied, other necessary vibrational matrix elements can only be derived after specifying the rovibrational Hamiltonian. Formulae for the Eckart–Watson Hamiltonian of Eq. (10) (DEWE) and for the general Hamiltonian of Eq. (60) (GENIUSH) are given in Sections 2.6.2 and 2.6.3, respectively.

There are several choices for defining the $2J+1$ rotational basis functions for a given J: (a) simple $|JKM\rangle$ symmetric top eigenfunctions, (b) Wang functions (see Eq. (38) for their definition), and (c) rigid-rotor eigenfunctions. The third option was preferred during the VS studies, namely the $2J+1$ rigid-rotor eigenfunctions computed with equilibrium rotational constants were utilized as a rotational basis, as this choice gives rise to straightforward computation of the RRD coefficients.

The first step is to set up the $\mathbf{H}_{\mathrm{RR}}$ matrix representation in the basis of the W_i Wang functions of the

$$\hat{H}_{\mathrm{RR}} = A\hat{J}_x^2 + B\hat{J}_y^2 + C\hat{J}_z^2 \tag{111}$$

rigid-rotor Hamiltonian with A, B, C being the rotational constants of the molecule. After finding the $\mathbf{d}_i$ eigenvectors of $\mathbf{H}_{\mathrm{RR}}$, the R_i rotational basis functions take the form

$$R_i = \sum_{k=1}^{2J+1} d_{ik} W_k. \tag{112}$$

The $\langle R_i|\hat{J}_\alpha|R_j\rangle$ and $\langle R_i|J_\alpha\hat{J}_\beta|R_j\rangle$ matrix elements are

$$\langle R_i|\hat{J}_\alpha|R_j\rangle = \sum_{k=1}^{2J+1}\sum_{l=1}^{2J+1} d_{ik}d_{jl}\langle W_k|\hat{J}_\alpha|W_l\rangle, \tag{113}$$

and

$$\langle R_i|\hat{J}_\alpha\hat{J}_\beta|R_j\rangle = \sum_{k=1}^{2J+1}\sum_{l=1}^{2J+1} d_{ik}d_{jl}\langle W_k|\hat{J}_\alpha\hat{J}_\beta|W_l\rangle \tag{114}$$

in terms of the Wang basis matrix elements.

This new contraction-like technique, denoted as VS, exhibits the following significant advantages over previous approaches: (a) the vibrational subspace is very compact (it consists of typically the first few hundred vibrational eigenstates of the molecule), which results in a Hamiltonian of modest size even for high J values; (b) the RRD analysis, which facilitates the labeling of the variationally computed rovibrational states, is especially simple, as the RRD coefficients are equal to the absolute squares of the components of the eigenvectors of the rotational-vibrational Hamiltonian; (c) the vibrational basis functions are automatically symmetry adapted (as they are basis functions of the irreducible representations of the point group), which facilitates the exploitation of molecular symmetry during the computation; (d) once the necessary vibrational matrix elements for the construction of the representation of $\hat{T}^{\mathrm{r}}$ and $\hat{T}^{\mathrm{rv}}$ have been computed, they can be saved for later use, which greatly reduces the cost of further computations; and (e) due to the modest size of the final Hamiltonian one can use direct eigensolvers instead of the iterative Lanczos algorithm; thus, the spectral density of the rovibrational energy levels does not affect the convergence speed of the diagonalization (for larger matrices one can, of course, return to Lanczos techniques). For this study a parallel eigensolver of the Math Kernel Library [82] was chosen.

2.6.2 DEWE-VS matrix elements

According to Eq. (40), the $\mu_{\alpha\beta}$ and $\mu_{\alpha\beta}\hat{\pi}_\beta$ operators ($\alpha,\beta = x,y,z$) appear in the $\hat{T}^{\mathrm{r}}$ and $\hat{T}^{\mathrm{rv}}$ operators of the Eckart–Watson Hamiltonian. The forthcoming equations are based on the following facts: (a) in DVR, matrix representations of operators depending only on the internal coordinates are diagonal, (b) diagonal matrix elements of the coordinate dependent operators are given by evaluating them at the DVR grid points, (c) components of the variational vibrational eigenvectors are real.

Elements of the $\mu_{\alpha\beta}$ matrix in the basis of the Φ_i variational vibrational wave functions are given by

$$\langle\Phi_i|\mu_{\alpha\beta}|\Phi_j\rangle = \sum_{k=1}^{n}\sum_{l=1}^{n} c_k^i c_l^j \langle F_k|\mu_{\alpha\beta}|F_l\rangle = \sum_{k=1}^{n} c_k^i c_k^j \mu_{\alpha\beta}(\mathbf{q}_k), \tag{115}$$

where the $3N-6$-dimensional F_k DVR basis functions defined by Eq. (26) have been applied and $\mathbf{q}_k$ is the direct product grid point associated with F_k. The $\mu_{\alpha\beta}\hat{\pi}_\beta$ matrix elements can be derived by inserting the approximate resolution of identity amongst the $\mu_{\alpha\beta}$ and $\hat{\pi}_\beta$ operators:

$$\langle\Phi_i|\mu_{\alpha\beta}\hat{\pi}_\beta|\Phi_j\rangle = \sum_{k=1}^{n}\sum_{l=1}^{n}\sum_{m=1}^{n} c_k^i c_l^j \langle F_k|\mu_{\alpha\beta}|F_m\rangle\langle F_m|\hat{\pi}_\beta|F_l\rangle = \tag{116}$$

$$= \sum_{k=1}^{n}\sum_{l=1}^{n} c_k^i c_l^j \mu_{\alpha\beta}(\mathbf{q}_k)\langle F_k|\hat{\pi}_\beta|F_l\rangle,$$

Further explanation of the $\langle F_k|\mu_{\alpha\beta}|F_l\rangle$ and $\langle F_m|\hat{\pi}_\beta|F_l\rangle$ matrix elements has been outlined in Section 2.1.2.

2.6.3 GENIUSH-VS matrix elements

In view of Eqs. (70) and (71), one has to consider the matrix representations of the $G_{k+D,l+D}$ rotational (D is the number of the active vibrational degrees of freedom, $k,l=1,2,3$), and $\tilde{g}^{-1/4}\hat{p}_k^\dagger G_{k,l+D}\,\tilde{g}^{1/4}$ and $\tilde{g}^{1/4}G_{k,l+D}\,\hat{p}_k\tilde{g}^{-1/4}$ rovibrational coupling operators ($k=1,\ldots,D$ and $l=1,2,3$) in the basis spanned by the Φ_i variational vibrational wave functions. The forthcoming equations are based on features described at the beginning of Section 2.6.2.

The rotational $G_{k+D,l+D}$ matrix elements are expressed as

$$\langle\Phi_i|G_{k+D,l+D}|\Phi_j\rangle = \sum_{a=1}^{n}\sum_{b=1}^{n} c_a^i c_b^j \langle F_a|G_{k+D,l+D}|F_b\rangle = \sum_{a=1}^{n} c_a^i c_a^j G_{k+D,l+D}(\mathbf{q}_a), \tag{117}$$

where F_a denotes the ath $3N-6$-dimensional vibrational DVR basis function and $\mathbf{q}_a$ is the grid point associated with F_a. Matrix elements of the $\tilde{g}^{-1/4}\hat{p}_k^\dagger G_{k,l+D}\,\tilde{g}^{1/4}$ operator take the form

$$\langle\Phi_i|\tilde{g}^{-1/4}\hat{p}_k^\dagger G_{k,l+D}\,\tilde{g}^{1/4}|\Phi_j\rangle = \sum_{a=1}^{n}\sum_{b=1}^{n} c_a^i c_b^j \langle F_a|\tilde{g}^{-1/4}\hat{p}_k^\dagger G_{k,l+D}\,\tilde{g}^{1/4}|F_b\rangle =$$

$$= \sum_{a=1}^{n}\sum_{b=1}^{n}\sum_{c=1}^{n}\sum_{d=1}^{n}\sum_{e=1}^{n} c_a^i c_b^j \langle F_a|\tilde{g}^{-1/4}|F_c\rangle\langle F_c|\hat{p}_k^\dagger|F_d\rangle\langle F_d|G_{k,l+D}\,|F_e\rangle\langle F_e|\tilde{g}^{1/4}|F_b\rangle = \tag{118}$$

$$= \sum_{a=1}^{n}\sum_{b=1}^{n} c_a^i c_b^j \langle F_a|\tilde{g}^{-1/4}|F_a\rangle\langle F_a|\hat{p}_k^\dagger|F_b\rangle\langle F_b|G_{k,l+D}\,|F_b\rangle\langle F_b|\tilde{g}^{1/4}|F_b\rangle =$$

$$= \sum_{a=1}^{n}\sum_{b=1}^{n} c_a^i c_b^j \tilde{g}^{-1/4}(\mathbf{q}_a)\langle F_a|\hat{p}_k^\dagger|F_b\rangle G_{k,l+D}(\mathbf{q}_b)\tilde{g}^{1/4}(\mathbf{q}_b),$$

where three approximate resolutions of identity have been applied. The same technique leads to the

$$\langle\Phi_i|\tilde{g}^{1/4}G_{k,l+D}\,\hat{p}_k\tilde{g}^{-1/4}|\Phi_j\rangle = \sum_{a=1}^{n}\sum_{b=1}^{n} c_a^i c_b^j \langle F_a|\tilde{g}^{1/4}G_{k,l+D}\,\hat{p}_k\tilde{g}^{-1/4}|F_b\rangle = \tag{119}$$

$$= \sum_{a=1}^{n}\sum_{b=1}^{n} c_a^i c_b^j \tilde{g}^{1/4}(\mathbf{q}_a)G_{k,l+D}(\mathbf{q}_a)\langle F_a|\hat{p}_k|F_b\rangle\tilde{g}^{-1/4}(\mathbf{q}_b)$$

matrix element expression of the $\tilde{g}^{1/4}G_{k,l+D}\,\hat{p}_k\tilde{g}^{-1/4}$ operator. Section 2.2.4 gives the details on the DVR matrix elements appearing in the previous equations.

2.6.4 Symmetry considerations

For Abelian groups the symmetry labels can be generated by simple analysis of the rotational-vibrational wave functions expanded in the basis defined by Eq. (108). This analysis builds upon the following: (a) only Abelian molecular symmetry groups are considered; (b) the vibrational basis is built upon the vibrational states of the molecule which are basis functions of the irreducible representations of the point group; (c) the rotational basis consists rigid-rotor eigenfunctions which are basis functions of the irreducible representations of the rotational group (D_2 for asymmetric tops); and (d) symmetry elements of the molecular symmetry group are products of point-group and rotational-group elements (see Sec. 2.3 for a more detailed description). If an arbitrary $\hat{A}$ MS operator is given by

$$\hat{A} = \hat{B}\hat{C}, \tag{120}$$

where $\hat{B}$ is a point-group (PG) and $\hat{C}$ is a rotational-group (RG) element, the effect of $\hat{A}$ on a $\Phi_i R_k$ basis function is the following:

$$\hat{A}(\Phi_i R_k) = (\hat{B}\Phi_i)(\hat{C}R_k) = \chi_b^{\mathrm{PG}}(\hat{B})\chi_c^{\mathrm{RG}}(\hat{C})\Phi_i R_k = \chi_a^{\mathrm{MS}}(\hat{A})\Phi_i R_k, \tag{121}$$

where a, b, and c refer to the irreducible representations of the molecular symmetry, point and rotational groups, respectively, and

$$\hat{B}\Phi_i = \chi_b^{\mathrm{PG}}(\hat{B})\Phi_i \tag{122}$$

and

$$\hat{C}R_k = \chi_c^{\mathrm{RG}}(\hat{C})R_k, \tag{123}$$

as all the groups are Abelian. In view of these equations it is evident that the $\Phi_i R_k$ (where $i = 1, \ldots, n$ and $k = 1, \ldots, 2J+1$) functions are basis functions of the one-dimensional irreducible representations of the molecular symmetry group. After finding the dominant (or any other nonzero) $\Phi_i R_k$ contribution in the variational expansion of the rotational-vibrational wave functions the characters of the irreducible representation spanned by this $\Phi_i R_k$ product are to be computed, according to Eq. (121), for all the conjugacy classes. The symmetry species of a given rovibrational state is obviously the same as that of the examined $\Phi_i R_k$ contribution.

3 Results and discussion

In this section a number of results are described which utilize the theory and codes I developed and described in the theoretical section. Section 3.1 summarizes the variational rovibrational computations I have executed with GENIUSH for the four-atomic NH_3 molecule. Besides the full-dimensional results, reduced-dimesional rovibrational models have also been examined and their quality is determined by comparison with results obtained from the full-dimensional treatment. Section 3.2 gives a detailed analysis of the rovibrational spectroscopy of the five-atomic H_2CCO (ketene) molecule. The variational rovibrational results obtained with DEWE and DEWE-VS have been interpreted by the NMD, RRD, and SAL procedures. New assignments in the experimental infrared spectrum of H_2CCO are proposed based on the results of variational and MARVEL [43] analyses. Finally, Section 3.3 describes the validation of the labels of the MARVEL energy levels of $H_2{}^{16}O$, for which I have executed variatonal rovibrational computations for large values of the J rotational quantum number with the GENIUSH-VS program.

3.1 Rovibrational states of NH_3 computed by GENIUSH

The capabilities of the rovibrational GENIUSH algorithm were tested on the ammonia ($^{14}NH_3$) molecule, exhibiting one large-amplitude motion usually called "umbrella motion". Rovibrational results from five reduced-dimensional models, with dimensions ranging from 1D to 4D, are compared to the full-dimensional treatment of coupled internal and rotational motions of ammonia.

Table II. Z-matrix representation of the internal coordinates of NH_3.

N						
X	N	1.0				
H_1	N	r_1	X	θ		
H_2	N	r_2	X	θ	H_1	β_1
H_3	N	r_3	X	θ	H_1	$-\beta_2$

3.1.1 Computational details

The potential energy surface (PES) of $^{14}NH_3$ was taken from Ref. 83. It corresponds to the PES called "refined" in that study. Atomic masses, m_H = 1.007 825 u and m_N = 14.003 074 u, were employed throughout the nuclear motion computations. The set of internal coordinates applied is summarized in Table II. The embedding of the rotational axes was done as follows: (a) the origin of the body-fixed frame is placed on the first atom (N); (b) the x axis is directed towards the second atom (X, a dummy atom); (c) the $x-y$ plane is defined by the first three atoms (N, X, H_1); (d) the z axis is oriented according to the right-hand rule; and (e) the origin is shifted to the center of mass of the nuclei. For reference purposes, full-dimensional variational rovibrational computations employing the complete rovibrational Hamiltonian without constraints on the coordinates were carried out.

Besides the full-dimensional, 6-D, model, five reduced-dimensional models, henceforth called 1-D, 2-D, 3-D, 4-D_1, and 4-D_2, were also implemented, where the number of dimensions refers to the number of active vibrational coordinates. In all reduced-dimensional models the coordinate θ, describing the inversion motion, was kept active. Different symmetrized and nonsymmetrized stretching and bending coordinates were added to it in order to investigate their effect on the rovibrational states. The models are shown in Table III, detailing both the active and the constrained coordinates. The constrained coordinates were fixed at their equilibrium values given by the PES, $r_1 = r_2 = r_3$ = 1.010 31 Å and $\beta_1 = \beta_2 = 120^o$. Fixing these coordinates is equivalent to the deletion of rows and columns corresponding to the constrained coordinates from the full-dimensional **g** matrix. An alternative method had also been implemented for the 4-D_1 model, whereby values of the constrained β_1 and β_2 coordinates were allowed to relax at each grid point of the active coordinates. For the lower-lying vibrational levels computed the "relaxed" and "fixed" results show no significant deviations. This result validates our choice of equilibrium values for the constrained coordinates, at least for the lower-lying vibrational levels. Implementation of all these different models is straightforward within the GENIUSH protocol.

Potential-optimized (PO) [49, 84, 85] Hermite-DVR basis functions were utilized for the vibrational degrees of freedom. The DVR intervals for the internal coordinates can be summarized as follows: $r_1, r_2, r_3 \in [0.35, 2.5]$ Å, $\beta_1, \beta_2 \in [20, 220]^\circ$, and $\theta \in [5, 175]^\circ$. For all the present computations the Podolsky form [32] of the rovibrational Hamiltonian has been applied. It requires the evaluation of only the first derivatives of the Cartesian coordinates

in the body-fixed frame with respect to the internal coordinates, unlike the "rearranged" form [32] often used in (ro)vibrational computations [36, 38, 40], which requires not only the first but also the second and third derivatives.

The customary ordering of the vibrational quantum numbers is employed for labeling the computed $J = 0$ states: 1 = totally symmetric stretch, 2 = inversion mode, 3 = doubly degenerate stretch, and 4 = doubly degenerate bend. The inversion-mode states are labeled, however, not by v_2 but by $v_{\rm inv}$, to account for the doubling of the levels. The molecular symmetry (MS) [73, 86] group D_{3h}(M) is used to provide labels for the symmetries of the rotational-vibrational states of ammonia.

The pure electronic and effective one-dimensional, vibrationally averaged barriers to inversion of $^{14}NH_3$ are computed to be 1777 ± 10 and 2021 ± 20 cm^{-1}, respectively [87, 88]. The latter value is in full agreement with a set of effective one-dimensional spectroscopic results in the 2018 ± 10 cm^{-1} interval [89, 90, 91, 92]. This energy is smaller than all but 5 of the vibrational state energies of $^{14}NH_3$. The vibrational band origins (VBO) of $^{14}NH_3$ lower than this energy have quantum numbers $v_{\rm inv} = 0$, 1, 2, and 3, and $v_4 = 1$. This investigation focuses only on the rotational-vibrational states characterized by $v_{\rm inv} = 0$, 1, 2, 3, 4, and 5 and $v_4 = 1$ while all other vibrational quantum numbers are kept at zero.

Ideally, each inversion state holds a set of $2J + 1$ "rotational" energy levels which can be characterized as symmetric top levels using the usual quantum numbers J and K [73]. To label the rovibrational states of ammonia further, two routes can be followed. The clearest one is to use the $v_{\rm inv}$ quantum number to distinguish between the inversion doublets and employ the irreducible representations of the D_{3h}(M) MS group. The less preferred alternative is to designate the doublets with superscripted + and − symbols, indicating the lower- and higher-energy member of the pairs, respectively. Note also that nuclear spin statistics makes some of the computed rovibrational levels (those with species A_1' and A_1'') "missing" [73]. Finally, we mention that for the $\{\nu_2^+, \nu_2^-\}$ diad and especially for the $\{2\nu_2^+, \nu_4^+, \nu_4^-\}$ triad the energy order of the rotational-vibrational eigenstates does not strictly follow the order of the VBOs (the $J = 0$ eigenstates). The rotational-vibrational states were sorted according to the prescription of the RRD procedure.

Table III. Characteristics of the reduced-dimensional models of NH_3 employed in this study.

model	active coordinates	constrained coordinates	no. of BFs for the active DOFs[a]
1-D	θ	$r_1, r_2, r_3, \beta_1, \beta_2$	40 (100)
2-D	$\theta, \frac{1}{\sqrt{3}}(r_1 + r_2 + r_3)$	$\frac{1}{\sqrt{6}}(2r_1 - r_2 - r_3), \frac{1}{\sqrt{2}}(r_2 - r_3), \beta_1, \beta_2$	25 (80), 15 (80)
3-D	θ, β_1, β_2	r_1, r_2, r_3	25 (80), 15 (80), 15 (80)
4-D_1	θ, r_1, r_2, r_3	β_1, β_2	25 (80), 15 (80), 15 (80), 15 (80)
4-D_2	$\theta, \frac{1}{\sqrt{3}}(r_1 + r_2 + r_3), \beta_1, \beta_2$	$\frac{1}{\sqrt{6}}(2r_1 - r_2 - r_3), \frac{1}{\sqrt{2}}(r_2 - r_3)$	25 (80), 15 (80), 15 (80), 15 (80)

[a] BF = PO DVR basis function. DOF = degree of freedom. The number of primitive DVR vibrational basis functions are given in parentheses.

3.1.2 Full-dimensional results

The full (6-D)-dimensional VBOs obtained with the PES and the exact kinetic energy operator employed for the present computations within the GENIUSH protocol have been reported in Ref. [32]. A few of these results are reproduced in Table IV along with the experimental values taken from Ref. 93. The basis set used here is large enough to converge all the VBOs of interest to better than 0.01 cm^{-1}. Thus, the computed full-dimensional rotational-vibrational energy levels, some of which are reported in Table V, serve as benchmark numbers.

As clear from Table V, the present PES [83], at least for the low J values investigated in this study, provides rotational-vibrational energies in good agreement with the experimental results. The agreement is not as outstanding as has been observed for the recent exceedingly high quality ab initio and ab initio-based PESs of water [13, 95, 96], but the average accuracy of the computed lines is down to the 0.1 cm^{-1} level.

It is interesting to compare the present benchmark energy values to those obtained using the TROVE algorithm employing truncated kinetic and potential energy operators [83, 94] during solution of the nuclear-motion problem. The appropriate vibrational and rovibrational results are reported in Tables IV and V, respectively. In all cases the TROVE energy values are higher than the GENIUSH ones. However, the differences are very small, on the order of 0.01–0.03 cm^{-1}, both for the pure vibrational and rovibrational states, considerably smaller than the accuracy of the PES employed, on the order of 0.1 cm^{-1} for the states considered. This proves the validity and utility of the approximations introduced in the TROVE algorithm.

Finally, a few words about the rotational wavenumbers corresponding to the different rotational axes. The rotational energies at about 20 cm^{-1} for $J = 1$ are considerably larger

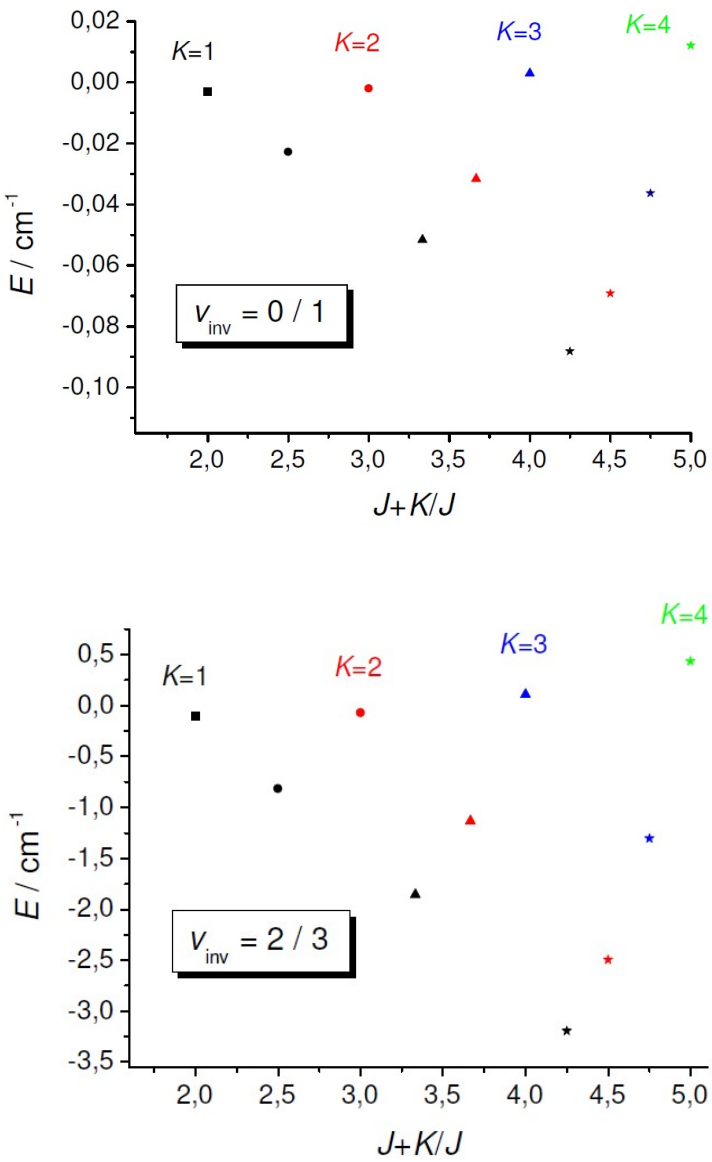

Figure 1: Relative splittings between rovibrational states of $^{14}NH_3$ sharing the same K value for a given J for the $v_{\rm inv} = 0/1$ ($v_2 = 0$) and $v_{\rm inv} = 2/3$ ($v_2 = 1$) pairs, referenced to the corresponding $J = 0$ values. Relative splittings for different J values are denoted according to the following pattern: rectangle: $J = 1$, circle: $J = 2$, triangle: $J = 3$, star: $J = 4$.

Table IV. Relevant full and reduced-dimensional zero-point vibrational energies (GS = ground state) and vibrational band origins of $^{14}NH_3$ relative to the vibrational ground state energy, all in cm^{-1}. The molecular symmetry group $D_{3h}(M)$ is used to label the rotational-vibrational states of ammonia. The $D_{3h}(M)$ symmetry labels are given in parentheses. The 1-D, 2-D, and 4-D_1 models do not exhibit the ν_4^+ and ν_4^- vibrations as the β_1 and β_2 vibrational coordinates are fixed in these cases.

	1-D	2-D	3-D	4-D_1	4-D_2	6-D	Expt.[a]
0^+ ($A_1^{'}$, GS)	521.43	2256.74	2158.70	5828.91	3911.34	7436.82	–
0^- ($A_2^{''}$)	1.13	1.28	1.70	0.58	1.74	0.79	0.79
ν_2^+ ($A_1^{'}$)	930.57	900.48	904.48	945.65	881.01	932.41	932.43
ν_2^- ($A_2^{''}$)	979.80	952.80	970.68	973.89	946.02	968.15	968.12
$2\nu_2^+(A_1^{'})$	1586.97	1537.6	1550.06	1626.11	1511.43	1597.26	1597.47
ν_4^+ ($E^{'}$)	–	–	1659.43	–	1649.71	1625.62	1626.28
ν_4^- ($E^{''}$)	–	–	1662.12	–	1652.08	1626.73	1627.37
$2\nu_2^-(A_2^{''})$	1918.86	1868.39	1917.98	1884.43	1867.66	1882.18	1882.18

[a] Experimental results are taken from Ref. 93 and have higher accuracy than indicated here. The VBOs obtained with TROVE [83, 94], using the same PES and following the same order, are 7436.82, 0.80, 932.42, 968.16, 1597.29, 1625.64, 1626.75, and 1882.20 cm^{-1}.

than the splitting between the 0^+ and 0^- states, about 1 cm^{-1}. Thus, resonance interactions should be limited. One further expects that rotation about the principal symmetry axis increases the inversion splitting and those about the perpendicular axes act in the opposite direction. As shown in Figure 1, the splittings between the E' and E'' states can both increase and decrease as a function of J and K, though these changes are rather small for the small J values considered. The relative splittings change almost linearly as a function of K. For each J, the relative splitting is positive only for the largest K pair.

3.1.3 Convergence of the rovibrational levels

Convergence of the rovibrational levels of NH_3 was examined extensively with respect to the size of the vibrational basis. Full-dimensional computations were carried out from $J = 0$ up to $J = 4$. The reported "converged" results were computed using 25 vibrational basis functions for the inversion and 10 vibrational basis functions for the other five degrees of freedom. For the approximate rovibrational levels a considerably smaller vibrational basis, containing 14 functions for the inversion and 5 for the others, was utilized. The basis functions mentioned refer to PO DVR functions for all degrees of freedom, each of them were generated by employing 80 primitive DVR functions (see Table III for a summary

about basis functions for the reduced-dimensional models).

A pictorial representation of the deviations between the "converged" and approximate rovibrational levels is given in Figure 2, where the minimum unsigned, maximum unsigned, and mean values of these deviations are plotted for six vibrational states.

As expected, deviations between the "converged" and the approximate rovibrational levels increase with vibrational excitation. For the vibrational ground state the small vibrational basis is able to reproduce the exact rovibrational levels very well, while the biggest deviations are present for the fifth VBO. These findings suggest that (a) the incompleteness of the vibrational basis plays an important role in the error of the rovibrational levels (unless they are referenced to the actual VBO); and (b) even small vibrational basis sets are able to supply rovibrational levels of appropriate precision for some of the vibrational band origins.

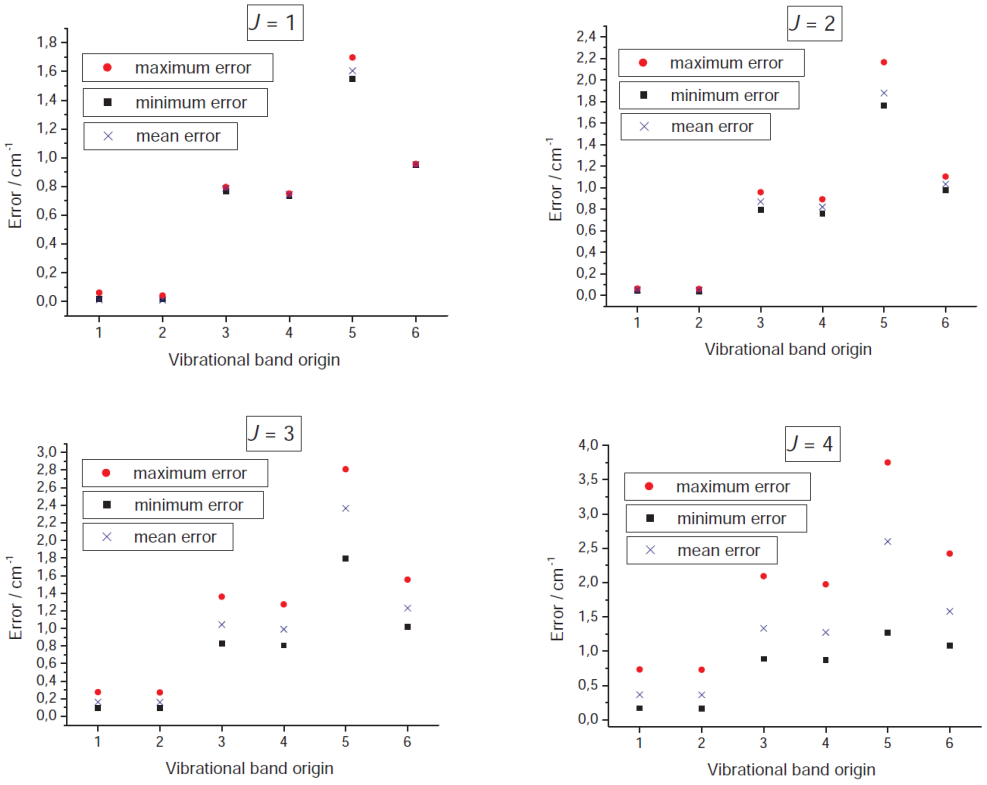

Figure 2: Convergence of the rovibrational levels of $^{14}NH_3$ from $J = 1$ up to $J = 4$. Maximum unsigned, minimum unsigned, and mean absolute deviations between the converged (25 basis functions for the inversion and 10 for the other degrees of freedom, respectively) and small (14 basis functions for the inversion and 5 for the other degrees of freedom, respectively) vibrational basis sets are shown. Note that 1, 2, 3, 4, 5, and 6 on the x axis refer to the 0^+, 0^-, ν_2^+, ν_2^-, $2\nu_2^+$, and $2\nu_2^-$ vibrational states, in order.

Table V. Selected computed full-dimensional rotational-vibrational energy levels of $^{14}NH_3$ for $J = 1 - 4$, in cm^{-1}, referenced to the zero-point energy of the system (all vibrational modes other than the umbrella motion remain in their ground state). See text for the meaning of the labels $\{v_{inv}\ J\ K\}$ of the rotational-vibrational states. Symmetry labels correspond to the $D_{3h}(M)$ molecular symmetry group.

J	K	v_{inv}	symm. label	GENIUSH	TROVE
1	0	0	A_2'	19.907	19.907
1	1	0	E''	16.188	16.188
1	1	1	E'	16.979	16.981

1	0	2	$A_2^{'}$	952.558	952.570
1	1	2	$E^{''}$	948.578	948.589
1	1	3	$E^{'}$	984.209	984.219
2	1	0	$E^{''}$	55.988	55.988
2	2	0	$E^{'}$	44.838	44.838
2	0	1	$A_2^{''}$	60.465	60.467
2	1	1	$E^{'}$	56.759	56.761
2	2	1	$E^{''}$	45.630	45.632
2	1	2	$E^{''}$	988.860	988.872
2	2	2	$E^{'}$	976.928	976.940
2	0	3	$A_2^{''}$	1027.507	1027.517
2	1	3	$E^{'}$	1023.781	1023.792
2	2	3	$E^{''}$	1012.596	1012.606
3	0	0	$A_2^{'}$	119.341	119.342
3	1	0	$E^{''}$	115.637	115.638
3	2	0	$E^{'}$	104.516	104.516
3	3	0	$A_2^{''}$	85.943	85.944
3	1	1	$E^{'}$	116.380	116.382
3	2	1	$E^{''}$	105.278	105.280
3	3	1	$A_2^{''}$	86.740	86.742
3	0	2	$A_2^{'}$	1053.171	1053.183
3	1	2	$E^{''}$	1049.216	1049.228
3	2	2	$E^{'}$	1037.327	1037.340
3	3	2	$A_2^{''}$	1017.453	1017.465
3	1	3	$E^{'}$	1083.098	1083.109
3	2	3	$E^{''}$	1071.935	1071.946
3	3	3	$A_2^{'}$	1053.302	1053.313
4	1	0	$E^{''}$	195.076	195.077
4	2	0	$E^{'}$	183.991	183.992
4	3	0	$E^{''}$	165.482	165.482
4	4	0	$E^{'}$	139.492	139.492
4	0	1	$A_2^{'}$	199.466	199.469
4	1	1	$E^{'}$	195.781	195.784

4	2	1	E''	184.716	184.719
4	3	1	A_2'	166.239	166.242
4	4	1	E''	140.298	140.300
4	1	2	E''	1129.566	1129.579
4	2	2	E'	1117.734	1117.747
4	3	2	A_2''	1097.956	1097.969
4	4	2	E'	1070.140	1070.152
4	0	3	A_2''	1165.817	1165.829
4	1	3	E'	1162.108	1162.121
4	2	3	E''	1150.975	1150.988
4	3	3	A_2'	1132.390	1132.403
4	4	3	E''	1106.313	1106.324

3.1.4 Reduced-dimensional results

Five reduced-dimensional models of the $^{14}NH_3$ molecule have been tested, ranging from 1-D to 4-D. Table IV gives the computed full and reduced-dimensional vibrational band origins of interest for this study. All of the computed rovibrational levels were referenced to the appropriate VBOs and the differences of these full and reduced-dimensional levels were then computed. The maximum unsigned, minimum unsigned, and mean absolute (MAD) deviations are summarized in Table VI for $J = 1$ and 4.

The ZPVE for the 1-D model is 521.4 cm^{-1}. The considerable increase in the effective one-dimensional barrier height mentioned before is due to the significant tightening of bonding at the transition state, as reflected in the PES. In the 1-D model, similarly to the full 6-D model, there are 4 vibrational states below the barrier, while the fifth state ($v_{inv} = 4$) is already slightly beyond it.

Though there is a considerable shift (see the MAD values of Table VI) of the rovibrational energy levels due to the incompleteness of the vibrational model for the ground state, deviations from the MADs are considerably smaller, up to a factor of 6. Thus, the computed reduced-dimensional rovibrational energies have considerable predictive power.

The deviations of the reduced-dimensional rovibrational results from the full rovibra-

tional results show clearly the considerable approximations characterizing the 1-D vibrational model. Interestingly, the 2-D model, having the two fully symmetric motions of ammonia active, does not improve substantially the 1-D results, except for the 0^+ and 0^- states. For example, the difference between the $2\nu_2^+(A_1')$ and $2\nu_2^-(A_1'')$ VBOs is 285 cm^{-1} experimentally, while the {1-D, 2-D} splittings are {332, 331} cm^{-1}, a gross overestimation in both cases. In fact, none of the reduced-dimensional models are successful in predicting this splitting.

By far the best model for describing the inversion motion of ammonia is the 4-D_1 model. This is a somewhat nonintuitive result and perhaps stems from a considerable coupling between the umbrella mode and the overtones of the non-symmetric stretching modes. Nevertheless, even this best reduced-dimensional model produces errors an order of magnitude larger than the intrinsic accuracy of the PES. Even in the most favorable cases the improvement in the maximum unsigned error is only about a factor of two. Thus, it is surprisingly hard to improve upon the simplest 1-D model by the inclusion of further degrees of freedom in the active set of coordinates. This is a serious warning when treating larger, more complex systems and what can be expected from models including several degrees of freedom in the active set designed to improve upon the physically simplest model. However, in the many cases when the smallest reasonable treatment of the molecular system does require the active treatment of several coordinates, the present procedure provides a straightforward way for the interpretation of the measured rotational-vibrational spectra.

3.2 Rovibrational results for the C_2H_2O computed by DEWE

The semirigid five-atomic ketene (C_2H_2O) molecule has proven to be an ideal candidate for variational rovibrational computations with DEWE as the following characteristics of its rovibrational spectrum hinder perturbative treatments: (a) its three lowest fundamental vibrations ($\nu_5(B_1) \approx 587$, $\nu_6(B_1) \approx 526$, and $\nu_9(B_2) \approx 439$ cm^{-1} in the Mulliken notation) cluster in the narrow $430-590$ cm^{-1} window; (b) the next two fundamentals, $\nu_4(A_1) \approx 1116$ and $\nu_8(B_2) \approx 977$ cm^{-1}, occur next to each other at about twice the frequency of the three bends; (c) complications also arise from the fact that there is a C_{2v} to C_s bifurcation on the ground-state PES of ketene, marking the advent of the out-of-plane bent (C_s^{I}) dissociation path when the C=C bond is elongated by just about 0.15 Å over its equilibrium value; (d) there are a number of vibrational (Fermi and Darling–Dennison) and rovibrational

Table VI. Maximum unsigned, minimum unsigned, and mean absolute (MAD) deviations between the computed full and reduced-dimensional results, in cm^{-1}, for the $J = 1$ and $J = 4$ states of $^{14}NH_3$. Both the full- and the reduced-dimensional rovibrational levels are referenced to the appropriate vibrational band origins given in Table IV.

		$J = 1$					$J = 4$				
Label		1-D	2-D	3-D	4-D_1	4-D_2	1-D	2-D	3-D	4-D_1	4-D_2
0^+	maximum	0.243	0.129	1.360	0.343	0.461	2.697	1.376	6.570	3.282	4.606
	minimum	0.208	0.121	1.087	0.195	0.271	1.909	1.351	2.360	1.050	1.571
	MAD	0.219	0.127	1.178	0.244	0.334	2.357	1.362	4.815	2.359	3.344
0^-	maximum	0.247	0.130	1.448	0.338	3.444	2.731	1.377	6.527	3.239	4.516
	minimum	0.211	0.121	1.180	0.193	0.268	1.939	1.357	2.401	1.049	1.587
	MAD	0.223	0.127	1.270	0.242	1.327	2.390	1.365	4.806	2.334	3.297
ν_2^+	maximum	0.440	0.491	2.542	0.125	0.698	4.742	5.114	9.500	4.755	7.790
	minimum	0.254	0.290	2.163	0.075	0.351	1.450	1.716	1.243	0.438	1.441
	MAD	0.316	0.357	2.416	0.092	0.467	3.351	3.685	5.263	1.645	4.930
ν_2^-	maximum	0.596	0.530	0.349	0.024	0.529	6.181	5.417	6.557	3.650	5.308
	minimum	0.372	0.332	0.074	0.015	0.309	2.420	2.155	0.499	0.148	0.611
	MAD	0.447	0.398	0.166	0.018	0.382	4.607	4.053	4.155	0.860	3.576
ν_4^+	maximum	–	–	1.063	–	0.932	–	–	8.502	–	5.589
	minimum	–	–	0.014	–	0.256	–	–	1.386	–	0.065
	MAD	–	–	0.622	–	0.552	–	–	6.207	–	3.829
ν_4^-	maximum	–	–	1.079	–	0.942	–	–	8.431	–	5.483
	minimum	–	–	0.030	–	0.273	–	–	1.384	–	0.097
	MAD	–	–	0.587	–	0.508	–	–	5.684	–	3.219
$2\nu_2^+$	maximum	0.500	0.617	3.462	0.275	0.470	4.950	6.061	3.781	2.573	4.564
	minimum	0.293	0.396	3.332	0.086	0.319	1.795	2.716	1.919	0.199	2.358
	MAD	0.362	0.470	3.419	0.149	0.369	3.717	4.749	3.082	1.598	3.723
$2\nu_2^-$	maximum	1.012	0.894	1.713	0.424	0.478	10.209	8.957	6.359	4.231	4.799
	minimum	0.607	0.529	1.505	0.171	0.313	3.683	3.117	3.075	0.197	2.148
	MAD	0.742	0.651	1.574	0.255	0.368	7.495	6.530	4.990	2.558	3.695

(Coriolis) resonances in different regions of the spectrum of ketene, occasionally causing localized level crossings distorting the rotational structures of some of the bands.

Perturbation-based analyses of the spectroscopic features of ketene have been summarized nicely by East et al. [98], who performed one of the most careful ab initio studies of the spectral features of ketene, based on a quartic force field representation of the PES and the traditional vibrational perturbation theory carried out to second order (VPT2) [99]. Understanding the various resonances, detecting and assigning their spectral signatures, including irregular subband origins and unusual isotopic frequency shifts, and treating them with perturbative theoretical techniques meant that spectroscopists encountered severe difficulties while working on the measured spectra of ketene isotopologues and thus had to leave a considerable number of spectral features unassigned even at the low energies considered. The most practical way out of the messy situation concerning the spectroscopy of ketene is to employ variational nuclear motion techniques.

This section discusses the results of the variational rovibrational computations done for C_2H_2O. Zeroth-order vibrational and rotational quantum numbers and symmetry labels were evaluated by the NMD, RRD and SAL procedures. Rovibrational energy levels and wave functions with high J rotational quantum numbers were computed by the DEWE-VS program. Then, the MARVEL analysis based on the measured rovibrational transitions of C_2H_2O is summarized. Finally, new experimental transitions are assigned based on the variational and MARVEL results.

3.2.1 Model of the PES

The empirically adjusted ab initio quartic internal coordinate force field of Ref. [98] was employed as a model of the PES of ketene around the equilibrium structure. This simple representation of the ground-state PES of ketene was obtained by East et al. [98] as a result of two cycles of refinements. In the interior cycle A the harmonic (quadratic) part of the force field was refined by scaling it according to the scaled quantum mechanical (SQM) force field recipe [100, 101] to harmonized frequencies, obtained via the VPT2 protocol, while keeping the reference (equilibrium) geometry fixed. In the exterior cycle B, corrections to the rotational constants based on lowest-order vibration-rotation interaction constants computed from the actual cubic force field, augmented with small centrifugal distortion and electronic corrections, were applied to the experimental ground-state rotational constants in order to get an improved estimate of the equilibrium molecular structure of ketene. The

exterior and interior cycles were repeated until self-consistency was achieved, resulting in a quartic force field which reproduced the available experimental fundamentals within the VPT2 protocol by about 1 cm^{-1} on average.

In order to make the internal coordinate quartic force field of Ref. [98] optimal for use in variational nuclear motion computations, the simple stretching coordinates were replaced by Simons–Parr–Finlan coordinates [102]. The necessary nonlinear transformations were performed analytically by employing the INTDER2000 program system [103, 104, 105]. The final quartic internal coordinate force field employed in this study is defined in the Supplementary Material of Ref. [22].

3.2.2 Rovibrational energy levels and wave functions

All the nuclear motion computations utilized the DEWE program package. The atomic masses employed for all the computations are $m(\mathrm{H}) = 1.007\,825$ u, $m(^{12}\mathrm{C}) = 12.000\,000$ u, and $m(^{16}\mathrm{O}) = 15.994\,910$ u. The reference structure and the definition of the rectilinear coordinates are given in the Supplementary Material of Ref. [22]. Following a considerable number of test computations, the vibrational basis was chosen as follows for the results reported hereby: 6, 8, and 10 basis functions for the four stretching motions, the two highest bends, and the three lowest bends, respectively. The size of the corresponding vibrational Hamiltonian thus became 82 944 000. This basis allowed execution of vibration-only computations on a personal computer within a few weeks resulting in the lowest 100 eigenvalues and eigenfunctions.

The rotational-vibrational computations were performed in two different ways. First, the DEWE algorithm was employed up to $J = 3$ with a vibrational basis of 21 781 872 functions (7 basis functions for the five bends and 6 for the four stretching motions). Second, the DEWE-VS procedure was applied for the computation of rotational-vibrational energy levels up to $J = 50$ (for the full list of rovibrational states corresponding to the first four VBOs, GS (ground state), $\nu_9 = 9^1$, $\nu_6 = 6^1$, and $\nu_5 = 5^1$, see the Supplementary Material of Ref. [22]). During the DEWE-VS computations the previously mentioned lowest 100 vibrational wave functions defined the vibrational subspace employed.

The NMD and RRD analyses of the computed rovibrational wave functions were performed according to the recipes of Section 2.5.

3.2.3 MARVEL analysis

The MARVEL [43] analysis of the measured rovibrational transitions resulted in a set of "experimental" energy levels. In order to keep the experimental sources of the measured transition data searchable, each experimental source received a tag (see Table VII). Table VII contains the intervals characterizing the measured transitions as well as the number of the available (A) and validated (V) transitions present in a given source.

We could not use the several hundred assigned transitions in 87DuFeHaToa [106], as not the individual transitions but the effective spectroscopic constants deduced from them were reported in the paper. We did, however, employ many previously assigned but so far unpublished high-resolution mid-infrared transitions [107], which became part of Ref. [22] and thus received the tag 11FaMaFuNe (see Table VII). There are many pure rotational transitions reported in the Cologne Database for Molecular Spectroscopy (CDMS) [108], which come from several known sources [109, 110, 112, 113, 114, 115]. Thanks to the kind help of Dr. Müller, maintaining the CDMS, these transitions received their original tag and at the end no explicit reference is made in the MARVEL input to the CDMS. Transitions reported in Ref. [112] are also listed under their original sources in the MARVEL input file.

Due to the symmetry of the molecule, the rotational-vibrational energy levels of ketene form two spectroscopic networks (SN) [116], called ortho and para. There are no ortho-para transitions measured.

Since the MARVEL energy levels determined do not have the same dependability (the uncertainties resulting from the least-squares fit can not always be trusted, especially when the energy level is determined by a single transition), we attached quality classifications to the levels, distributing them into three categories: A (best), B, and C (worst). A MARVEL energy level is of A quality if it is determined by at least 5 transitions coming from at least 3 different data sources. Energy levels of B quality participate in at least 4 transitions coming from at least 2 data sources. All other MARVEL energy levels, in fact the majority of the MARVEL levels, are tagged as C.

Table VII. Data sources for line information and their characteristics for $H_2{}^{12}C{=}{}^{12}C{=}{}^{16}O$ employed during the present MARVEL analysis.

Tag	Range (cm^{-1})[a]	Trans. (A / V)[b]
77FaKrMu [114]	0.013 – 0.038	2 / 2
03GuHu [112]	0.076 – 10.882	97 / 65
52JoSt [109]	0.264 – 2.041	29 / 24[c]
72JoStWi [117]	0.264 – 6.123	53 / 45
01SuDr [110]	0.674 – 0.674	1 / 1
63CoEs [111]	0.674 – 1.361	15 / 9
90BrGoMcPi [113]	0.674 – 12.140	37 / 20
92JoNeYaWa [115]	0.692 – 24.445	146 / 77
96HiZeDoGu [122]	1.337 – 5.445	130 / 89
11FaMaFuNe [22]	332.638 – 1021.930	2345 / 1945
94EsDoCaOr [118]	3049. 661 – 3089.528	276 / 175
03StNeGr [121]	4269.605 – 6271.494	851 / 742

[a] Note that (a) the range indicated does not mean the actual spectral range covered by the experiment but simply the lowest- and highest-energy transition present in the database and (b) the ranges are not always indicative of the vibrational states covered by the experiment.
[b] Trans. = transitions, A = available in the original data source, V = validated by MARVEL during the present work.
[c] The 52JoSt.24 transition was removed manually from the database as it has the same lower and upper level assignments in the original publication.

3.2.4 Vibrational band origins

The vibrational energy levels computed with the DEWE program package are collected in Table VIII. Since the present quartic force field does not take into account the dissociation path bifurcation occuring on the ground-state PES of ketene at about 4000 cm^{-1}, we report computed vibrational band origins (VBO) only up to about 2200 cm^{-1}, i.e., up to the neighborhood of the C=O stretch fundamental $2^1 = \nu_2(A_1)$. The NMD tables of the parent isotopologue of ketene, close to the same energy cut-off value, are reported in Tables IX-XII for the four irreducible representations of the C_{2v} point group.

The very strong mixing within some of the vibrational states of ketene is clearly evident from the NMD data of Tables IX-XII. Therefore, the zeroth-order normal-mode labeling given in Table VIII becomes rather approximate in certain cases even at the low energies and low excitations considered. The most striking example concerns the A_1-symmetry states at 1402.3 and 1415.9 cm^{-1} (variational results), which have an almost perfect 50-50 mixing of the ω_3 and (ω_8 + ω_9) harmonic oscillator basis states. This means that it is unclear, based on the present variational quantum chemical computations, whether the $3^1 = \nu_3(A_1)$ fundamental of parent ketene is at 1402 or at 1416 cm^{-1}. The NMD analysis prefers the higher assignment by NMD coefficients 50 to 43. However, we prefer the lower assignment, though clearly this is somewhat arbitrary and can be supported only if comparison with experimental and harmonic results is considered. The strong Fermi resonance behind this result has been noted before, for example by Duncan et al. [106]. The $4^1 = \nu_4(A_1)$ fundamental of parent ketene at 1113 cm^{-1} also mixes strongly with the 5^16^1 combination state at 1169 cm^{-1}, though for this fundamental the largest NMD coefficient is a much more indicative 61. Nevertheless, here there are also strong Fermi resonance interactions as indicated by the mixing of the ω_4, $2\omega_5$, and (ω_5 + ω_6) basis states. The mixing of the $2\omega_6$ state, predicted by Duncan et al. [106], is weak and thus could almost be neglected. It is also important to point out that $8^1 = \nu_8(B_2)$ is not strongly mixed with the other vibrational states. This is principally due to the fact that there are no nearby B_2-symmetry vibrational states. Finally, we note that the strict harmonic order of the vibrational states changes in several instances. This happens, for example, for the (ω_6 + ω_9) – ω_8 and $2\omega_6$ – (ω_5 + ω_9) pairs at about 970 and 1050 cm^{-1}, respectively, in the first case due to anharmonic corrections of different sign.

The anharmonic corrections to the fundamentals 9^1, 6^1, 5^1, 8^1, 4^1, 3^1, 2^1 are +5.0, +26.3, +7.1, –17.9, –29.7, –25.9, –44.4 and +3.5, +31.4, +21.6, –23.4, –32.8, –12.9, –43.5 cm^{-1} for VPT2 and DEWE, respectively. Clearly, in some cases the two approaches provide considerably different VBOs for this molecule; for example, VPT2 and DEWE differ by a factor of 3 and 2 for the anharmonic corrections to the fundamentals 5^1 and 3^1, respectively. These large discrepancies should be compared to the ability of the refined quartic force field employed to reproduce measured band origins by an average accuracy of 1 cm^{-1} based on the VPT2 treatment [98]. This also points to the need of using variational results when refining quartic force fields for molecules exhibiting strong and extensive anharmonic resonances. Another peculiar feature of the computed results is that there is a very large

positive anharmonicity for the out-of-plane C=C=O bending fundamental, $6^1 = \nu_6(B_1)$, and its overtones, it is +31.4, +66.5, +99.4, +123.2 cm^{-1} for the VBOs 6^1, 6^2, 6^3, 6^4, showing some irregularity.

As clear from Table VIII, the variationally computed VBOs deviate substantially from the experimental MARVEL ones (discussion of the MARVEL levels is given in Section 3.2.6). Since the variational protocol employed uses an exact kinetic energy operator and includes also the complete PES, these discrepancies are the result of slight problems with the empirically adjusted ab initio quartic force field approximation of the PES employed. Nevertheless, it is more important to emphasize that the discrepancies are only on the order of a few cm^{-1}, making all semi-quantitative conclusions of this study about the rovibrational characteristics of the ketene molecule valid.

Of the four vibrational resonance interactions identified in Table IX of Ref. [98], three and one within the A_1 and B_2 irreducible representations, respectively, the two lower-energy ones can be investigated here: the tetrad (ν_4, $2\nu_5$, $2\nu_6$, $\nu_5 + \nu_6$) at 1100–1200 cm^{-1} and the diad (ν_3, $\nu_8 + \nu_9$) at about 1410 cm^{-1}. Our NMD analysis presented in Table IX clearly confirms the existence of both resonance schemes.

For the Fermi resonance tetrad, the present variational and the previous VPT2 results [98] show moderate agreement, perhaps somewhat worse than anticipated. For the lower two states ($2\nu_6$ and ν_4) the variational and the VPT2 eigenvalues agree well, within 8 cm^{-1}. We clearly confirm ν_4 to be around 1113 cm^{-1}. Otherwise, the variational and VPT2 results disagree to some extent. In all cases the variational wave functions suggest stronger interactions than those indicated in Ref. [98]. Furthermore, for the higher two eigenvalues the disagreement between the two protocols is quite substantial, 23 cm^{-1} for ψ_{11} and 48 cm^{-1} for ψ_{10}.

As to the Fermi diad, the variational separation of the two states, 14 cm^{-1}, is just half as large as the separation computed via VPT2. Furthermore, while the VPT2 interaction between the two states was labeled as "weak", the variational results indicate a rather strong interaction, whereby the NMD coefficients are almost 50:50.

There are other moderate or strong resonance interactions identified by our NMD analysis below a relative energy of about 2100 cm^{-1}. Most notably, in the A_1 block there is the ψ_{38}–ψ_{42} diad, in the A_2 block the ψ_{45}–ψ_{49}–ψ_{53}–ψ_{56} tetrad, in the B_1 block the ψ_{37}–ψ_{43} diad and the ψ_{21}–ψ_{23}–ψ_{25}–ψ_{26}–ψ_{28} pentad, and in the B_2 block the ψ_{19}–ψ_{22}, ψ_{30}–ψ_{32}, and ψ_{44}–ψ_{48} diads. The number and extent of all the vibrational resonance interactions identi-

fied suggest that further analysis of the high-resolution rotational-vibrational spectrum of ketene should be based on extensive and accurate variational computations.

Table VIII. Active database (MARVEL) and variational quantum mechanical (DEWE) vibrational band origins (VBO, cm^{-1}) for $H_2{}^{12}C{=}{}^{12}C{=}{}^{16}O$ in order of increasing energy, with zeroth-order normal-mode (NMD) assignments, symmetry labels (Sym.), and MARVEL uncertainties (Unc., 10^{-6} cm^{-1}). The number of validated rotational-vibrational levels (RL) associated with the vibrational bands in the present database and traditional characterization of the fundamentals are also given.

NMD label	Sym.	MARVEL	Unc.[a]	RL	DEWE[b]	Characterization
GS	A_1	0	0	329	6832.0	ground state
9^1	B_2	439.386511	235	148	437.1	in-plane C=C=O bend
6^1	B_1	526.070043	236	248	534.0	out-of-plane C=C=O bend
5^1	B_1	587.428312	231	200	603.5	CH_2 wag
9^2	A_1				873.8	
8^1	B_2			234	972.6	CH_2 rocking
6^19^1	A_2				975.0	
5^19^1	A_2				1047.1	
6^2	A_1				1071.7	
4^1	A_1				1113.3	
5^16^1	A_1				1169.1	
5^2	A_1				1211.4	
9^3	B_2				1310.1	
3^1	A_1				1402.3	CH_2 scissor[c]
6^19^2	B_1				1412.4	
8^19^1	A_1				1415.9	
5^19^2	B_1				1490.5	
6^18^1	A_2				1508.2	
6^29^1	B_2				1516.2	
4^19^1	B_2				1558.2	
5^18^1	A_2				1567.3	
6^3	B_1				1607.2	
$5^16^19^1$	B_2				1612.7	

$4^1 6^1$	B_1	1637.7	
$5^2 9$	B_2	1659.0	
$4^1 5^1$	B_1	1702.3	
[d]	B_1	1714.8	
9^4	A_1	1745.9	
[d]	B_1	1784.2	
5^3	B_1	1808.0	
$8^1 9^2$	B_2	1836.0	[e]
$6^1 9^3$	A_2	1847.0	
$3^1 9^1$	B_2	1854.2	[e]
$5^1 9^3$	A_2	1933.6	
8^2	A_1	1940.9	
$6^1 8^1 9^1$	B_1	1943.3	
$6^2 9^2$	A_1	1953.2	
$3^1 6^1$	B_1	1966.9	
$4^1 9^2$	A_1	2001.0	
$5^1 8^1 9^1$	B_1	2013.2	
$6^2 8^1$	B_2	2044.9	
$6^3 9^1$	A_2	2051.0	
$5^1 6^1 9^2$	A_1	2052.1	
$3^1 5^1$	B_1	2077.8	
$4^1 8^1$	B_2	2080.1	
$4^1 6^1 9^1$	A_2	2085.9	
$5^2 9^2$	A_1	2108.1	
6^4	A_1	2133.6	
$5^1 6^1 8^1$	B_2	2133.6	
[d]	A_2	2147.5	
2^1	A_1	2153.7	C=O stretch
$5^2 8^1$	B_2	2161.5	
$4^1 6^2$	A_1	2162.9	
[d]	A_2	2166.9	
9^5	B_2	2178.1	

[a] The uncertainties (Unc.) are given in units of 10^{-6} cm^{-1}. VBOs not determined by the experimental data available are left blank in the MARVEL and Unc. columns. Two further MARVEL VBOs have been determined as part of the present analysis: 1^2 (A_1) = 6068.373106(50) and 7^2 (A_1) = 6262.909106(50) cm^{-1}, holding 130 and 59 RLs, respectively. The 1^1, 8^1, 1^17^1, and 2^2 VBOs could not be determined via the MARVEL analysis but in the present database they hold 107, 234, 201, and 65 RLs, respectively.

[b] The vibrational basis was chosen as follows for the VBOs computed by DEWE: 6, 8, and 10 basis functions for the four stretching motions, the two highest bends, and the three lowest bends, respectively.

[c] There is a very strong mixing between the 3^1 and 8^19^1 states (see Table IX), in fact for this state 3^1 and 8^19^1 have NMD contributions of 43 and 50 %, respectively.

[d] No reasonable assignment can be given due to extremely heavy mixing of several states.

[e] Note the very strong mixing of the 8^19^2 and 3^19^1 states, see Table XII.

Table IX. The lowest-energy part of the normal-mode decomposition (NMD) table of ketene for A_1 point-group symmetry.

NMD(ν,ω)[a,b]		6891.5	867.2	1005.2	1084.5	1146.0	1163.8	1415.2	1429.6	1734.4	1872.4	1951.7	1992.0	2010.4	2013.2	2031.0	2089.7	2151.2	2169.0	2197.2	2230.5	2248.3	2282.4	2292.0	2296.8	2309.8	2327.6	2420.4	2434.8	2499.7	2514.1	2561.2	2575.6	2579.0	2593.4	2601.6	2739.6	2818.9	2830.4	2844.8	2859.2	2877.6	2880.4	2898.2	
		ZPV	$2\omega_9$	$2\omega_8$	$\omega_5+\omega_6$	ω_4	$2\omega_5$	ω_3	$\omega_8+\omega_9$	$4\omega_9$	$2\omega_8+2\omega_9$	$\omega_7+\omega_8+2\omega_9$	$2\omega_8$	$4\omega_8$	$\omega_4+2\omega_9$	$2\omega_8+2\omega_9$	$\omega_5+3\omega_6$	$\omega_4+2\omega_6$	$2\omega_5+2\omega_6$	ω_2	$\omega_1+\omega_5+\omega_6$	$3\omega_5+\omega_6$	$\omega_3+2\omega_9$	$2\omega_4$	$\omega_8+3\omega_9$	$\omega_4+2\omega_5$	$4\omega_5$	$\omega_3+2\omega_6$	$2\omega_7+\omega_8+\omega_9$	$\omega_7+\omega_5+\omega_6$	$\omega_7+\omega_6+\omega_8+\omega_9$	$\omega_3+\omega_4$	$\omega_4+\omega_8+\omega_9$	$\omega_3+2\omega_5$	$2\omega_5+\omega_8+\omega_9$	$6\omega_9$	$2\omega_7+4\omega_9$	$\omega_5+\omega_6+4\omega_9$	$2\omega_3$	$\omega_3+\omega_8+\omega_9$	$2\omega_7+2\omega_9$	$4\omega_7+2\omega_9$	$\omega_7+4\omega_9$	$2\omega_7+4\omega_9$		Σ
6832.0	ψ_0	98	0	0	0	0	0	0	0	0	0	0	0	0	0	0	0	0	0	0	0	0	0	0	0	0	0	0	0	0	0	0	0	0	0	0	0	0	0	0	0	0	0	...	99
873.8	ψ_4	0	94	0	0	1	0	0	0	0	0	0	0	0	0	0	0	0	0	0	0	0	0	0	0	0	0	0	0	0	0	0	0	0	0	0	0	0	0	0	0	0	0	...	97
1071.7	ψ_8	0	0	79	14	0	0	2	0	0	0	0	0	1	0	0	0	0	0	0	0	0	0	0	0	0	1	0	0	0	0	0	0	0	0	0	0	0	0	0	0	0	0	...	98
1113.3	ψ_9	0	1	6	20	61	8	0	0	0	0	0	0	0	0	0	0	0	0	0	0	0	1	0	0	0	0	0	0	0	0	0	0	0	0	0	0	0	0	0	0	0	0	...	98
1169.1	ψ_{10}	0	0	4	45	33	10	1	0	0	0	0	0	0	0	0	0	0	0	0	0	0	1	0	0	0	0	0	0	0	0	0	0	0	0	0	0	0	0	0	0	0	0	...	97
1211.4	ψ_{11}	0	0	1	12	0	76	0	0	0	0	0	0	0	0	0	0	0	1	0	0	0	0	0	0	0	0	0	0	0	0	0	0	0	0	0	0	0	0	0	0	0	0	...	94
1402.3	ψ_{13}	0	0	1	1	0	0	43	50	0	0	0	0	0	0	0	0	0	0	0	0	0	0	0	0	0	0	0	0	0	0	0	0	0	0	0	0	0	0	0	0	0	0	...	97
1415.9	ψ_{15}	0	0	2	0	0	0	50	45	0	0	0	0	0	0	0	0	0	0	0	0	0	0	0	0	0	0	0	0	0	0	0	0	0	0	0	0	0	0	0	0	0	0	...	98
1745.9	ψ_{27}	0	0	0	0	0	0	0	0	80	0	0	0	0	7	1	0	0	0	0	0	0	1	0	0	0	0	0	0	0	0	0	0	0	0	0	0	0	0	0	0	0	0	...	90
1940.9	ψ_{34}	0	0	0	0	0	0	0	0	0	0	0	95	0	0	0	0	0	0	0	0	0	0	0	0	0	0	0	0	0	0	0	0	0	0	0	0	0	0	0	0	0	0	...	97
1953.2	ψ_{36}	0	0	0	0	0	0	0	0	0	80	0	0	1	1	0	0	1	0	0	0	3	0	0	0	0	0	0	0	0	0	0	0	0	0	0	0	0	0	0	0	1	0	0	...	91
2001.0	ψ_{38}	0	0	0	0	0	0	0	0	6	1	22	0	0	58	0	0	0	0	0	1	0	0	2	1	0	0	0	0	0	0	0	0	0	0	0	0	0	0	0	0	0	0	...	93
2052.1	ψ_{42}	0	0	0	0	0	0	0	0	2	0	58	0	0	23	0	0	0	0	0	1	0	1	1	0	0	0	0	0	0	0	0	0	0	0	0	0	0	0	0	0	0	0	...	90
2108.1	ψ_{46}	0	0	0	0	0	0	0	0	1	0	0	0	0	1	81	0	0	0	0	0	1	0	0	0	2	1	0	0	0	0	0	0	0	0	0	0	0	0	0	0	0	0	...	90
2133.6	ψ_{47}	0	0	0	0	0	0	0	0	0	1	0	0	63	0	0	7	0	0	0	0	0	0	0	0	0	0	13	0	1	0	0	0	0	0	0	0	0	0	0	0	0	0	...	92
2153.7	ψ_{50}	0	0	0	0	0	0	0	0	0	0	0	0	0	0	0	0	0	0	92	0	0	0	1	0	0	0	0	0	0	0	0	0	0	0	0	0	0	0	0	0	0	0	...	98
2162.9	ψ_{52}	0	0	0	0	0	0	0	0	0	1	2	0	1	0	0	23	45	7	0	7	0	0	0	0	0	0	1	0	1	0	1	0	0	0	0	0	0	0	0	0	0	0	...	93
2209.4	ψ_{55}	0	0	0	0	0	0	0	0	0	0	1	0	0	1	2	10	0	6	1	33	5	0	20	0	8	1	0	0	1	0	0	0	0	0	0	0	0	0	0	0	0	0	...	91
2252.4	ψ_{57}	0	0	0	0	0	0	0	0	0	0	0	0	0	0	0	28	31	3	1	1	1	0	11	0	2	0	5	0	3	0	1	0	0	0	0	0	0	0	0	0	0	0	...	92
2270.0	ψ_{59}	0	0	0	0	0	0	0	0	1	1	2	0	0	0	0	0	0	1	0	0	0	35	1	44	0	0	0	0	0	0	1	2	0	0	0	0	0	0	0	0	0	0	...	90
2272.2	ψ_{60}	0	0	0	0	1	0	0	0	0	0	0	0	0	1	0	0	6	31	1	2	3	1	37	1	1	0	0	0	1	0	1	0	1	0	0	0	0	0	0	0	0	0	...	92
2291.4	ψ_{62}	0	0	0	0	0	0	0	0	0	2	0	0	0	0	0	0	0	0	0	0	1	45	0	34	2	0	0	0	0	0	1	2	0	0	0	0	0	0	0	0	0	0	...	91
2292.6	ψ_{63}	0	0	0	0	0	0	0	0	0	0	0	0	0	0	2	0	0	6	0	0	19	3	11	2	34	8	0	0	0	0	0	0	1	0	0	0	0	0	0	0	0	0	...	89
2347.3	ψ_{64}	0	0	0	0	0	0	0	0	0	0	0	0	0	0	0	1	2	17	0	43	10	0	6	0	0	2	1	0	4	0	1	0	1	0	0	0	0	0	0	0	0	0	...	92
2381.3	ψ_{68}	0	0	0	0	0	0	0	0	0	0	0	0	0	0	1	0	0	0	0	0	35	0	0	0	17	14	0	0	1	0	0	0	5	0	0	0	0	0	0	0	0	0	...	80
2404.2	ψ_{71}	0	0	0	0	0	0	0	0	0	0	0	0	0	0	0	0	0	1	0	1	3	0	0	0	25	57	0	0	0	0	0	0	0	0	0	0	0	0	0	0	0	0	...	90
2481.8	ψ_{77}	0	0	0	0	0	0	0	0	0	1	0	0	0	0	0	0	0	0	0	0	0	0	0	0	0	0	1	76	4	0	0	1	0	0	0	0	0	0	2	0	0	0	...	89
2510.4	ψ_{79}	0	0	0	0	0	0	0	0	0	0	0	0	2	0	0	1	1	0	0	0	0	1	0	0	0	0	10	2	22	6	24	12	9	0	0	0	0	0	1	0	0	0	...	94
2529.5	ψ_{83}	0	0	0	0	0	0	0	0	0	0	0	0	1	0	0	0	0	0	0	0	0	0	2	0	0	6	3	8	22	2	43	2	0	0	0	0	0	1	0	0	0	0	...	94
2545.2	ψ_{84}	0	0	0	0	0	0	0	0	0	0	0	0	4	0	0	0	1	0	0	0	0	0	0	0	0	18	1	6	3	56	0	1	0	0	0	0	1	0	0	0	0	0	...	94
2573.8	ψ_{88}	0	0	0	0	0	0	0	0	0	0	0	0	0	0	0	0	0	0	0	0	0	0	1	0	0	1	0	0	49	1	30	1	3	0	0	0	0	1	0	0	0	0	...	88
2613.5	ψ_{92}	0	0	0	0	0	0	0	0	1	0	0	0	0	0	0	0	0	0	0	0	0	0	0	0	0	0	0	0	0	0	0	0	61	1	0	0	0	0	0	13	1	...	81
2618.1	ψ_{95}	0	0	0	0	0	0	0	0	0	0	0	0	0	0	0	0	0	0	0	1	0	0	0	0	0	1	0	0	2	0	3	1	81	0	0	0	0	0	0	0	0	...	90
2634.5	ψ_{96}	0	0	0	0	0	0	0	0	0	0	0	0	4	0	0	2	1	1	0	0	1	0	0	0	0	0	16	0	6	1	4	0	43	2	0	0	0	6	0	0	0	0	...	93

[a] Rows of variational vibrational wave functions (Ψ_i) with energy levels ν_i are decomposed in terms of columns of harmonic oscillator (HO) basis states with reference energy levels ω_i. NMD coefficients in percent; energies in cm^{-1} relative to the corresponding variational or harmonic zero-point vibrational (ZPV) level appearing in row 1 or column 1, respectively.

[b] The decomposition was extended to the first 92 A_1 HO states in each row; Σ values denote the corresponding sums of the NMD coefficients over these states.

Table X. The lowest-energy part of the normal-mode decomposition (NMD) table of ketene for A_2 point-group symmetry.

NMD (ν,ω)[a,b]		936.2	1015.5	1498.6	1577.9	1803.4	1882.7	1941.4	2020.7	2082.2	2100.0	2161.5	2179.3	2351.4	2365.8	2430.7	2445.1	2503.8	2583.1	2644.6	2662.4	2670.6	2723.9	2741.7	2749.9	2808.6	2887.9	2913.8	
		ω_6	ω_5	ω_4	ω_3	ω_2	ω_1	$3\omega_6$	$\omega_6+2\omega_4$	$\omega_4+\omega_6$	$2\omega_5+\omega_6$	$\omega_4+\omega_5$	$3\omega_5$	$\omega_5+\omega_6$	$\omega_6+\omega_8$	$\omega_5+\omega_6$	$\omega_5+\omega_8$	$3\omega_6$	$\omega_5+2\omega_6$	$\omega_4+\omega_6$	$2\omega_5+\omega_8$	$\omega_6+5\omega_5$	$\omega_4+\omega_5$	$3\omega_5+\omega_6$	$\omega_5+5\omega_5$	$3\omega_6+3\omega_5$	$\omega_5+2\omega_6$	$\omega_5+\omega_6$		Σ
975.0	ψ_6	94	1	0	0	0	0	0	0	0	0	0	0	0	0	0	0	0	0	0	0	0	0	0	0	0	0	0	...	97
1047.1	ψ_7	1	94	0	0	0	0	0	0	0	0	0	0	0	0	0	0	0	0	0	0	0	0	0	0	0	0	0	...	96
1508.2	ψ_{17}	0	0	93	2	0	0	0	0	0	0	0	0	0	0	0	0	0	0	0	0	0	0	0	0	0	0	0	...	97
1567.3	ψ_{20}	0	0	2	94	0	0	0	0	0	0	0	0	0	0	0	0	0	0	0	0	0	0	0	0	0	0	0	...	96
1847.0	ψ_{31}	0	0	0	0	82	0	1	0	4	0	0	0	1	0	0	0	0	0	0	0	0	0	0	0	0	0	0	...	90
1933.6	ψ_{33}	0	0	0	0	1	81	0	0	0	1	5	1	0	0	0	0	0	0	0	0	0	0	0	0	0	0	0	...	91
2051.0	ψ_{41}	0	0	0	0	1	0	74	2	2	0	0	0	8	0	0	0	0	0	0	0	0	0	0	0	0	0	0	...	91
2085.9	ψ_{45}	0	0	0	0	3	1	0	28	56	1	0	0	0	1	1	0	0	0	0	0	0	0	0	0	0	0	0	...	93
2147.5	ψ_{49}	0	0	0	0	1	2	0	26	12	7	33	2	2	0	2	0	0	0	0	0	0	0	0	0	0	0	0	...	89
2166.9	ψ_{53}	0	0	0	0	0	3	0	21	20	22	23	1	2	0	0	1	0	0	0	0	0	0	0	0	0	0	0	...	94
2230.0	ψ_{56}	0	0	0	0	0	1	0	0	0	49	29	1	1	0	3	0	0	0	0	0	0	0	0	0	0	0	0	...	88
2266.8	ψ_{58}	0	0	0	0	0	1	0	0	0	1	5	81	0	0	0	0	0	0	0	0	0	0	0	0	0	0	0	...	89
2378.4	ψ_{67}	0	0	0	0	1	0	0	1	0	0	0	0	5	75	4	0	0	0	1	0	0	0	0	0	0	0	0	...	90
2414.1	ψ_{72}	0	0	0	0	0	0	5	0	0	0	0	0	52	8	24	1	0	0	0	0	0	0	0	0	0	0	0	...	94
2458.2	ψ_{74}	0	0	0	0	0	0	0	0	0	1	0	0	1	1	0	81	0	0	0	0	0	2	1	0	0	0	0	...	90
2513.4	ψ_{80}	0	0	0	0	0	0	2	4	0	1	0	0	19	0	58	1	0	0	0	0	0	0	0	0	0	0	0	...	90
2570.8	ψ_{87}	0	0	0	0	0	0	1	0	0	0	0	0	0	0	0	0	72	0	1	0	0	0	0	0	0	0	9	...	85
2602.5	ψ_{91}	0	0	0	0	0	0	0	0	0	0	0	0	0	1	0	0	1	38	45	2	0	1	0	0	0	0	0	...	91
2651.0	ψ_{98}	0	0	0	0	0	0	0	0	0	0	0	0	0	0	0	1	0	13	7	21	0	37	3	0	0	0	1	...	87

[a] Rows of variational vibrational wave functions (Ψ_i) with energy levels ν_i are decomposed in terms of columns of harmonic oscillator (HO) basis states with reference energy levels ω_i. NMD coefficients in percent; energies in cm^{-1} relative to the corresponding variational or harmonic zero-point vibrational (ZPV) level appearing in row 1 or column 1 of Table IX, respectively.

[b] The decomposition was extended to the first 58 A_2 HO states in each row; Σ values denote the corresponding sums of the NMD coefficients over these states.

Table XI. The lowest-energy part of the normal-mode decomposition (NMD) table of ketene for B_1 point-group symmetry.

NMD(ν,ω)[a,b]		502.6	581.9	1369.8	1449.1	1507.8	1587.1	1648.6	1666.4	1727.9	1745.7	1917.8	1932.2	1997.1	2011.5	2237.0	2316.3	2375.0	2454.3	2494.6	2513.0	2515.8	2533.6	2573.9	2592.3	2595.1	2612.9	2653.8	2671.6	2699.8	2733.1	2750.9	2779.1	2785.0	2794.6	2799.4	2812.4	2830.2	2864.3	2873.9	2878.7	2891.7	2909.5	2923.0	2937.4	
		ω_8	ω_9	$\omega_4+2\omega_9$	$\omega_4+2\omega_9$	$3\omega_8$	$\omega_4+2\omega_8$	$\omega_4+\omega_8$	$2\omega_4+\omega_8$	$\omega_4+\omega_8$	$3\omega_9$	$\omega_4+\omega_8+\omega_9$	$\omega_4+\omega_8$	$\omega_4+\omega_8+\omega_9$	$\omega_4+4\omega_9$	$\omega_4+4\omega_9$	$3\omega_4+2\omega_9$	$\omega_4+2\omega_4+2\omega_9$	$\omega_4+2\omega_8$	$5\omega_9$	$\omega_4+\omega_8+2\omega_9$	$2\omega_4+\omega_8+2\omega_9$	$\omega_4+2\omega_8$	$\omega_4+4\omega_9$	$\omega_4+\omega_8+2\omega_9$	$3\omega_4+2\omega_9$	$\omega_4+3\omega_8$	$2\omega_4+3\omega_8$	$\omega_4+\omega_8$	$\omega_4+\omega_8+2\omega_9$	$3\omega_4+2\omega_8$	$\omega_4+\omega_8$	$\omega_4+\omega_8+2\omega_9$	$2\omega_4+\omega_8$	$\omega_4+\omega_8+3\omega_9$	$\omega_4+2\omega_4+\omega_8$	$4\omega_4+\omega_8$	$\omega_4+\omega_8+2\omega_9$	$2\omega_4+\omega_8$	$\omega_4+\omega_8+3\omega_9$	$\omega_4+3\omega_8$	$5\omega_8$	$\omega_4+3\omega_8$	$3\omega_4+\omega_8+\omega_9$		Σ
534.0	ψ_2	91	6	0	0	0	0	0	0	0	0	0	0	0	0	0	0	0	0	0	0	0	0	0	0	0	0	0	0	0	0	0	0	0	0	0	0	0	0	0	0	0	0	0	...	99
603.5	ψ_3	5	91	0	0	0	0	0	0	0	0	0	0	0	0	0	0	0	0	0	0	0	0	0	0	0	0	0	0	0	0	0	0	0	0	0	0	0	0	0	0	0	0	0	...	98
1412.4	ψ_{14}	0	0	90	0	0	0	1	0	0	0	0	0	0	0	0	0	0	0	0	0	0	0	0	0	0	0	0	0	0	0	0	0	1	0	0	0	0	0	0	0	0	0	0	...	94
1490.5	ψ_{16}	0	0	0	90	0	0	0	0	2	1	0	0	0	0	0	0	0	0	0	0	0	0	0	0	0	0	0	0	0	0	0	0	0	0	0	0	0	0	0	0	0	0	0	...	94
1607.2	ψ_{21}	0	0	1	0	68	16	1	1	0	0	6	0	0	0	0	0	0	0	0	1	0	0	0	0	0	0	0	0	0	0	0	0	0	0	0	0	0	0	0	0	0	1	0	...	96
1637.7	ψ_{23}	0	0	1	1	7	16	55	7	5	1	1	0	0	0	0	0	0	0	0	0	0	0	0	0	0	0	0	0	0	0	0	0	1	0	0	0	0	0	0	0	0	0	0	...	96
1702.3	ψ_{25}	0	0	0	1	1	15	0	12	50	8	1	0	1	0	0	0	0	0	0	0	0	0	0	0	0	0	1	0	0	0	0	0	0	0	0	0	0	1	0	0	0	0	0	...	93
1714.8	ψ_{26}	0	0	0	0	2	30	35	19	1	1	3	0	1	0	0	0	0	0	0	0	0	0	0	1	0	0	1	0	0	0	0	0	0	1	0	0	0	0	0	0	0	0	0	...	96
1784.2	ψ_{28}	0	0	0	0	0	4	1	39	36	4	2	0	3	0	0	0	0	0	0	0	0	0	0	0	0	0	0	1	0	1	0	0	0	0	0	0	0	0	1	0	0	0	0	...	93
1808.0	ψ_{29}	0	0	0	0	0	0	0	7	2	74	0	0	1	0	0	0	0	0	0	0	0	0	0	0	0	0	0	0	0	1	0	0	0	0	0	0	1	0	0	0	0	0	0	...	87
1943.3	ψ_{35}	0	0	0	0	1	1	0	0	0	0	7	77	6	0	0	0	0	0	0	0	0	0	0	0	0	0	0	0	0	0	0	0	0	0	0	0	0	0	0	0	0	0	0	...	95
1966.9	ψ_{37}	0	0	0	0	5	0	0	0	0	0	47	14	28	0	0	0	0	0	0	0	0	0	0	0	0	0	0	0	0	0	0	0	0	0	0	0	0	0	0	0	0	1	0	...	97
2013.2	ψ_{39}	0	0	0	0	0	0	0	1	0	0	1	0	0	91	0	0	0	0	0	0	0	0	0	0	0	0	0	0	0	0	0	0	0	0	0	0	0	0	0	0	0	0	0	...	94
2077.8	ψ_{43}	0	0	0	0	3	5	0	1	0	0	25	0	54	0	0	0	0	0	0	0	0	0	0	0	0	0	0	0	0	0	0	0	0	0	0	0	0	0	0	0	0	1	0	...	96
2279.4	ψ_{61}	0	0	0	0	0	0	0	0	0	0	0	0	0	0	72	2	1	0	0	0	6	0	0	0	0	0	0	0	0	0	0	0	1	0	0	0	0	0	0	0	0	0	0	...	84
2376.2	ψ_{66}	0	0	0	0	0	0	0	0	0	0	0	0	0	0	2	70	0	1	0	0	1	1	0	0	8	2	0	0	0	0	0	0	0	0	0	0	0	0	1	0	0	0	0	...	87
2475.9	ψ_{75}	0	0	0	0	0	0	0	0	0	0	0	1	0	0	0	0	1	0	90	0	0	0	0	0	0	0	0	0	0	0	0	0	0	0	0	0	0	0	0	0	0	0	0	...	93
2481.7	ψ_{76}	0	0	0	0	0	0	0	0	0	0	0	0	0	0	1	0	61	0	1	1	5	0	0	0	0	0	1	0	0	0	0	0	7	0	0	0	0	0	0	0	0	1	0	...	82
2528.0	ψ_{81}	0	0	0	0	0	0	0	0	0	0	0	0	0	0	0	0	0	0	0	1	0	91	0	0	0	0	0	0	0	0	0	0	0	0	0	0	0	0	0	0	0	0	0	...	94
2529.2	ψ_{82}	0	0	0	0	0	0	0	0	0	0	0	0	0	0	5	0	5	26	0	0	41	0	2	0	1	0	1	0	0	1	0	0	0	1	1	0	0	1	0	0	0	0	0	...	88
2586.9	ψ_{90}	0	0	0	0	0	0	0	0	0	0	0	0	0	0	3	1	0	25	0	0	24	6	0	0	15	0	0	0	0	0	0	0	2	1	0	1	0	2	1	0	0	0	0	...	84
2615.4	ψ_{93}	0	0	0	0	0	0	0	0	0	0	0	0	0	0	0	5	0	15	0	0	9	18	0	0	32	0	0	1	0	1	1	0	1	0	0	1	0	0	2	1	1	0	0	...	89
2635.4	ψ_{97}	0	0	0	0	0	0	0	0	0	0	0	0	0	0	0	0	2	0	0	49	0	0	0	0	0	0	1	0	0	0	0	0	0	0	0	0	0	0	0	0	0	18	0	...	74

[a] See footnote a to Table X.

[b] The decomposition was extended to the first 71 B_1 HO states in each row; Σ values denote the corresponding sums of the NMD coefficients over these states.

Table XII. The lowest-energy part of the normal-mode decomposition (NMD) table of ketene for B_2 point-group symmetry.

NMD(ν,ω)[a,b]		433.6	996.0	1300.8	1438.8	1518.1	1579.6	1597.4	1848.8	1863.2	2001.2	2080.5	2142.0	2159.8	2168.0	2306.0	2385.3	2411.2	2425.6	2444.0	2446.8	2464.6	2523.3	2584.8	2602.6	2630.8	2664.1	2681.9	2716.0	2725.6	2730.4	2743.4	2761.2	2854.0	2868.4	2933.3	2947.7	
		ω_9	ω_8	$3\omega_9$	$2\omega_8+\omega_9$	$\omega_8+\omega_6+\omega_9$	$\omega_8+\omega_9$	$2\omega_8+\omega_9$	$\omega_8+\omega_9$	$\omega_8+2\omega_9$	$2\omega_8+\omega_8$	$\omega_8+\omega_6+\omega_8$	$\omega_8+\omega_8$	$2\omega_8+\omega_8$	$5\omega_9$	$2\omega_8+3\omega_9$	$\omega_8+\omega_6+3\omega_9$	$\omega_8+\omega_8$	$2\omega_8+\omega_9$	$4\omega_8+\omega_9$	$\omega_8+3\omega_9$	$2\omega_8+3\omega_9$	$\omega_8+3\omega_6+\omega_9$	$\omega_8+2\omega_6+\omega_9$	$2\omega_8+2\omega_6+\omega_9$	$\omega_8+\omega_9$	$\omega_8+\omega_6+\omega_6+\omega_9$	$3\omega_8+\omega_6+\omega_9$	$\omega_8+3\omega_9$	$2\omega_8+\omega_9$	$\omega_8+4\omega_9$	$\omega_8+2\omega_8+\omega_9$	$4\omega_8+\omega_9$	$\omega_8+2\omega_6+\omega_9$	$2\omega_8+\omega_8+2\omega_9$	$\omega_8+\omega_8+\omega_6+\omega_9$	$\omega_8+\omega_8+2\omega_9$		Σ
437.1	ψ_1	98	0	0	0	0	0	0	0	0	0	0	0	0	0	0	0	0	0	0	0	0	0	0	0	0	0	0	0	0	0	0	0	0	0	0	...	98
972.6	ψ_5	0	97	0	0	0	0	0	0	0	0	0	0	0	0	0	0	0	0	0	0	0	0	0	0	0	0	0	0	0	0	0	0	0	0	0	...	98
1310.1	ψ_{12}	0	0	88	0	0	4	0	0	0	0	0	0	0	0	0	0	0	0	0	0	0	0	0	0	0	0	0	0	0	0	0	0	0	0	0	...	94
1516.2	ψ_{18}	0	0	0	85	4	0	0	2	0	0	0	0	0	0	0	0	0	0	1	0	0	0	0	0	0	0	0	0	0	0	0	1	0	0	0	...	95
1558.2	ψ_{19}	0	0	3	0	23	65	2	0	1	0	0	0	0	0	0	0	0	0	0	0	0	0	0	0	0	0	0	0	0	0	0	0	0	0	0	...	96
1612.7	ψ_{22}	0	0	1	2	60	27	1	1	0	0	0	0	0	0	0	0	0	0	0	0	0	1	0	0	0	0	0	0	0	0	0	0	0	0	0	...	94
1659.0	ψ_{24}	0	0	0	0	1	1	88	0	0	0	0	0	0	0	0	0	0	0	0	0	0	0	0	0	0	0	0	0	0	0	0	0	0	0	0	...	92
1836.0	ψ_{30}	0	0	0	1	1	0	0	40	48	0	0	1	0	0	0	0	0	0	0	0	0	0	0	0	0	0	0	0	0	0	0	0	0	0	0	...	94
1854.2	ψ_{32}	0	0	0	2	0	0	0	50	41	0	0	1	0	0	0	0	0	0	0	0	0	0	0	0	0	0	0	0	0	0	0	0	0	0	0	...	95
2044.9	ψ_{40}	0	0	0	0	0	0	0	0	0	84	5	0	0	0	0	0	3	0	0	0	0	0	0	0	0	0	0	0	0	0	0	0	0	0	0	...	96
2080.1	ψ_{44}	0	0	0	0	0	0	0	0	1	1	33	54	5	0	0	0	0	1	0	0	0	0	0	0	0	0	0	0	0	0	0	0	0	0	0	...	96
2133.6	ψ_{48}	0	0	0	0	0	0	0	0	0	1	51	36	0	0	0	0	1	0	0	0	0	0	0	0	0	0	0	0	0	0	0	0	0	0	0	...	94
2161.5	ψ_{51}	0	0	0	0	0	0	0	0	0	0	0	4	87	0	0	0	0	0	0	0	0	0	0	0	0	0	0	0	0	0	0	0	0	0	0	...	93
2178.1	ψ_{54}	0	0	0	0	0	0	0	0	0	0	0	0	0	71	1	0	0	0	0	10	1	0	0	0	0	0	0	1	0	0	0	0	0	0	0	...	86
2364.0	ψ_{65}	0	0	0	0	0	0	0	0	0	2	1	0	0	0	0	0	50	38	0	0	0	0	0	0	0	0	0	0	0	0	0	0	0	0	0	...	94
2384.3	ψ_{69}	0	0	0	0	0	0	0	0	0	1	0	0	0	0	20	0	28	37	1	1	0	0	1	0	0	0	0	1	0	0	0	0	0	0	0	...	92
2384.9	ψ_{70}	0	0	0	0	0	0	0	0	0	0	0	0	0	0	50	0	11	16	1	2	0	0	2	0	0	0	0	2	0	0	0	0	1	0	0	...	87
2442.0	ψ_{73}	0	0	0	0	0	0	0	0	0	0	0	0	0	8	2	19	0	0	0	48	0	0	1	0	0	2	0	0	5	1	0	0	0	0	0	...	89
2489.3	ψ_{78}	0	0	0	0	0	0	0	0	0	0	0	0	0	3	0	50	0	0	0	21	2	1	0	0	0	2	1	0	2	0	0	0	0	0	0	...	85
2557.8	ψ_{85}	0	0	0	0	0	0	0	0	0	0	0	0	0	1	0	3	0	0	0	2	69	0	0	1	0	1	1	0	0	0	5	3	0	0	0	...	87
2568.2	ψ_{86}	0	0	0	0	0	0	0	0	0	0	0	0	0	0	2	0	0	0	55	0	0	0	5	0	1	0	0	0	0	0	0	0	13	0	0	...	79
2585.5	ψ_{89}	0	0	0	0	0	0	0	0	0	0	0	0	0	0	0	0	0	0	0	0	0	0	0	0	93	0	0	0	1	0	0	0	0	0	0	...	95
2615.8	ψ_{94}	0	0	0	0	0	0	0	0	0	0	0	0	0	0	3	2	0	0	5	0	0	32	37	0	0	0	0	0	0	0	0	0	1	3	0	...	87
2662.2	ψ_{99}	0	0	0	0	0	0	0	0	0	0	0	0	0	0	1	2	0	0	0	2	1	5	9	12	0	35	0	0	14	0	0	0	0	0	2	1	...	86

[a] See footnote a to Table X.

[b] The decomposition was extended to the first 69 B_2 HO states in each row; Σ values denote the corresponding sums of the NMD coefficients over these states.

3.2.5 Rovibrational energy levels

The ketene molecule is very nearly a prolate symmetric top, with (A_0, B_0, C_0) rotational constants close to (9.41, 0.34, 0.33) cm^{-1}, in order. Thus, the pure rotational levels can be approximated very well by the simple expression $E(J, K_a) = 0.34J(J+1) + 9.07K_a^2$. Accordingly, a near double degeneracy for all values of $K_a \geq 1$ can be expected and this is seen in the rovibrational levels in Tables XIII and XIV, listing selected variational (DEWE) and experimental (MARVEL) levels (the complete Table XIV can be found in the Supplementary Material of Ref. [22]). Closing of the doubly-degenerate pairs becomes more pronounced when one goes to higher energies and K_a values though occasionally perturbations cause deviations from this trend. Figure 3 shows the deviations of the pure rotational DEWE (panel A) and MARVEL (panel B) levels from the rigid-rotor (RR) picture, based on the ground-state rotational constants [117] $A_0 = 9.409\ 209$, $B_0 = 0.343\ 370$, and $C_0 = 0.330\ 737$ cm^{-1}. Both the DEWE and the MARVEL levels show the expected pronounced degeneracy (note, however, that the scales of panels A and B of Figure 3 are very different). The DEWE and the MARVEL results also show a clear J-independence and K_a-dependence of the deviations.

The variational differences between the $J_{K_a,J+1-K_a}$ and $J_{K_a,J-K_a}$ pairs are often an order of magnitude smaller than the "measured" ones (see Supplementary Material of Ref. [22]). This is most likely due to deficiencies of the force field used as a model of the PES of ketene.

As to the performance of the VS method, it is worth comparing the energies obtained from a computation with the complete vibrational space of size $8 \cdot 10^7$ (DEWE in Table XIII), performed up to $J = 3$, to those obtained with a reduced vibrational space of dimension 10^2 (DEWE-VS in Tables XIII and XIV). In spite of the 10^6-fold reduction of the size of the rovibrational basis and the corresponding reduction in storage and other resources required to perform the computations, the overall agreement of the first few hundred rovibrational states is better than 1 cm^{-1}. Thus, the error introduced due to this truncation of the vibrational space is less than the uncertainty of the underlying PES. The accuracy of the rovibrational energy levels obtained within the DEWE-VS protocol could easily be increased further by including more vibrational eigenstates in the computation. This would preferentially include all the fundamentals of the molecule and all states in between. Naturally, by increasing the size of the vibrational subspace in the second stage of the rovibrational computation the rovibrational limit corresponding to the complete set

of the original primitive vibrational basis functions is approached.

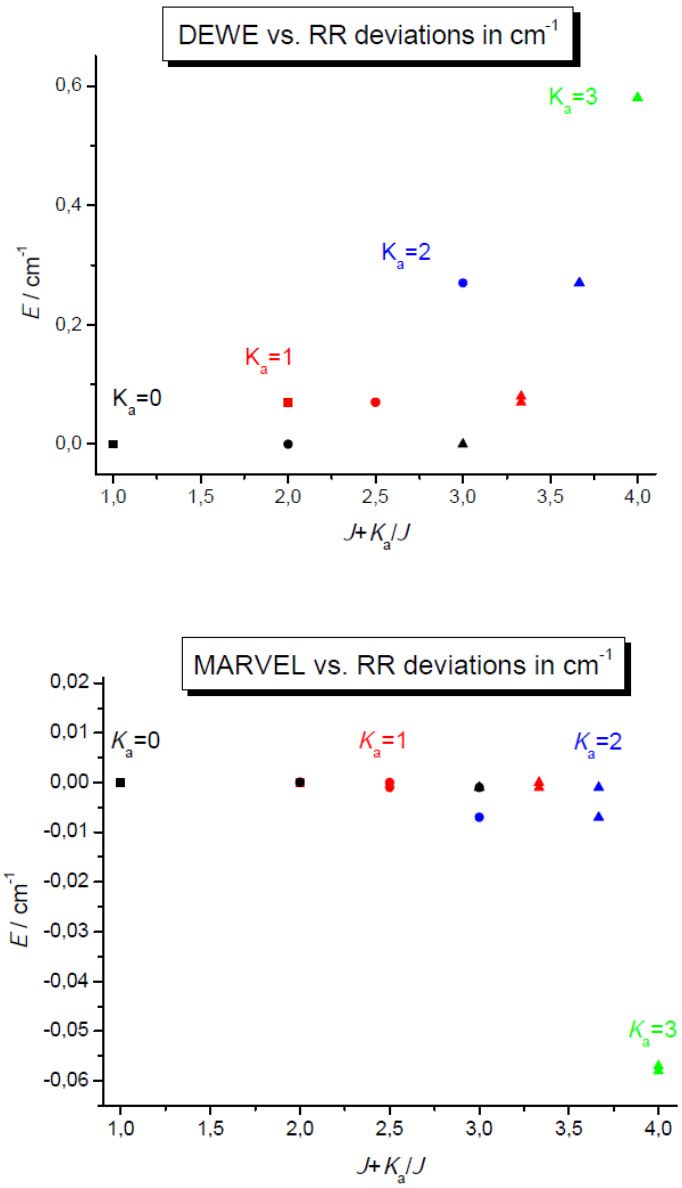

Figure 3: Deviations of the variational DEWE and the MARVEL pure rotational energy levels from those levels (RR) corresponding to a rigid rotor picture with rotational constants $A_0 = 9.409209$, $B_0 = 0.343370$, and $C_0 = 0.330737$ cm^{-1}. Squares, circles, and triangles correspond to $J = 1$, 2, and 3, respectively.

Table XIII. Active database (MARVEL) and variational quantum mechanical (DEWE) rotational-vibrational energy levels (cm^{-1}) for $J = 1-3$ for $H_2{}^{12}C{=}{}^{12}C{=}{}^{16}O$ in order of increasing J and energy for the vibrational states GS, $9^1 = \nu_9$, $6^1 = \nu_6$, and $5^1 = \nu_5$, with asymmetric-top rotational labels (J K_a K_c), symmetry (S) information, and MARVEL classification (Class., see text for details) and uncertainties (U, 10^{-6} cm^{-1}). The DEWE-VS - DEWE deviations (Δ, cm^{-1}) are reported under DEWE, in parentheses. The size of the vibrational basis for the DEWE computations is $10^3 \cdot 8^2 \cdot 6^4$, that is $8 \cdot 10^7$, while that of the DEWE-VS computations is 10^2.

	GS				ν_9				ν_6				ν_5			
J K_a K_c	S	Class.	MARVEL [U]	DEWE (Δ)	S	Class.	MARVEL [U]	DEWE (Δ)	S	Class.	MARVEL [U]	DEWE (Δ)	S	Class.	MARVEL [U]	DEWE (Δ)
1 0 1	A_2	A	0.6741 [1]	0.67 (0.01)	B_1	A	440.0612 [231]	440.06 (0.01)	B_2	A	526.7454 [224]	526.72 (0.04)	B_2	A	588.1028 [226]	588.09 (0.02)
1 1 1	B_1	A	9.7395 [1]	9.81 (0.08)	A_2			447.28 (0.10)	A_1	B	536.0447 [387]	536.58 (0.13)	A_1		598.3116 [273]	598.05 (0.28)
1 1 0	B_2	A	9.7521 [1]	9.82 (0.08)	A_1			447.30 (0.11)	A_2			536.59 (0.15)	A_2		598.3229 [358]	598.06 (0.32)
2 0 2	A_1	A	2.0223 [1]	2.02 (0.01)	B_2	A	441.4109 [216]	441.41 (0.01)	B_1	A	528.0947 [226]	528.07 (0.03)	B_1	A	589.4521 [220]	589.43 (0.03)
2 1 2	B_2	A	11.0750 [1]	11.15 (0.07)	A_1			448.62 (0.10)	A_2	A	537.3827 [384]	537.92 (0.15)	A_2	B	599.6491 [261]	599.38 (0.28)
2 1 1	B_1	A	11.1128 [1]	11.18 (0.08)	A_2			448.66 (0.11)	A_1			537.95 (0.13)	A_1	B	599.6843 [354]	599.42 (0.32)
2 2 1	A_2	A	38.3011 [164]	38.58 (0.29)	B_1		470.4844 [355]	470.65 (0.36)	B_2		565.0305 [299]	567.17 (0.44)	B_2		630.2861 [316]	629.34 (1.00)
2 2 0	A_1	A	38.3001 [463]	38.58 (0.29)	B_2		470.4845 [340]	470.65 (0.39)	B_1		565.0305 [345]	567.17 (0.57)	B_1		630.2863 [290]	629.34 (1.15)
3 0 3	A_2	A	4.0446 [1]	4.04 (0.01)	B_1	B	443.4389 [215]	443.44 (0.01)	B_2	B	530.1176 [281]	530.09 (0.04)	B_2	B	591.4766 [221]	591.46 (0.03)
3 1 3	B_1	A	13.0783 [1]	13.15 (0.07)	A_2			450.63 (0.10)	A_1	B	539.3884 [381]	539.92 (0.16)	A_1	B	601.6561 [256]	601.38 (0.29)
3 1 2	B_2	A	13.1539 [1]	13.23 (0.07)	A_1			450.71 (0.11)	A_2			539.99 (0.13)	A_2		601.7264 [354]	601.46 (0.32)
3 2 2	A_1	A	40.3230 [164]	40.6 (0.29)	B_2	B	472.5122 [352]	472.67 (0.37)	B_1	B	567.0534 [298]	569.19 (0.44)	B_1	B	632.3104 [315]	631.36 (1.01)
3 2 1	A_2	A	40.3221 [463]	40.6 (0.29)	B_1	B	472.5123 [337]	472.67 (0.40)	B_2	B	567.0535 [345]	569.19 (0.57)	B_2	B	632.3106 [286]	631.36 (1.15)
3 3 1	B_1	B	85.6354 [168]	86.27 (0.64)	A_2			510.13 (0.79)	A_1		612.4090 [527]	616.96 (1.12)	A_1			681.34 (2.12)
3 3 0	B_2	A	85.6360 [142]	86.27 (0.64)	A_1			510.13 (0.86)	A_2		612.4081 [682]	616.96 (1.41)	A_2			681.35 (2.43)

Table XIV. Selected higher-J ($J \geq 4$) variational quantum mechanical (DEWE-VS) rotational-vibrational energy levels (cm^{-1}) which have active database (MARVEL) counterparts for $H_2{}^{12}C{=}{}^{12}C{=}{}^{16}O$ in order of increasing J and energy for the vibrational states GS, $9^1 = \nu_9$, $6^1 = \nu_6$, and $5^1 = \nu_5$, with asymmetric-top rotational labels (J K_a K_c), symmetry (S) information, and MARVEL classification (Class.) and uncertainties (U, 10^{-6} cm^{-1}). See Table IX in the Supplementary Material of Ref. [22] for the full table containing 238 rows.

	GS				ν_9				ν_6				ν_5			
J K_a K_c	S	Class.	MARVEL [U]	DEWE-VS	S	Class.	MARVEL [U]	DEWE-VS	S	Class.	MARVEL [U]	DEWE-VS	S	Class.	MARVEL [U]	DEWE-VS
4 0 4	A_1	A	6.7408 [1]	6.74	B_2	B	446.1430 [137]	446.15	B_1	B	532.8153 [146]	532.82	B_1	B	594.1760 [144]	594.17
4 1 4	B_2	A	15.7494 [1]									15.89	A_2	B	604.3319 [256]	604.33
4 1 3	B_1	A	15.8753 [1]	16.01												
4 2 3	A_2	A	43.0189 [164]	43.58					B_2	B	569.7509 [197]	572.45	B_2	B	635.0096 [164]	635.05
4 2 2	A_1	A	43.0191 [184]	43.58					B_1	B	569.7508 [169]	572.32	B_1	B	635.0115 [266]	635.20
4 3 2	B_2	A	88.3307 [168]	89.60												
4 3 1	B_1	A	88.3312 [142]	89.60					A_1	B	615.1058 [343]	620.77				
5 0 5	A_2	A	10.1110 [1]	10.11	B_1	B	449.5228 [132]	449.53	B_2	B	536.1874 [140]	536.19	B_2	B	597.5500 [140]	597.55
5 1 5	B_1	A	19.0882 [1]	19.23												
5 1 4	B_2	A	19.2770 [1]	19.42												
5 2 4	A_1	A	46.3887 [164]	46.95					B_1	B	573.1224 [107]	575.83	B_1	B	638.3833 [161]	638.43
5 2 3	A_2	A	46.3892 [184]	46.95					B_2	B	573.1225 [83]	575.69	B_2	B	638.3854 [264]	638.57
5 3 3	B_1	A	91.6997 [168]	92.97					A_1	B	618.4756 [305]	624.43				
5 3 2	B_2	A	91.7003 [142]	92.97					A_2	B	618.4765 [339]	624.14				
5 4 2					B_2	B	569.0673 [563]	571.21	B_1	B	681.0352 [545]	691.34	B_1	B	760.1568 [580]	760.91
5 4 1	A_2	B	155.0751 [420]	157.35	B_1	B	569.0685 [607]	571.32	B_2	B	681.0364 [590]	690.83	B_2	B	760.1577 [653]	761.45

	GS				ν_9				ν_6				ν_5			
J K_a K_c	S	Class.	MARVEL [U]	DEWE-VS	S	Class.	MARVEL [U]	DEWE-VS	S	Class.	MARVEL [U]	DEWE-VS	S	Class.	MARVEL [U]	DEWE-VS
5 5 1	B_2	A	236.4289 [505]	240.04												
5 5 0	B_1	A	236.4301 [554]	240.04												
6 0 6	A_1	A	14.1551 [1]	14.16	B_2	B	453.5782 [131]	451.28	B_1	B	540.2337 [138]	548.18	B_1	B	601.5987 [140]	617.70
6 1 6	B_2	A	23.0947 [1]	23.23					A_2	B	549.4172 [255]	558.05	A_2	B	611.6901 [240]	627.79
6 1 5	B_1	A	23.3590 [1]	23.50									A_1	B	611.9362 [188]	628.08
6 2 5	A_2	A	50.4324 [164]	50.99	B_1	B	482.6511 [181]	480.87	B_2	B	577.1682 [190]	587.82	B_2	B	642.4317 [160]	658.58
6 2 4	A_1	A	50.4334 [184]	50.99	B_2	B	482.6521 [177]	480.90	B_1	B	577.1687 [163]	587.68	B_1	B	642.4342 [265]	658.73
6 3 4	B_2	A	95.7426 [168]	97.01					A_2	B	622.5204 [303]	636.42				
6 3 3	B_1	A	95.7432 [142]	97.01					A_1	B	622.5213 [338]	636.13				
6 4 3					B_1	B	573.1209 [562]	572.96	B_2	B	685.0786 [544]	703.33	B_2	B	764.2030 [580]	781.06
6 4 2	A_1	B	159.1166 [420]	161.39	B_2	B	573.1221 [606]	573.06	B_1	B	685.0797 [589]	702.82	B_1	B	764.2031 [702]	781.60
6 5 2	B_2	A	240.4686 [505]	244.08												
6 5 1	B_1	A	240.4697 [554]	244.08												
7 0 7	A_2	A	18.8730 [1]	18.87	B_1	B	458.3092 [133]	456.01	B_2	B	544.9542 [140]	552.91	B_2	B	606.3220 [141]	622.42
7 1 7	B_1	A	27.7688 [1]	27.91					A_1	B	554.0971 [254]	562.73	A_1	B	616.3726 [240]	632.47
7 1 6	B_2	A	28.1213 [1]	28.26									A_2	B	616.7007 [185]	632.84
7 2 6	A_1	A	55.1500 [164]	55.71	B_2	B	487.3822 [182]	485.60	B_1	B	581.8882 [190]	592.54	B_1	B	647.1547 [162]	663.30
7 2 5	A_2	A	55.1517 [184]	55.71	B_1	B	487.3843 [174]	485.64	B_2	B	581.8892 [164]	592.41	B_2	B	647.1479 [271]	663.45
7 3 5	B_1	A	100.4593 [168]	101.73					A_1	B	627.2393 [303]	641.14				
7 3 4	B_2	A	100.4599 [142]	101.73					A_2	B	627.2402 [339]	640.85				
7 4 4					B_2	B	577.8502 [562]	577.69	B_1	B	689.7958 [544]	708.05				
7 4 3	A_2	A	163.8316 [420]	166.11	B_1	B	577.8513 [606]	577.80	B_2	B	689.7969 [589]	707.54				
7 5 3	B_1	A	245.1815 [505]	248.79												
7 5 2	B_2	A	245.1826 [554]	248.80												

	GS				ν_9				ν_6				ν_5			
J K_a K_c	S	Class.	MARVEL [U]	DEWE-VS	S	Class.	MARVEL [U]	DEWE-VS	S	Class.	MARVEL [U]	DEWE-VS	S	Class.	MARVEL [U]	DEWE-VS
8 0 8	A_1	A	24.2645 [1]	24.27	B_2	B	463.7157 [138]	461.42	B_1	B	550.3487 [144]	558.30	B_1	B	611.7197 [145]	627.81
8 1 8	B_2	A	33.1106 [1]	33.25					A_2	B	559.4454 [256]	568.08				
8 1 7	B_1	A	33.5638 [1]	33.70									A_1	B	622.1457 [187]	638.28
8 2 7	A_2	A	60.5415 [217]	61.10					B_2	B	587.2824 [194]	597.94	B_2	B	652.5524 [166]	668.69
8 2 6	A_1	A	60.5443 [184]	61.10	B_2	B	492.7927 [175]	491.05	B_1	B	587.2843 [168]	597.80	B_1	B	652.5465 [276]	668.84
8 3 6	B_2	A	105.8498 [168]	107.12												
8 3 5	B_1	A	105.8503 [142]	107.12					A_1	B	632.6332 [341]	646.24				
8 4 5									B_2	B	695.1868 [545]	713.44				
8 4 4	A_1	A	169.2202 [420]	171.49					B_1	B	695.1879 [591]	712.93				
8 5 4	B_2	A	250.5676 [505]	254.18												
8 5 3	B_1	A	250.5687 [554]	254.18												
9 0 9	A_2	A	30.3296 [1]	30.33												
10 0 10	A_1	A	37.0679 [220]	37.07												
11 0 11	A_2	A	44.4796 [220]	44.48												
12 0 12	A_1	A	52.5644 [220]	52.57												
13 0 13	A_2	A	61.3220 [220]	61.32												
14 0 14	A_1	A	70.7524 [313]	70.75												
15 0 15	A_2	A	80.8552 [313]	80.86												
20 0 20	A_1	A	141.4475 [576]	141.45												
25 0 25	A_2	A	218.8099 [789]	218.82												
30 0 30	A_1	B	312.9006 [1398]	312.92												
35 1 35	B_1	A	429.4011 [637]	429.57												
39 1 38	B_2	B	539.1255 [857]	539.27												
45 0 45	A_2			695.08	B_1			1133.92	B_2			1230.17	B_2			1299.51
50 0 50	A_1			855.58	B_2			1294.72	B_1			1391.01	B_1			1460.32

3.2.6 MARVEL energy levels

In order to improve our understanding of the measured spectra and validate the experimental assignments proposed for ketene lines, we analyzed simultaneously all the experimental line information available to us [109, 113, 117, 118, 119, 120, 121, 122], as indicated in Table VII.

The MARVEL analysis employed proved to be successful for a similar analysis of the rovibrational states of several water isotopologues [43, 123, 124, 125]. During the present study we utilized altogether 3 982 measured and assigned rovibrational transitions of $H_2{}^{12}C{=}{}^{12}C{=}{}^{16}O$. Due to nuclear spin symmetry, these transitions form part of two main spectroscopic networks (SN) [116], ortho and para. The selection rules governing the transitions are given in the Supplementary Material of Ref. [22].

We had two main difficulties with the measured data. First, in many of the original publications the uncertainties of the measured transitions were not given explicitly. Therefore, we had to assign reasonable uncertainties to several transitions based on the best available information deduced from the original sources. This, however, is not a serious problem as MARVEL adjusts, via robust reweighting, the uncertainties attached to the transitions until self-consistency within the database is achieved. Second, as almost always happens with measured transitions, some of them are not part of the main networks but are part of floating spectroscopic networks (FSNs) or are orphans. Since orphan energy levels and those taking part in FSNs cannot be validated, only 3 194 transitions could be validated in this work. Transitions which could not be validated are indicated in Table VII source by source.

The ortho and the para SNs contain 2 489 and 705 observed transitions and 1 251 and 471 MARVEL energy levels, respectively. The MARVEL energy levels of A and B quality go up to $J = 39$ for the vibrational ground state and up to $J = 8$ for the other states. Most highly excited rotational and rovibrational energy levels take part in only a single measured transition. Thus, their accuracy remain uncertain even after the MARVEL validation procedure.

Due to the sparsity of measurements for parent ketene, there are relatively few energy levels of A quality for all but the ground vibrational state (see Tables XIII and XIV). Thus, since in Tables XIII and XIV only MARVEL levels of A and B quality are given, for the excited vibrational states there are plenty of missing levels under the heading MARVEL. The computed levels of C quality should be handled with special care: they may be inaccurate

as they are determined by insufficient experimental information, by just a single measured and assigned transition. Thus, though they are given in the Supplementary Material of Ref. [22], they should be used only with caution.

Figure 4 presents a comparison of absolute differences, given on a semi-logarithmic scale and as a function of the energy of the levels, between the pure rotational MARVEL energy levels of this study and those reported in the CDMS database [108] and determined via an effective Hamiltonian based on fitted spectroscopic parameters. Note that energy values having K_a larger than 5 are missing from the figure as no validated experimental data, and thus no MARVEL energy levels, are available for them. The figure clearly shows deviations between the two sets of results. Since the MARVEL energy levels involved in creation of the figure are not only of A and B quality, it cannot be concluded that they present better representation for these levels. Only further experimental studies and a new list of relevant assigned transitions would be able to solve this problem.

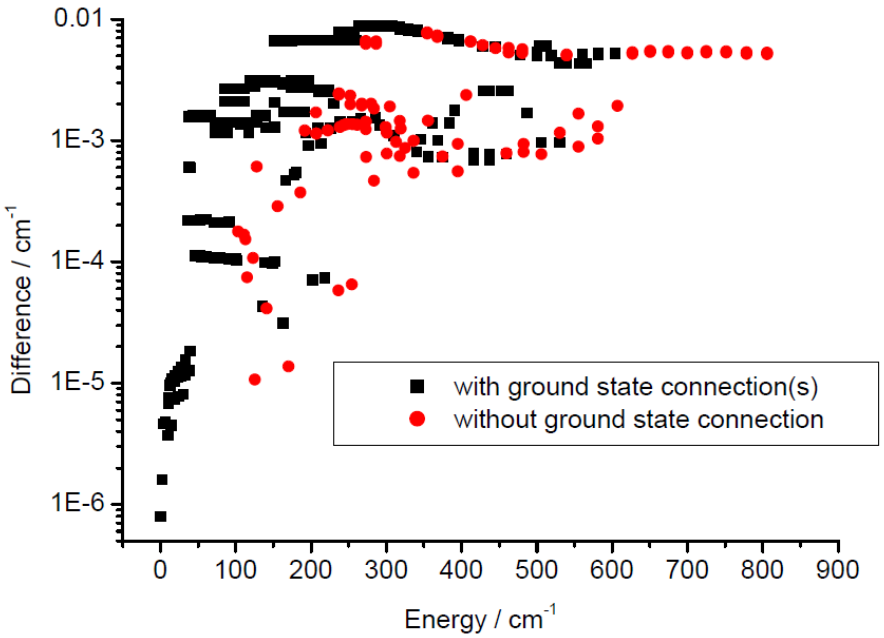

Figure 4: Absolute differences, on a semi-logarithmic scale, between the pure rotational MARVEL energy levels obtained in this study and those levels reported in the CDMS database [108] as a function of the energy of the level.

3.2.7 New assignments

The apodized resolution in the mid-infrared high resolution IR gas-phase spectra of ketene [107] was approximately 0.004 cm^{-1}, and the relative frequency calibration accuracy was better than 0.001 cm^{-1} as determined by comparison with extensive, known ground state combination differences (CD) [126]. The absolute wavenumbers have errors smaller than the apodized resolution, a conservative estimate is 0.001 cm^{-1}. These spectra contain several thousand lines, and a sizeable portion of these are difficult to assign using ground-state CDs, partly because of their low intensity or location in very congested spectral areas, and partly as combination differences require additional transitions involving some of the levels that are also involved in the transitions to be assigned. (The method of combination differences makes use of the fact that some transitions share a common level). In addition, there are localized resonances in the spectra that perturb regularity. Thus, there is a great need of an independently determined set of rotation-vibration energy levels to facilitate line identification. Such levels of high quality have been obtained in this work using the MARVEL technique validated via the variational nuclear motion DEWE-VS results. The complete list of MARVEL energy levels is presented in the Supplementary Material of Ref. [22]. The presently available energy levels allow a host of new assignments relative to those obtained in previous works [127, 128, 129]. Note also that the vibration-rotation transitions used in Refs. [127] and [128] were not published there explicitly.

We have searched the FTIR spectra [107] of ketene for regions that had previously not been analyzed by the usual CD methods and thus were not used in perturbation calculations by least-squares fits. In what follows two specific series are given involving lines of rovibrational branches of two fundamentals. The specific examples of newly assigned sets of transitions are given in Table XV, which convincingly show the great utility of experimental-quality MARVEL energy levels to make progress in assigning a high-resolution spectrum.

The first branch is the ${}^{r}R_1(J)$ series of the $\nu_5 = 5^1$ vibrational fundamental that extends from 621.24 to 627.75 cm^{-1} for lines involving lower state $J = 2$ up to $J = 11$ (10 lines). The assignment of this clearly visible series was not attempted earlier due to lack of CD transition partners. These lines occur in a congested region but are clearly indentifiable due to their narrow profiles and no lines in their close neighbourhood. The differences between the MARVEL and experimental lines are nowhere greater than a couple of times 10^{-4} cm^{-1}; thus, the line identifications are unique. (Note also that although we give

Table XV. New line identifications, based on MARVEL energy levels and associated transitions, of two series of lines (GS-$J_{1J} - 5^1$-$(J+1)_{2J}$ for ν_5 and GS-$J_{1J} - 8^1$-$(J+1)_{0(J+1)}$ for ν_8) in the infrared spectrum of ketene, with line data in cm^{-1}.

ν_5	Expt. trans.[a]	MARVEL pred.	DEWE-VS[b]	ν_8	Expt. trans.[a]	MARVEL pred.	DEWE-VS[d]
$^rR_1(2)$	621.2357(20)	621.2354(2)	621.2353	$^pR_1(5)$	972.7856(10)	972.7855(4)	972.7862
$^rR_1(3)$	621.9312(20)	621.9312(2)	621.9311	$^pR_1(8)^c$	974.9959(20)	974.9954(4)	974.9949
$^rR_1(4)$	622.6339(20)	622.6339(2)	622.6339	$^pR_1(11)^c$	977.2859(20)	977.2858(4)	977.2866
$^rR_1(5)$	623.3436(20)	623.3435(2)	623.3436				
$^rR_1(6)$	624.0602(20)	624.0600(2)	623.0603				
$^rR_1(7)$	624.7835(20)	624.7836(2)	624.7838				
$^rR_1(8)$	625.5141(20)	625.5150(4)	625.5143				
$^rR_1(9)$	626.2517(20)	626.2519(4)	626.2518				
$^rR_1(10)$	626.9962(20)	626.9962(4)	626.9962				
$^rR_1(11)$	627.7478(20)	627.7474(3)	627.7473				

[a] See beginning of Section 3.2.7 for the discussion of experimental uncertainties.
[b] Obtained from the directly computed first-principles results via the following quadratic correction form fitted to all MARVEL – DEWE-VS differences: $-16.013366 + 0.000759J + 0.000143J^2$.
[c] Slightly blended line.
[d] Obtained from the directly computed first-principles results via the following quadratic correction form fitted to all ($J = 5$ to 13) MARVEL – DEWE-VS differences: $-5.233293 + 0.002764J - 0.001535J^2$.

in Table XV a comparison for all 10 lines, only a single MARVEL prediction suffices for definitive assignments using standard spectroscopic techniques based on series regularity for all unperturbed lines in the series having sufficient intensity and no line blending.)

The next series is the $^pR_1(J)$ branch of the fundamental vibration $\nu_8 = 8^1$. This branch is located between 972.78 and 978.87 cm^{-1} and contains clearly resolved rotational features, characterized with J values ranging from 5 to 13. Three new lines have been assigned and all show outstanding agreement with the MARVEL predicted transitions. Other members of this series ($J = 5$ to 13) have been identified before and were included in the MARVEL analysis.

3.3 GENIUSH-VS computations for $H_2{}^{16}O$

The MARVEL procedure [43] is able to compute energy levels of experimental quality provided an initial database of experimental transitions is available. The experimental transitions present in the input database need to be assigned with unique labels describing

the upper and lower energy levels. Usually the labels refer to the well-known zeroth-order vibrational and rotational quantum numbers. The MARVEL energy levels, being the output of the MARVEL analysis, can be used to predict a huge number of transitions that are of experimental quality and can be utilized for the identification of unassigned experimental spectral lines. This is the main reason why validity of the labels of the MARVEL energy levels is crucial. Therefore, we decided to validate the MARVEL energy levels of the $H_2{}^{16}O$ isotopologue by comparing their approximate labels to those of the energy levels computed by the GENIUSH-VS algorithm.

To facilitate the validation process the first 800 vibrational energy levels and wave functions were computed by GENIUSH in a vibrational basis of dimension $45 \cdot 35^2$. 45 potential-optimized Legendre-DVR and 35 potential-optimized Laguerre-DVR basis functions were applied to the θ bending, and r_1 and r_2 stretching coordinates, respectively. Rovibrational energy levels and wave functions up to $J = 25$ were computed by the GENIUSH-VS procedure employing the first 800 vibrational states as a vibrational basis. During the computations the Eckart frame, which has proven to be beneficial for the accuracy of the GENIUSH-VS results, was used. The resulting rovibrational energy levels and wave functions were analyzed by the RRD procedure by evaluating J, K_a, K_c rigid rotor quantum numbers and C_{2v}(M) symmetry labels. NMD labels used for this examination were taken from Ref. [9].

The results of the validation procedure form a part of an IUPAC Task Group effort to describe the full spectroscopy of water vapor and are summarized in Table XVI. A cut-off value of 0.7 was chosen for the largest RRD coefficient, *i.e.*, only cases where the labelling is unambiguously provided by the RRD scheme were investigated. Rovibrational states with an energy larger than 25000 cm^{-1} were also not investigated since for them there appear to be very few states which can clearly be labeled via an RRD table. This means that for a large number of MARVEL energy levels no validation via the RRD scheme was attempted. The extent of validated labels for the different vibrational band origins (VBO) is given in Table XVI, which also gives the J_{max} values for a large number of VBOs. Clearly, it is more problematic to provide unambiguous rotational labels for VBOs which contain a high level of bending excitation (note that starting from the (0 10 0) VBO no rotational labels on pure bending VBOs can be performed) and as the energy of excitation increases the highest J value where RRD can be used to validate the MARVEL labels decreases.

Table XVI. Validation of the rotational labels of the rovibrational levels determined by the final MARVEL analysis via the RRD protocol. RRD labels have been determined only for states with J less equal than 25. VBO = vibrational band origin. $J_{\rm max}$ gives the maximum J value for rovibrational MARVEL states determined on the particular VBO. $J_{\rm v}$ is the maximum J value for wich all labels have been validated.

VBO	$J_{\rm max}$	$J_{\rm v}$	No. of val. labels	No. of labels without val.
(000)	42	23	581	95
(010)	39	14	475	201
(020)	36	10	338	322
(100)	36	22	458	193
(001)	37	23	506	162
(030)	28	10	271	244
(110)	32	14	319	173
(011)	35	15	421	173
(040)	26	8	191	90
(120)	24	10	209	43
(021)	33	12	280	141
(200)	29	9	284	63
(101)	33	9	321	112
(002)	32	9	304	35
(050)	20	6	127	64
(130)	15	6	129	9
(031)	29	8	213	72
(210)	15	8	145	13
(111)	31	9	271	79
(060)	17	5	78	39
(012)	29	12	222	10
(140)	13	6	95	17
(041)	25	7	152	80
(070)	13	3	34	32
(220)	13	9	111	16
(121)	22	7	159	64
(022)	26	9	151	36

(300)	25	7	186	68
(201)	32	7	210	58
(102)	27	6	209	23
(003)	26	10	209	15
(150)	10	5	6	11
(051)	24	6	73	48
(080)	11	3	7	24
(230)	14	7	88	16
(131)	22	7	126	27
(032)	19	8	104	22
(310)	22	7	128	33
(211)	27	7	168	56
(160)	12	4	5	17
(112)	16	8	128	13
(090)	10	4	3	9
(013)	15	8	131	7
(061)	19	5	30	33
(240)	13	4	77	30
(141)	14	4	88	29
(042)	16	5	79	9
(320)	14	6	81	32
(221)	14	6	94	37
(170)	10	6	4	6
(400)	20	6	108	31
(301)	24	7	120	40
(071)	11	6	11	7
(0 10 0)	7	6	0	3
(122)	12	6	80	12
(023)	14	9	99	6
(202)	14	7	107	13
(103)	23	8	137	11
(004)	22	22	124	2
(250)	8	6	0	11

(151)	11	5	35	16
(052)	10	8	0	7
(180)	10	6	0	6
(081)	10	8	0	4
(330)	10	6	42	18
(231)	10	4	66	19
(0 11 0)	0	0	0	0
(410)	11	7	74	14
(311)	15	4	92	21
(132)	9	7	36	1

4 Future plans

There are a few areas where the results obtained during my PhD research have not been published. I include them in this section and I plan to publish the most important findings in the near future.

4.1 Clustering of the highly-excited rovibrational states of CH_4

The ability to compute highly-excited rovibrational states with the VS procedure of Section 2.6 means that a peculiar feature of rovibrational spectra, the clustering of highly-excited rovibrational states of molecules can be studied. Such clustering was first predicted perhaps by Dorney and Watson [130] for the case of spherical top molecules (e.g., CH_4). The most familiar and most widely studied rotational level clustering effects include asymmetric tops [131] (for example, H_2O, H_2S, H_2Se and H_2Te) and those of XY_3 symmetric tops, like PH_3 [132, 133], BiH_3 [134], and SbH_3 [134].

Figures 5, 6, and 7 shows interesting clustering effects of the five-atomic CH_4 molecule for its lowest vibrational states ((00)(00) (A_1), (00)(01) ($\nu = 1311.74$ cm^{-1}, F_2), and (00)(10) ($\nu = 1533.25$ cm^{-1}, E), respectively). The computations employed the PES of Ref. [135] and the DEWE-VS program. First, the first 100 vibrational energy levels and wave functions were computed by DEWE in a Hermite-DVR vibrational basis of dimension $7^5 \cdot 6^4$. Then, rovibrational energy levels and wave functions were computed by DEWE-VS employing the previously obtained 100 vibrational states as a vibrational basis. In the end, rovibrational states corresponding to the lowest vibrational states were selected by the RRD procedure and assigned with $T_\mathrm{d}(\mathrm{M})$ symmetry labels. The VS method allows the accurate computation of highly excited rotational-vibrational eigenpairs, the fully quantum mechanical determination of energy clusters, and thus the detailed analysis of the semi-classical results of Dorney and Watson [130] and Sadovskii [136].

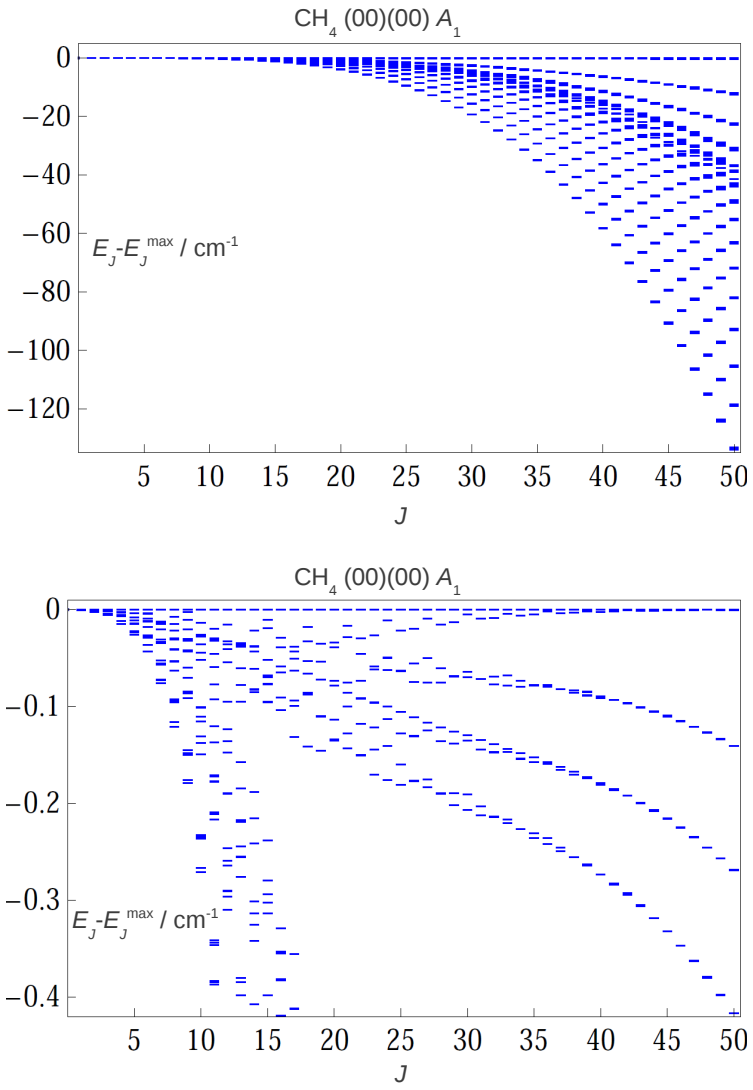

Figure 5: Rotational clustering effects shown on two different scales for the (00)(00) A_1 vibrational ground state of the parent isotopologue of the methane molecule. $E_J - E_J^{\max}$ differences, in cm^{-1}, are plotted against the J rotational quantum number, where E_J and $E_J^{\max}$ denote an arbitrary and the maximum energy level for a given value of J, respectively. The computations are based on the PES of Ref. [135] and were obtained with the DEWE-VS program.

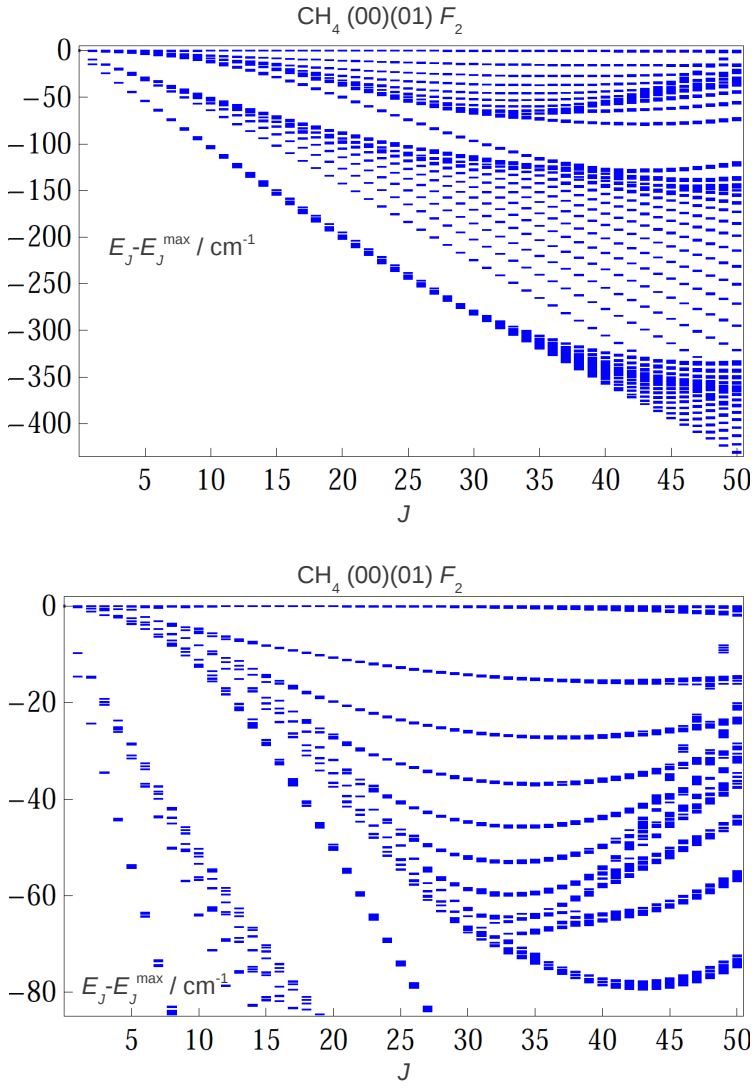

Figure 6: Rotational clustering effects shown on two different scales for the (00)(01) F_2 vibrational state ($\nu = 1311.74$ cm^{-1}) of the parent isotopologue of the methane molecule. $E_J - E_J^{\max}$ differences, in cm^{-1}, are plotted against the J rotational quantum number, where E_J and $E_J^{\max}$ denote an arbitrary and the maximum energy level for a given value of J, respectively. The computations are based on the PES of Ref. [135] and were obtained with the DEWE-VS program.

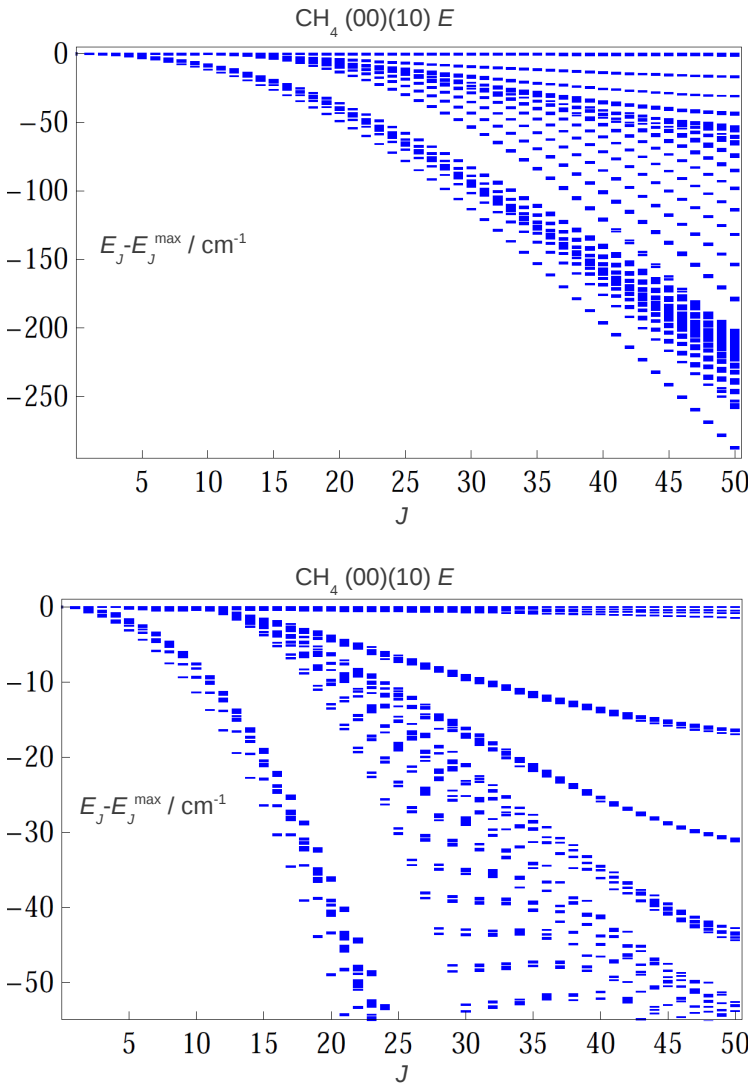

Figure 7: Rotational clustering effects shown on two different scales for the (00)(10) E vibrational state ($\nu = 1533.25$ cm^{-1}) of the parent isotopologue of the methane molecule. $E_J - E_J^{\max}$ differences, in cm^{-1}, are plotted against the J rotational quantum number, where E_J and $E_J^{\max}$ denote an arbitrary and the maximum energy level for a given value of J, respectively. The computations are based on the PES of Ref. [135] and were obtained with the DEWE-VS program.

4.2 Eckart embedding for the NH_3 molecule

Rovibrational energy levels and wave functions for the first ten vibrational states of the ammonia molecule were computed by GENIUSH for $J = 1, 2$, and 3 for the 6D full and 3D stretch-only models. The Eckart embedding was utilized with equilibrium (C_{3v}) and planar (D_{3h}) point-group symmetry reference structures besides the embedding described in Section 3.1, called the old frame henceforth. Results of the RRD computations were compared for the three different embedding choices.

For the 6D full model (active inversion), the largest RRD coefficients were obtained by the Eckart frame employing the D_{3h} reference structure. The second largest RRD coefficients belong to the old frame, while the Eckart frame with C_{3v} reference structure had the worst performance. In case of the 3D stretch-only model (inactive inversion) the following quality order of the RRD coefficients were found: Eckart frame with C_{3v} reference structure, old frame, Eckart frame employing D_{3h} reference structure.

My aim is to perform a deeper analysis of the RRD results, testing the GENIUSH-VS algorithm for the three different embeddings mentioned, and consider a special Eckart reference structure following the large amplitude inversion motion of NH_3.

5 Summary

A considerable part of my research efforts was dedicated to the DEWE (Discrete variable representation of the Eckart–Watson Hamiltonian with a numerically Exact inclusion of arbitrary potential energy surfaces) algorithm. DEWE employs the universal and exact Eckart–Watson Hamiltonian and the iterative Lanczos eigensolver for obtaining the eigenvalues and eigenvectors of the Hamiltonian matrix. Though DEWE can be applied for N-atomic systems it is limited to the case of semirigid molecules with a single well-defined minimum structure. My contribution to DEWE was to add the capability of computing rotational-vibrational energy levels and wave functions to the original vibrational-only code. Detailed description of the variational solution of the rotational-vibrational problem within the framework of DEWE was discussed.

My program development efforts also resulted in an improved GENIUSH (General rovibrational code with Numerical, Internal coordinate, User-Specified Hamiltonians) algorithm. The GENIUSH approach successfully circumvents the main drawback of DEWE and thus can be applied to N-atomic molecules exhibiting multiple accessible PES minima and large amplitude motions. The main idea behind GENIUSH is the numerical representation of the rovibrational kinetic energy operator which allows us to employ arbitrary sets of internal coordinates and body-fixed frame embeddings during the rovibrational computations. Another important characteristics of GENIUSH is the possibility to introduce reduced-dimensional computational models in a straightforward manner. My task was to formulate and add the rotational functionality to the original vibrational-only GENIUSH code. Formulation of the general N-atomic rovibrational Hamiltonian and the variational solution of the rovibrational problem were described.

During my research, I also addressed the problem of assigning symmetry labels to the computed rovibrational energy levels and wave functions. For this purpose I adopted the symmetry-adapted Lanczos (SAL) method. After a brief review of the Lanczos algorithm and the general theory of the SAL method I described my own SAL implementation within the DEWE program.

I also considered the problem how to maintain the rotational Eckart condition. After a brief summary of the theory of the rotational Eckart condition I introduced my implementation of the Eckart embedding within the GENIUSH algorithm.

I solved the problem of labelling of the computed rovibrational energy levels and wave functions with zeroth-order harmonic oscillator and rigid rotor quantum numbers. I gave

an insight into the rigid-rotor decomposition (RRD) algorithm I used extensively for the interpretation of the computed rovibrational states.

I proposed an efficient algorithm for the computation of highly-excited rovibrational states. I developed efficient VS implementations within the DEWE and GENIUSH program packages.

I computed rovibrational energy levels and wave functions for the four-atomic NH_3 by GENIUSH with a special emphasis on the quality of the results computed with the full-dimensional and different reduced-dimensional rovibrational models. Next, the rovibrational spectroscopy of the five-atomic C_2H_2O (ketene) molecule was examined. Variational computations (employing the DEWE, VS, NMD, RRD and SAL methods) and the MARVEL procedure were applied to propose new assignments in the experimental spectrum of C_2H_2O. Finally, labels of the MARVEL energy levels of $H_2{}^{16}O$ up to $J = 25$ were validated by the VS procedure implemented within GENIUSH.

My future plans include rovibrational computations for CH_4 in order to study the rovibrational clustering of the energy levels corresponding to high J rotational quantum number values. For NH_3, rovibrational computations employing the Eckart frame have been executed and the results with different choices of the Eckart reference structure have been analysed briefly.

A Appendix

A.1 Angular momentum algebra

As angular momentum algebra is of great importance in the field of computational molecular spectroscopy, a brief summary of some of its elements is given here. A more detailed description can be found in the literature and in several textbooks [52, 74, 137, 138, 139, 140].

The starting point is that generalized angular momentum operators obey the

$$[\hat{J}^2, \hat{J}_\alpha] = 0 \tag{124}$$

and

$$[\hat{J}_\alpha, \hat{J}_\beta] = -i \sum_\gamma \epsilon_{\alpha\beta\gamma} \hat{J}_\gamma \tag{125}$$

commutation relations. In Eq. (125), $\alpha, \beta, \gamma = x, y, z$, $\epsilon_{\alpha\beta\gamma}$ denotes the Levi–Cività-symbol. The so-called anomalous commutation relations of Eq. (125) apply to the angular momentum components expressed in the molecule-fixed frame.

As $[\hat{J}^2, \hat{J}_z] = 0$, the eigenfunction sets of $\hat{J}^2$ and $\hat{J}_z$, denoted by $|JKM\rangle$, coincide:

$$\hat{J}^2 |JKM\rangle = J(J+1)|JKM\rangle \tag{126}$$

and

$$\hat{J}_z |JKM\rangle = K|JKM\rangle. \tag{127}$$

The $|JKM\rangle$ eigenfunctions can be parametrized with the ϕ, θ, and χ Euler angles:

$$|JKM\rangle = \sqrt{\frac{2J+1}{8\pi^2}} D^{J*}_{MK}(\phi, \theta, \chi), \tag{128}$$

where $D^J_{MK}(\phi, \theta, \chi)$ stands for the Wigner rotation matrix. The $|JKM\rangle$ functions satisfy the

$$\langle JKM|J'K'M'\rangle = \delta_{JJ'}\delta_{KK'}\delta_{MM'} \tag{129}$$

orthogonality relations.

It is advantageous to introduce the $\hat{J}_+$ step-up and $\hat{J}_-$ step-down ladder operators as

$$\hat{J}_\pm = \hat{J}_x \pm i\hat{J}_y. \tag{130}$$

The $\hat{J}_\pm$ operators satisfy the

$$[\hat{J}^2, \hat{J}_\pm] = 0 \tag{131}$$

and

$$[\hat{J}_z, \hat{J}_\pm] = \pm\hat{J}_\pm \tag{132}$$

commutation relations. According to the previous equations,

$$\hat{J}^2\hat{J}_\pm|JKM\rangle = \hat{J}_\pm\hat{J}^2|JKM\rangle = J(J+1)\hat{J}_\pm|JKM\rangle \tag{133}$$

and

$$\hat{J}_z\hat{J}_\pm|JKM\rangle = \hat{J}_\pm\hat{J}_z|JKM\rangle \pm \hat{J}_\pm|JKM\rangle = (K\pm 1)\hat{J}_\pm|JKM\rangle. \tag{134}$$

In view of Eq. (134), the effect of the ladder operators on the $|JKM\rangle$ functions can be expressed as

$$\hat{J}_\pm|JKM\rangle = C_\pm|J(K\pm 1)M\rangle. \tag{135}$$

The absolute value of the $C_\pm$ coefficients equals to

$$|C_\pm|^2 = \langle JKM|\hat{J}_\mp\hat{J}_\pm|JKM\rangle = \langle JKM|\hat{J}^2 - \hat{J}_z(\hat{J}_z \pm 1)|JKM\rangle = \tag{136}$$

$$= J(J+1) - K(K\pm 1),$$

where the $\hat{J}_\pm^\dagger = \hat{J}_\mp$ relation is used. If the phase of $C_\pm$ is chosen to be zero,

$$\hat{J}_\pm|JKM\rangle = \sqrt{J(J+1) - K(K\pm 1)}|J(K\pm 1)M\rangle. \tag{137}$$

The next step is to give the matrix representations of the $\hat{J}_x$ and $\hat{J}_y$ operators in the body-fixed frame. As

$$\hat{J}_x = \frac{\hat{J}_+ + \hat{J}_-}{2} \tag{138}$$

and

$$\hat{J}_y = \frac{\hat{J}_+ - \hat{J}_-}{2i}, \tag{139}$$

nonzero elements of the $\mathbf{J}_x$ and $\mathbf{J}_y$ matrices are

$$\langle JKM|\hat{J}_x|J(K\pm 1)M\rangle = \frac{1}{2}\sqrt{J(J+1)-K(K\pm 1)}$$

$$\langle JKM|\hat{J}_y|J(K\pm 1)M\rangle = \mp\frac{i}{2}\sqrt{J(J+1)-K(K\pm 1)} \tag{140}$$

$$\langle JKM|\hat{J}_z|JKM\rangle = K.$$

A.2 Elements of the g matrix

The rotational $\mathbf{g}$ matrix elements are equal to

$$g_{k+D,l+D} = \sum_{i=1}^{N} m_i \frac{\partial \mathbf{X}_i^{\mathrm{T}}}{\partial \alpha_k}\frac{\partial \mathbf{X}_i}{\partial \alpha_l} = \sum_{i=1}^{N} m_i \mathbf{x}_i^{\mathrm{T}}\frac{\partial \mathbf{C}^{\mathrm{T}}}{\partial \alpha_k}\frac{\partial \mathbf{C}}{\partial \alpha_l}\mathbf{x}_i = \sum_{i=1}^{N} m_i \mathbf{x}_i^{\mathrm{T}}\frac{\partial \mathbf{C}^{\mathrm{T}}}{\partial \alpha_k}\mathbf{C}\mathbf{C}^{\mathrm{T}}\frac{\partial \mathbf{C}}{\partial \alpha_l}\mathbf{x}_i =$$

$$= \sum_{i=1}^{N} m_i \left(\mathbf{C}^{\mathrm{T}}\frac{\partial \mathbf{C}}{\partial \alpha_k}\mathbf{x}_i\right)^{\mathrm{T}}\left(\mathbf{C}^{\mathrm{T}}\frac{\partial \mathbf{C}}{\partial \alpha_l}\mathbf{x}_i\right) = \sum_{i=1}^{N} m_i (\mathbf{e}_k \times \mathbf{x}_i)^{\mathrm{T}}(\mathbf{e}_l \times \mathbf{x}_i), \tag{141}$$

where α_k is the kth rotational coordinate, $\mathbf{e}_k$ is a unit vector giving the direction of the rotational axis associated with α_k, $\mathbf{x}_i$ is the position vector of the ith nucleus expressed in the body-fixed frame, and $k, l = 1(x), 2(y), 3(z)$. In Eq. (141) the equalities

$$\mathbf{C}\mathbf{C}^{\mathrm{T}} = \mathbf{I}, \tag{142}$$

and

$$\mathbf{C}^{\mathrm{T}}\frac{\partial \mathbf{C}}{\partial \alpha_k}\mathbf{r} = \mathbf{e}_k \times \mathbf{r} \tag{143}$$

have been utilized. In these equations $\mathbf{I}$ is the identity matrix of dimension three and the $\mathbf{C}^{\mathrm{T}}\frac{\partial \mathbf{C}}{\partial \alpha_k}$ matrix in Eq. (143) is antisymmetric and its effect on an arbitrary $\mathbf{r}$ vector corresponds to the $\mathbf{e}_k \times \mathbf{r}$ cross product. See Section A.3 for the derivation of Eq. (143).

The vibrational $\mathbf{g}$ matrix elements are given as

$$g_{kl} = \sum_{i=1}^{N} m_i \frac{\partial \mathbf{X}_i^{\mathrm{T}}}{\partial q_k} \frac{\partial \mathbf{X}_i}{\partial q_l} = \sum_{i=1}^{N} m_i \frac{\partial \mathbf{x}_i^{\mathrm{T}}}{\partial q_k} \mathbf{C}^{\mathrm{T}} \mathbf{C} \frac{\partial \mathbf{x}_i}{\partial q_l} = \sum_{i=1}^{N} m_i \frac{\partial \mathbf{x}_i^{\mathrm{T}}}{\partial q_k} \frac{\partial \mathbf{x}_i}{\partial q_l}, \tag{144}$$

where q_k is the kth internal coordinate.

The $\mathbf{g}$ matrix elements of the rovibrational coupling block have the form

$$g_{k,l+D} = \sum_{i=1}^{N} m_i \frac{\partial \mathbf{X}_i^{\mathrm{T}}}{\partial q_k} \frac{\partial \mathbf{X}_i}{\partial \alpha_l} = \sum_{i=1}^{N} m_i \frac{\partial \mathbf{x}_i^{\mathrm{T}}}{\partial q_k} \mathbf{C}^{\mathrm{T}} \frac{\partial \mathbf{C}}{\partial \alpha_l} \mathbf{x}_i = \sum_{i=1}^{N} m_i \frac{\partial \mathbf{x}_i^{\mathrm{T}}}{\partial q_k} (\mathbf{e}_l \times \mathbf{x}_i). \tag{145}$$

A.3 Derivation of Eq. (143)

Let us consider a three-dimensional orthogonal matrix $\mathbf{C}$ describing a rotation around $\mathbf{n}$, where $\mathbf{n}$ is a unit vector specifying the axis of the rotation and ϕ is the rotation angle. The antisymmetric property of $\mathbf{C}^{\mathrm{T}} \frac{\mathrm{d}\mathbf{C}}{\mathrm{d}\phi}$ is a direct consequence of the

$$\mathbf{C}^{\mathrm{T}} \mathbf{C} = \mathbf{I} \tag{146}$$

relation, where $\mathbf{I}$ indicates the identity matrix of dimension three. After differentiating Eq. (146) with respect to ϕ,

$$\frac{\mathrm{d}\mathbf{C}^{\mathrm{T}}}{\mathrm{d}\phi} \mathbf{C} + \mathbf{C}^{\mathrm{T}} \frac{\mathrm{d}\mathbf{C}}{\mathrm{d}\phi} = \mathbf{0}, \tag{147}$$

where $\mathbf{0}$ is the three-dimensional zero matrix. Rearrangement of Eq. (147) yields

$$\left(\mathbf{C}^{\mathrm{T}} \frac{\mathrm{d}\mathbf{C}}{\mathrm{d}\phi} \right)^{\mathrm{T}} = -\mathbf{C}^{\mathrm{T}} \frac{\mathrm{d}\mathbf{C}}{\mathrm{d}\phi}, \tag{148}$$

which demonstrates the antisymmetry of $\mathbf{C}^{\mathrm{T}} \frac{\mathrm{d}\mathbf{C}}{\mathrm{d}\phi}$.

The effect of $\mathbf{C}$ on an arbitrary $\mathbf{r}$ vector is given by the

$$\mathbf{r}' = \mathbf{C}\mathbf{r} = \mathbf{r} \cos\phi + (\mathbf{n} \cdot \mathbf{r})\mathbf{n}(1 - \cos\phi) + (\mathbf{n} \times \mathbf{r}) \sin\phi \tag{149}$$

general rotation formula, where $\mathbf{r}'$ is the result of the rotation. After expanding the vector

operations in Eq. (149), $\mathbf{C}$ can be expressed as

$$\mathbf{C} = \begin{pmatrix} \cos\phi+(1-\cos\phi)\cdot n_x^2 & (1-\cos\phi)\cdot n_x n_y-\sin\phi\cdot n_z & (1-\cos\phi)\cdot n_x n_z+\sin\phi\cdot n_y \\ (1-\cos\phi)\cdot n_x n_y+\sin\phi\cdot n_z & \cos\phi+(1-\cos\phi)\cdot n_y^2 & (1-\cos\phi)\cdot n_y n_z-\sin\phi\cdot n_x \\ (1-\cos\phi)\cdot n_x n_z-\sin\phi\cdot n_y & (1-\cos\phi)\cdot n_y n_z+\sin\phi\cdot n_x & \cos\phi+(1-\cos\phi)\cdot n_z^2 \end{pmatrix}, \tag{150}$$

where n_x, n_y and n_z are the three components of $\mathbf{n}$, and $n_x^2+n_y^2+n_z^2=1$. Since Eq. (150) gives the rotation matrix of arbitrary axis and angle, one can generally derive the matrix elements of $\mathbf{C}^{\mathrm{T}}\frac{\mathrm{d}\mathbf{C}}{\mathrm{d}\phi}$ as

$$\mathbf{C}^{\mathrm{T}}\frac{\mathrm{d}\mathbf{C}}{\mathrm{d}\phi} = \begin{pmatrix} 0 & -n_z & n_y \\ n_z & 0 & -n_x \\ -n_y & n_x & 0 \end{pmatrix}. \tag{151}$$

In light of Eq. (151) it becomes clear that the effect of $\mathbf{C}^{\mathrm{T}}\frac{\mathrm{d}\mathbf{C}}{\mathrm{d}\phi}$ on an arbitrary $\mathbf{r}$ vector is

$$\mathbf{C}^{\mathrm{T}}\frac{\mathrm{d}\mathbf{C}}{\mathrm{d}\phi}\mathbf{r} = \mathbf{n}\times\mathbf{r}. \tag{152}$$

References

[1] M. Born, J. R. Oppenheimer, Ann. Phys. (Leipzig) **84**, 457 (1927).

[2] M. Born, K. Huang, *Dynamical Theory of Crystal Lattices* (Oxford Univ. Press, New York, 1954).

[3] H. Goldstein, *Classical mechanics*, (Addison–Wesley, 1980).

[4] B. T. Sutcliffe, J. Tennyson, Int. J. Quant. Chem. **39**, 183 (1991).

[5] N. C. Handy, Mol. Phys. **61**, 207 (1987).

[6] A. G. Császár, N. C. Handy, J. Chem. Phys. **102**, 3962 (1995).

[7] G. Czakó, T. Furtenbacher, A. G. Császár, V. Szalay, Mol. Phys. **102**, 2411 (2004).

[8] T. Furtenbacher, G. Czakó, B. T. Sutcliffe, A. G. Császár, V. Szalay, J. Mol. Struct. **780-781**, 283 (2006).

[9] A. G. Császár, E. Mátyus, T. Szidarovszky, L. Lodi, N. F. Zobov, S. V. Shirin, O. L.Polyansky, J. Tennyson, J. Quant. Spectr. Rad. Transfer **111(9)**, 1043 (2010).

[10] T. Szidarovszky, A. G. Császár, G. Czakó, Phys. Chem. Chem. Phys. **12**, 8373 (2010).

[11] M. Pavanello, L. Adamowicz, A. Alijah, N. F. Zobov, I. I. Mizus, O. L. Polyansky, J. Tennyson, T. Szidarovszky, A. G. Császár, M. Berg, A. Petrignani, A. Wolf, Phys. Rev. Lett. **108**, 023002 (2012).

[12] J. Tennyson, M. A. Kostin, P. Barletta, G. J. Harris, J. Ramanlal, O. L. Polyansky, N. F. Zobov, Comp. Phys. Comm. **163**, 85 (2004).

[13] O. L. Polyansky, A. G. Császár, S. V. Shirin, N. F. Zobov, P. Barletta, J. Tennyson, D. W. Schwenke, P. J. Knowles, Science **299**, 539 (2003).

[14] M. J. Bramley, T. Carrington Jr., J. Chem. Phys. **99**, 8519 (1993).

[15] I. N. Kozin, M. M. Law, J. Tennyson, J. M. Hutson, Comp. Phys. Comm. **163**, 117 (2004).

[16] M. Mladenović, J. Chem. Phys. **112**, 1070 (2000).

[17] X.-G. Wang, T. J. Carrington Jr., Chem. Phys. **121**, 2937 (2004).

[18] J. K. G. Watson, Mol. Phys. **15**, 479 (1968).

[19] J. K. G. Watson, Mol. Phys. **19**, 465 (1970).

[20] E. Mátyus, G. Czakó, B. T. Sutcliffe, A. G. Császár, J. Chem. Phys. **127**, 084102 (2007).

[21] E. Mátyus, J. Šimunek, A. G. Császár, J. Chem. Phys. **131**, 074106 (2009).

[22] C. Fábri, E. Mátyus, T. Furtenbacher, B. Mihály, T. Zoltáni, L. Nemes, A. G. Császár, J. Chem. Phys. **135**, 094307 (2011).

[23] D. Searles, E. von Nagy-Felsobuki, *Ab Initio Variational Calculations of Molecular Vibration-Rotation Spectra, Lecture Notes in Chemistry No. 61* (Springer-Verlag, Berlin, 1993).

[24] O. Christiansen, Phys. Chem. Chem. Phys. **9**, 2942 (2007).

[25] R. J. Whitehead, N. C. Handy, Mol. Phys. **55**, 456 (1975).

[26] K. M. Dunn, J. E. Boggs, P. Pulay, J. Chem. Phys. **85**, 5838 (1986).

[27] K. M. Dunn, J. E. Boggs, P. Pulay, J. Chem. Phys. **86**, 5088 (1987).

[28] J. O. Jung, R. B. Gerber, J. Chem. Phys. **105**, 10332 (1996).

[29] J. M. Bowman, S. Carter, X. C. Huang, Int. Rev. Phys. Chem. **22**, 533 (2003).

[30] T. Yonehara, T. Yamamoto, S. Kato, Chem. Phys. Lett. **393**, 98 (2004).

[31] G. Rauhut, J. Chem. Phys. **121**, 9313 (2004).

[32] E. Mátyus, G. Czakó, A. G. Császár, J. Chem. Phys. **130**, 134112 (2009).

[33] C. Fábri, E. Mátyus, A. G. Császár, J. Chem. Phys. **134**, 074105 (2011).

[34] R. Meyer, H. H. Gunthard, J. Chem. Phys. **50**, 353 (1969).

[35] J. K. G. Watson, J. Mol. Spectrosc. **228**, 645 (2004).

[36] D. Luckhaus, J. Chem. Phys. **113**, 1329 (2000).

[37] D. Luckhaus, J. Chem. Phys. **118**, 8797 (2003).

[38] D. Lauvergnat, A. Nauts, J. Chem. Phys. **116**, 8560 (2002).

[39] D. Lauvergnat, E. Baloitcha, G. Dive, M. Desouter-Lecomte, Chem. Phys. **326**, 500 (2006).

[40] S. N. Yurchenko, W. Thiel, P. Jensen, J. Mol. Spectrosc. **245**, 126 (2007).

[41] C. Eckart, Phys. Rev. **47**, 552 (1935).

[42] E. Mátyus, C. Fábri, T. Szidarovszky, G. Czakó, W. D. Allen, A. G. Császár, J. Chem. Phys. **133**, 034113 (2010).

[43] T. Furtenbacher, A. G. Császár, J. Tennyson, J. Mol. Spectrosc. **245**, 115 (2007).

[44] C. Lanczos, J. Res. Natl. Bur. Stand. **45**, 255 (1950).

[45] L. D. Landau, E. M. Lifshitz, *Quantum Mechanics: Non-Relativistic Theory, Volume 3*, (Pergamon Press, 1977).

[46] D. O. Harris, G. G. Engerholm, W. D. Gwinn, J. Chem. Phys. **43**, 1515 (1965).

[47] V. Szalay, J. Chem. Phys. **105**, 6940 (1996).

[48] A. S. Dickinson, P. R. Certain, J. Chem. Phys. **49**, 4209 (1968).

[49] J. Echave, D. C. Clary, Chem. Phys. Lett. **190**, 225 (1992).

[50] J. C. Light, I. P. Hamilton, J. V. Lill, J. Chem. Phys. **82**, 1400 (1985).

[51] V. Szalay, J. Chem. Phys. **99**, 1978 (1993).

[52] R. N. Zare, *Angular Momentum: Understanding Spatial Aspects in Chemistry and Physics*, Wiley–Interscience, (New York, 1988).

[53] G. O. Sørensen, Top. Curr. Chem. **82**, 99 (1979).

[54] E. B. Wilson, J. C. Decius, P. C. Cross, *Molecular Vibrations*, McGraw-Hill: New York, 1955.

[55] B. Podolsky, Phys. Rev. **32**, 812 (1928).

[56] L. Halonen, Highly excited states and local modes, in *Computational Molecular Spectroscopy*, Eds. P. Jensen and P. R. Bunker, Wiley: Chichester, 2000, pp. 325-364.

[57] B. Schutz, *Geometrical methods in mathematical physics*, Cambridge University Press: Cambridge, 1980.

[58] T. J. Lukka, J. Chem. Phys. **102**, 3945 (1995).

[59] S. M. Colwell, N. C. Handy, Mol. Phys. **92**, 317 (1997).

[60] C. Fábri, G. Czakó, G. Tasi, A. G. Császár, J. Chem. Phys. **130**, 134314 (2009).

[61] D. T. Colbert, W. H. Miller, J. Chem. Phys. **96**, 1982 (1992).

[62] G. Arfken, *"Diagonalization of Matrices" §4.6 in Mathematical Methods for Physicists* (3rd ed. Orlando, FL: Academic Press, pp. 217-229, 1985).

[63] J. K. Cullum, R. A. Willoughby, Lanczos Algorithms for Large Symmetric Eigenvalue Computations (Birkhauser, Boston, 1985).

[64] L. W. Wang, A. Zunger, J. Chem. Phys. **100**, 2394 (1994).

[65] I. J. Farkas, I. Derényi, A. L. Barabási, T. Vicsek, Phys. Rev. E **64**, 026704 (2001).

[66] J. Grcar, Analyses of the Lanczos Algorithm and of the Approximation Problem in Richardson′s method, PhD. Thesis, University of Illinois (1981).

[67] H. D. Simon, Math. Comp. **42**, 115 (1984).

[68] K. Wu, H. D. Simon, Thick-restart Lanczos method for the symmetric eigenvalue problems, Lawrence Berkeley National Laboratory Report No. 41412 (1998).

[69] K. Wu, A. Canning, H. D. Simon, L. W. Wang, J. Comput. Phys. **154**, 156 (1999).

[70] N. M. Poulin, M. J. Bramley, T. Carrington, H. G. Kjaergaard, B. R. Henry, J. Chem. Phys. **104**, 7807 (1996).

[71] X-G. Wang, T. Carrington, J. Chem. Phys. **114**, 1473 (2001).

[72] R. Chen, H. Guo, J. Chem. Phys. **114**, 1467 (2001).

[73] P. R. Bunker, P. Jensen, *Molecular Symmetry and Spectroscopy* (NRC, Ottawa, 1998).

[74] E. P. Wigner, *Group Theory and its Application to the Quantum Mechanics of Atomic Spectra*, (New York: Academic Press, 1959).

[75] H. M. Pickett, H. L. Strauss, J. Am. Chem. Soc. **92**, 7281 (1970).

[76] A. Y. Dymarsky, K. N. Kudin, J. Chem. Phys. **122**, 124103 (2005).

[77] H. Wei, T. Carrington, J. Chem. Phys. **107**, 2813 (1997).

[78] H. Wei, T. Carrington, J. Chem. Phys. **107**, 9493 (1997).

[79] H. Wei, T. Carrington, Chem. Phys. Lett. **287**, 289 (1998).

[80] C. R. Le Sueur, S. Miller, J. Tennyson, B. T. Sutcliffe, Mol. Phys. **76**, 1147 (1992).

[81] H. Wei, J. Chem. Phys. **118**, 7202 (2003).

[82] http://software.intel.com/en-us/articles/intel-mkl/

[83] S. N. Yurchenko, J. Zheng, H. Lin, P. Jensen, W. Thiel, J. Chem. Phys. **123**, 134308 (2005).

[84] H. Wei, T. Carrington Jr., J. Chem. Phys. **97**, 3029 (1992).

[85] V. Szalay, G. Czakó, Á. Nagy, T. Furtenbacher, A. G. Császár, J. Chem. Phys. **119**, 10512 (2003).

[86] H. C. Longuet-Higgins, Mol. Phys. **6**, 445 (1963).

[87] A. G. Császár, W. D. Allen, H. F. Schaefer, J. Chem. Phys. **108**, 9751 (1998).

[88] W. Klopper, C. C. M. Samson, G. Tarczay, A. G. Császár, J. Comp. Chem. **22**, 1306 (2001).

[89] J. D. Swalen, J. A. Ibers, J. Chem. Phys. **36**, 1914 (1962).

[90] D. Papoušek, V. Špirko, Top. Curr. Chem. **68**, 59 (1976).

[91] V. Špirko, J. Mol. Spectrosc. **101**, 30 (1983).

[92] V. Špirko, W. P. Kraemer, J. Mol. Spectrosc. **133**, 331 (1989).

[93] T. Rajamäki, A. Miani, L. Halonen, J. Chem. Phys. **118**, 6358 (2003).

[94] S. N. Yurchenko, personal communication (2010).

[95] A. G. Császár, G. Czakó, T. Furtenbacher, J. Tennyson, V. Szalay, S. V. Shirin, N. F. Zobov, O. L. Polyansky, J. Chem. Phys. **122**, 214305 (2005).

[96] S. V. Shirin, O. L. Polyansky, N. F. Zobov, R. I. Ovsyannikov, A. G. Császár, J. Tennyson, J. Mol. Spectrosc. **236**, 216 (2006).

[97] M. Artamonov, T.-S. Ho, H. Rabitz, Chem. Phys. **328**, 147 (2006).

[98] A. L. L. East, W. D. Allen, S. J. Klippenstein, J. Chem. Phys. **102**, 8506 (1995).

[99] D. Papoušek, M. R. Aliev, *Molecular Vibrational-Rotational Spectra* (Elsevier, Amsterdam, 1982).

[100] P. Pulay, G. Fogarasi, G. Pongor, J. E. Boggs, A. Vargha, J. Am. Chem. Soc. **105**, 7037 (1983).

[101] W. D. Allen, A. G. Császár, D. A. Horner, J. Am. Chem. Soc. **114**, 6834 (1992).

[102] G. Simons, R. G. Parr, J. M. Finlan, J. Chem. Phys. **59**, 3229 (1973).

[103] INTDER2000 is a connected set of FORTRAN programs developed by W. D. Allen and co-workers for performing general curvilinear transformations and associated tasks often encountered in the calculation of anharmonic molecular force fields.

[104] W. D. Allen, A. G. Császár, V. Szalay, I. M. Mills, Mol. Phys. **89**, 1213 (1996).

[105] W. D. Allen, A. G. Császár, J. Chem. Phys. **98**, 2983 (1993).

[106] J. L. Duncan, A. M. Ferguson, J. Harper, K. H. Tonge, F. Hegelund, J. Mol. Spectrosc. **122**, 72 (1987).

[107] These data originated from the laboratory of Dr. John W. C. Johns at the Herzberg Institute of Astrophysics, Ottawa, Canada, and were taken using a BOMEM DA3.002 FTIR instrument in 1986. The apodized resolution was approximately 0.004 cm^{-1}, and the relative frequency calibration accuracy was better than 0.001 cm^{-1}, as determined by comparison with extensive, known ground-state combination differences.

The absolute wavenumbers have errors smaller than the apodized resolution. The spectral analysis was performed by L. Nemes.

[108] (a) H. S. P. Müller, S. Thorwirth, D. A. Roth, G. Winnewisser; Astron. Astrophys. **370** L49 (2001).
(b) H. S. P. Müller, F. Schlöder, J. Stutzki, G. Winnewisser, J. Mol. Struct. **742**, 215 (2005).
(c) For data on parent ketene, see the web page http://www.ph1.uni- koeln.de/cgi-bin/cdmsinfo?file=e042501.cat (accessed on January 10, 2011).

[109] H. R. Johnson, M. W. P. Strandberg, J. Chem. Phys. **20**, 687 (1952).

[110] D. H. Sutter, H. Dreizler, Z. Naturforsch. **55A**, 695 (2001).

[111] P. Cox, A. S. Esbitt, J. Chem. Phys. **38**, 1636 (1963).

[112] A. Guarnieri, A. Huckauf, Z. Naturforsch. **58A**, 275 (2003).

[113] R. D. Brown, P. D. Godfrey, D. McNaughton, A. P. Pierlot, W. H. Taylor, J. Mol. Spectrosc. **140**, 340 (1990).

[114] B. Fabricant, D. Krieger, J. S. Muenter, J. Chem. Phys. **67**, 1576 (1977).

[115] J. W. C. Johns, L. Nemes, K. M. T. Yamada, T. Y. Wang, J. L. Domenech, J. Santos, P. Cancio, D. Bermejo, J. Ortigoso, R. Escribano, J. Mol. Spectrosc. **156**, 501 (1992).

[116] A. G. Császár, T. Furtenbacher, J. Mol. Spectrosc. **266**, 99 (2011).

[117] J. W. C. Johns, J. M. R. Stone, G. Winnewisser, J. Mol. Spectrosc. **42**, 523 (1972).

[118] R. Escribano, J. L. Domenech, P. Cancio, J. Ortigoso, J. Santos, D. Bermejo, J. Chem. Phys. **101**, 937 (1994).

[119] B. Bak, F. A. Andersen, J. Chem. Phys. **22**, 1050 (1954).

[120] L. Nemes, J. Demaison, G. Wlodarczak, Acta Phys. Hung. **61**, 135 (1987).

[121] B. Strickler, L. Nemes, M. Gruebele, J. Mol. Spectrosc. **219**, 335 (2003).

[122] R. Hinze, H. Zerbe-Foese, J. Doose, A. Guarnieri, J. Mol. Spectrosc. **176**, 133 (1996).

[123] A. G. Császár, G. Czakó, T. Furtenbacher, E. Mátyus, Ann. Rep. Comp. Chem. **3**, 155 (2007).

[124] J. Tennyson, P. F. Bernath, L. R. Brown, A. Campargue, M. R. Carleer, A. G. Császár, R. R. Gamache, J. T. Hodges, A. Jenouvrier, O. V. Naumenko, O. L. Polyansky, L. S. Rothman, R. A. Toth, A. C. Vandaele, N. F. Zobov, L. Daumont, A. Z. Fazliev, T. Furtenbacher, I. F. Gordon, S. N. Mikhailenko, S. V. Shirin, J. Quant. Spectr. Rad. Transfer **110**, 573 (2009).

[125] J. Tennyson, P. F. Bernath, L. R. Brown, A. Campargue, M. R. Carleer, A. G. Császár, L. Daumont, R. R. Gamache, J. T. Hodges, A. Jenouvrier, O. V. Naumenko, O. L. Polyansky, L. S. Rothman, R. A. Toth, A. C. Vandaele, N. F. Zobov, A. Z. Fazliev, T. Furtenbacher, I. F. Gordon, S.-M. Hu, S. N. Mikhailenko, B. Voronin, J. Quant. Spectr. Rad. Transfer **111**, 2160 (2010).

[126] L. Nemes, J. W. C. Johns, Acta Phys. Hung. **74**, 367 (1994).

[127] M. C. Campina, E. Domingo, M. Fernandez-Liencres, R. Escribano, L. Nemes, Anales de Quimica-Internatl. Ed. **94**, 23 (1998).

[128] M. Gruebele, J. W. C. Johns, L. Nemes, J. Mol. Spectrosc. **198**, 376 (1999).

[129] L. Nemes, D. Luckhaus, M. Quack, J. W. C. Johns, J. Mol. Struct. **517-518**, 217 (2000).

[130] A. J. Dorney, J. K. G. Watson, J. Mol. Spectrosc. **42**, 135 (1972).

[131] I. N. Kozin, I. M. Pavlichenkov, J. Chem. Phys. **104**, 4105 (1996).

[132] S. N. Yurchenko, W. Thiel, S. Patchkovskii, P. Jensen, Phys. Chem. Chem. Phys. **7**, 573 (2005).

[133] S. V. Petrov, B. M. Kozlovskii, J. Mol. Spectrosc. **243**, 245 (2007).

[134] S. N. Yurchenko, W. Thiel, P. Jensen, J. Mol. Spectrosc. **240**, 174 (2006).

[135] D. W. Schwenke, H. Partridge, Spectrochim. Acta Part A **58**, 849 (2002).

[136] D. A. Sadovskii, B. I. Zhilinskii, J. P. Champion, G. Pierre, J. Chem. Phys. **92**, 1523 (1990).

[137] D. A. Varschalovich, A. N. Moskalev, V. K. Khersonskii, *Quantum Theory of Angular Momentum*, World Scientific, (Singapore, 1988).

[138] D. M. Brink, G. R. Satchler, *Angular Momentum*, Oxford Science Publications, (Oxford, 1993).

[139] K. A. Nasyrov, J. Phys. A: Math. Gen. **32**, 6663 (1999).

[140] E. P. Wigner, Am. J. Math. **63**, 57 (1941).

Abstract

During my doctoral work I have developed and implemented general algorithms for the accurate and efficient variational computation and interpretation of rotational-vibrational energy levels and wave functions of N-atomic molecules.

First, I extended the original vibrational-only DEWE and GENIUSH programs, developed principally by Dr. Edit Mátyus, with the capability of variational computation of rotational-vibrational energy levels and wave functions. The DEWE program employs the exact and general N-atomic Eckart–Watson nuclear kinetic energy operator, thus it is limited to semirigid molecules exhibiting a single well-defined minimum on their PES. The GENIUSH program successfully circumvents the main drawback of DEWE and can be applied to N-atomic molecules exhibiting multiple accessible PES minima and large amplitude motions. In GENIUSH arbitrary internal coordinates, molecule-fixed frames, and either full- or reduced-dimensional rovibrational models can be employed during the computations. The Eckart frame, giving a good separation between rotational and vibrational motions, is also available within GENIUSH.

As a next step, the rigid rotor decomposition (RRD) and symmetry-adapted Lanczos (SAL) procedures were implemented to facilitate the interpretation of the computed rovibrational states. The RRD and SAL algorithms are extremely helpful in the assignment of the rovibrational states with zeroth-order quantum numbers and molecular symmetry group symmetry labels, respectively.

Finally, I developed the vibrational subspace (VS) method allowing the variational computation and assignment of rovibrational states for high values of the J rotational quantum number. Practical VS implementations were done for the DEWE and GENIUSH programs.

The power of the computational framework developed was demonstrated for the three-atomic H_2O, four-atomic NH_3, and five-atomic C_2H_2O (ketene) and CH_4 molecules.

Összefoglalás

Doktori munkám során olyan általános módszereket fejlesztettem ki, melyek lehetővé teszik N-atomos molekulák rezgési-forgási energiaszintjeinek és hullámfüggvényeinek variációs alapú számítását és értelmezését.

Elsőként a Dr. Mátyus Edit által fejlesztett, eredetileg csak rezgési számítások elvégzésére alkalmas DEWE és GENIUSH programokat fejlesztettem tovább. Munkám eredményeképpen a DEWE és a GENIUSH programokkal variációs rezgési-forgási számításokat végezhetünk N-atomos molekulákra. Mivel a DEWE az N-atomos molekulákra általánosan alkalmazható Eckart–Watson Hamilton kinetikus energia operátoron alapul, úgynevezett félmerev molekulák vizsgálatára alkalmazható, melyek potenciális energia felülete egy jól definiált minimummal rendelkezik. Ezt a problémát sikeresen orvosolja a GENIUSH eljárás, ugyanis a GENIUSH segítségével olyan nagy amplitúdójú mozgásokkal rendelkező flexibilis molekulákra is sikerrel végezhetünk variációs rezgési-forgási számításokat, melyek potenciális energia felületén több hozzáférhető minimumot találunk. A GENIUSH programban tetszőleges belső koordinátákat és molekulacetrált koordináta-rendszereket használhatunk a számítások során, többek között az Eckart-rendszert is, mely minimalizálja a rezgések és forgások közti csatolást. A GENIUSH lehetővé teszi redukált dimenziójú modellek használatát is.

Következő lépésként a számítási eredmények értelmezését segítő RRD (rigid rotor decomposition, *merev pörgettyű felbontás*) és SAL (symmetry adapted Lanczos, *szimmetria adaptált Lánczos*) eljárásokat vizsgáltam. Míg az RRD segítségével elvégezhetjük a számított rezgési-forgási állapotok nulladrendű (harmonikus oszcillátor és merev pörgettyű) kvantumszámokkal való asszignációját, a SAL eljárás alkalmas a számított rezgési-forgási állapotok szimmetriájának vizsgálatára.

Végül kifejlesztettem és beprogramoztam a VS (vibrational subspace, *rezgési altér*) módszert, mely lehetővé teszi a magas J forgási kvantumszám értékekhez tartozó rezgési-forgási állapotok számítását és asszignációját. Mind a DEWE, mind pedig a GENIUSH program alkalmas VS számítások elvégzésére.

A munkám során kifejlesztett pontos és hatékony elméleti molekulaspektroszkópiai módszereket sikeresen alkalmaztam a háromatomos H_2O, a négyatomos NH_3, illetve az ötatomos C_2H_2O (ketén) és CH_4 molekulákra.